

Journal of Mechanics of Materials and Structures

Special issue

Trends in Continuum Physics
(TRECOP 2010)

Volume 7, No. 3

March 2012



JOURNAL OF MECHANICS OF MATERIALS AND STRUCTURES

jomms.net

Founded by Charles R. Steele and Marie-Louise Steele

EDITORS

CHARLES R. STEELE Stanford University, USA
DAVIDE BIGONI University of Trento, Italy
IWONA JASIUK University of Illinois at Urbana-Champaign, USA
YASUhide SHINDO Tohoku University, Japan

EDITORIAL BOARD

H. D. BUI École Polytechnique, France
J. P. CARTER University of Sydney, Australia
R. M. CHRISTENSEN Stanford University, USA
G. M. L. GLADWELL University of Waterloo, Canada
D. H. HODGES Georgia Institute of Technology, USA
J. HUTCHINSON Harvard University, USA
C. HWU National Cheng Kung University, Taiwan
B. L. KARIHALOO University of Wales, UK
Y. Y. KIM Seoul National University, Republic of Korea
Z. MROZ Academy of Science, Poland
D. PAMPLONA Universidade Católica do Rio de Janeiro, Brazil
M. B. RUBIN Technion, Haifa, Israel
A. N. SHUPIKOV Ukrainian Academy of Sciences, Ukraine
T. TARNAI University Budapest, Hungary
F. Y. M. WAN University of California, Irvine, USA
P. WRIGGERS Universität Hannover, Germany
W. YANG Tsinghua University, China
F. ZIEGLER Technische Universität Wien, Austria

PRODUCTION contact@msp.org

SILVIO LEVY Scientific Editor

Cover design: Alex Scorpan

See <http://jomms.net> for submission guidelines.

JoMMS (ISSN 1559-3959) is published in 10 issues a year. The subscription price for 2012 is US \$555/year for the electronic version, and \$735/year (+\$60 shipping outside the US) for print and electronic. Subscriptions, requests for back issues, and changes of address should be sent to Mathematical Sciences Publishers, Department of Mathematics, University of California, Berkeley, CA 94720-3840.

JoMMS peer-review and production is managed by EditFLOW[®] from Mathematical Sciences Publishers.

PUBLISHED BY
 **mathematical sciences publishers**
<http://msp.org/>

A NON-PROFIT CORPORATION

Typeset in L^AT_EX

Copyright ©2012 by Mathematical Sciences Publishers

PREFACE

BOGDAN T. MARUSZEWSKI, WOLFGANG MUSCHIK,
JOSEPH N. GRIMA AND KRZYSZTOF W. WOJCIECHOWSKI

Guest Editors

The International Symposia on Trends in Continuum Physics have been held every three years since 1998. The first three events took place at the Poznan University of Technology in Poznan, Poland. The fourth one took place in Lviv, Ukraine, for the first time outside the European Union. The fifth jubilee Symposium was held July 16–20, 2010 in Msida, Malta.

The first four Symposia were jointly planned and organized by B. T. Maruszewski (Poznan University of Technology), W. Muschik (Technische Universität Berlin) and A. Radowicz (Kielce University of Technology). Organization of the fifth one was possible by courtesy of Joseph N. Grima (University of Malta, Msida, Malta).

One of the main aims of those meetings has been to bring together scientists from Eastern Europe working in different fields of continuum physics, broadly understood, as well as those from Western and Central Europe, in order to extend their cooperation and to create new connections and acquaintances.

Special emphasis was placed on the representation of various concepts applied to different physical fields interacting with each other. The scope of the Symposia includes fundamentals of continuum physics, new trends in thermodynamics and in electrodynamics, physics of materials (encompassing defective crystals, ferroic crystals, liquid crystals, molecular crystals, high-temperature superconductors, semiconductors, plasma, polymers, amorphous media, smart materials, and anomalous phenomena such as auxetics and negative thermal expansion), biophysics, multiphase systems, and multiscale problems. These fields have been developing fast in recent years.

The chairs of the Fifth International Symposium on Trends in Continuum Physics (TRECOP'10), where most of the articles in this issue were presented, would like to acknowledge support by the sponsoring institutions who made the meeting possible. They are:

- Institute of Applied Mechanics, Poznan University of Technology
- Institute of Theoretical Physics, Technical University of Berlin, Berlin, Germany
- Kielce University of Technology, Kielce, Poland
- University of Malta, Msida, Malta
- Institute of Molecular Physics, Polish Academy of Sciences, Poznan, Poland
- Foundation for Development of Poznan University of Technology, Poznan, Poland
- Poznan Division of the Polish Society of Theoretical and Applied Mechanics, Poznan, Poland
- Institute of Environmental Mechanics and Applied Computer Science, Kazimierz Wielki University, Bydgoszcz, Poland,
- Department of Solid State Physics, Gdansk University of Technology, Gdansk, Poland

Krzysztof W. Wojciechowski
Chair of the Scientific Committee

Bogdan T. Maruszewski
 Joseph N. Grima
 Wolfgang Muschik
Symposium Chairs

Scientific Committee

Krzysztof W. Wojciechowski (Institute of Molecular Physics, Polish Academy of Sciences, Poznan, Poland)

Jan Awrejcewicz (Lodz University of Technology, Lodz, Poland)

Vladimir Alshits (Institute of Crystallography, Russian Academy of Sciences, Moscow, Russia)

Arkadi Berezovski (CENS – Institute of Cybernetics, Tallinn, Estonia)

Yaroslav Burak (Institute of Applied Mathematics and Mechanics, Ukrainian National Academy of Sciences, Lviv, Ukraine)

Enzo Ciancio (University of Messina, Messina, Italy)

Yevhen Czaplya (Pidstryhach Institute of Applied Problems of Mechanics and Mathematics, Ukrainian National Academy of Sciences, Lviv, Ukraine)

Juri Engelbrecht (Estonian Academy of Sciences, Tallinn, Estonia)

Joseph N. Grima (University of Malta, Msida, Malta)

Karl H. Hoffmann (Chemnitz University of Technology, Chemnitz, Germany)

David Jou (University of Barcelona, Barcelona, Spain)

Jan A. Kołodziej (Institute of Applied Mechanics, Poznan University of Technology, Poznan, Poland)

Józef Kubik (Kazimierz Wielki University, Bydgoszcz, Poland)

Gerard A. Maugin (University of Paris VI, Paris, France)

Stanisław Matysiak (Warsaw University, Warsaw, Poland)

Wolfgang Muschik (Institute of Theoretical Physics, Technical University of Berlin, Berlin, Germany)

Henryk Petryk (Institute of Fundamental Technological Research, Polish Academy of Sciences, Warsaw, Poland)

Liliana Restuccia (University of Messina, Messina, Italy)

Czesław Rymarz (Institute of Fundamental Technological Research, Polish Academy of Sciences, Warsaw, Poland)

Jarostaw Rybicki (Gdansk University of Technology, Gdansk, Poland)

Igor Selezov (Institute of Hydromechanics, Ukrainian National Academy of Sciences, Kiev, Ukraine)

Stanisław Sieniutycz (Warsaw University of Technology, Warsaw, Poland)

Gwidon Szefer (Cracow University of Technology, Cracow, Poland)

Alfons A. F. van de Ven (Eindhoven University of Technology, Eindhoven, The Netherlands)

Organizing Committee

Chairs:

Bogdan T. Maruszewski (Poznan University of Technology, Institute of Applied Mechanics, Poznan, Poland)

Wolfgang Muschik (Technische Universität Berlin, Institut für Theoretische Physik, Berlin, Germany)

Joseph N. Grima (University of Malta, Msida, Malta)

Secretary:

Roman Starosta (Institute of Applied Mechanics, Poznan University of Technology, Poznan, Poland)

Members:

Jacek Buskiewicz (Institute of Applied Mechanics, Poznan University of Technology, Poznan, Poland)

Andrzej Drzewiecki (Institute of Applied Mechanics, Poznan University of Technology, Poznan, Poland)

Pawel Fritzkowski (Institute of Applied Mechanics, Poznan University of Technology, Poznan, Poland)

Henryk Kaminski (Institute of Applied Mechanics, Poznan University of Technology, Poznan, Poland)

Jerzy Lewinski (Institute of Applied Mechanics, Poznan University of Technology, Poznan, Poland)

Andrzej Radowicz (Kielce University of Technology, Kielce, Poland)

Grazyna Sypniewska-Kaminska (Institute of Applied Mechanics, Poznan University of Technology, Poznan, Poland)

Tomasz Walczak (Institute of Applied Mechanics, Poznan University of Technology, Poznan, Poland)

THE INVERSE DETERMINATION OF THE VOLUME FRACTION OF FIBERS IN A UNIDIRECTIONALLY REINFORCED COMPOSITE FOR A GIVEN EFFECTIVE THERMAL CONDUCTIVITY

MAGDALENA MIERZWICZAK AND JAN ADAM KOŁODZIEJ

We consider the problem of determining the volume fraction of fibers in a unidirectionally reinforced composite in order to provide the appropriate effective thermal conductivity. The problem is formulated in such a way as to be treated as an inverse heat transfer problem. The thermal conductivities of the constituents (fibers and matrix) and fiber arrangement are known. The calculations are carried out for a perfect thermal contact between the fibers and matrix.

1. Introduction

In the literature the following problems are considered to be classical inverse heat conduction problems:

- determination of heat sources [Yan et al. 2008],
- determination of the heat transfer coefficient [Hon and Wei 2004],
- the Cauchy problem [Marin 2005], and
- determination of the temperature dependent thermal conductivity [Chantasiriwan 2002].

These problems usually apply to homogeneous media. In the case of composite materials (nonhomogeneous media) other practically important issues might have to be considered. One of them is the inverse problem of determination of the volume fraction of constituents in order to obtain the appropriate effective thermal conductivity. Let's consider a unidirectional fibrous composite with regular arrangement of fibers (Figure 1, left). If the thermal conductivity coefficients of constituents and their volume fractions are known then the composite can be treated as a homogeneous region for which effective thermal conductivity can be determined as a function of known parameters. Currently there are many papers in which the effective thermal conductivity coefficient is determined for a regular arrangement of fibers for given thermal conductivity of constituents and volume fraction of fibers (the direct problem). The method of determination is usually based on the solution of the heat transfer equation at a microstructure level in repeated elements of an array [Han and Cosner 1981]. But to our knowledge no paper has considered the inverse problem of determination of the volume fraction of fibers for a given effective thermal conductivity. Here we propose an analytic-numerical algorithm for determination of the volume fraction of fibers in order to obtain a given value of the transverse effective thermal conductivity λ_z (the inverse problem).

Keywords: effective thermal conductivity, inverse heat transfer problem, boundary collocation method, Newton's method.

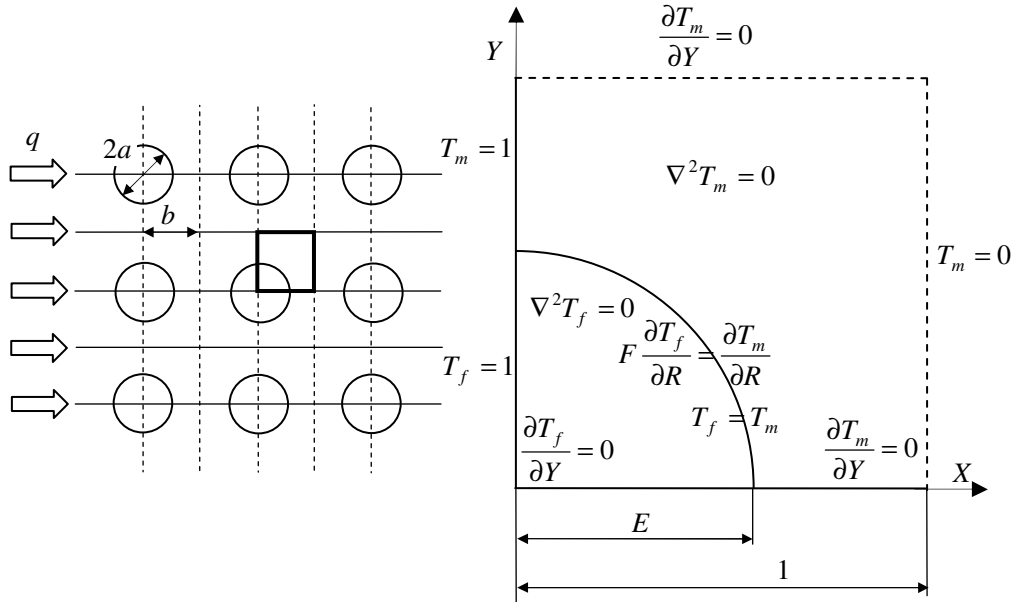


Figure 1. A unidirectional reinforced fibrous composite with fibers arranged in a square array. Left: general view, with marked repeated element. Right: formulation of the boundary value problem in the repeated element for nondimensional variables.

2. Direct problem: determination of the effective thermal conductivity coefficient of the composite material

Consider a unidirectional composite with fibers arranged in a matrix in a regular, square array with imperfect thermal contact between the fiber and matrix (Figure 1, left), where a is radius of the fibers, $2b$ is the distance between neighboring fibers, $E = a/b$, and $\varphi = \pi E^2/4$ is the volume fraction of the fibers. The ratio of the thermal conductivity of fibers λ_f to matrix λ_m is denoted as $F = \lambda_f/\lambda_m$, $R = r/b$ is the dimensionless radius, $X = x/b$ and $Y = y/b$ are the dimensionless Cartesian coordinates, $T = (\hat{T} - \hat{T}_R)/(\hat{T}_R - \hat{T}_L)$ is the dimensionless temperature field, and \hat{T}_R and \hat{T}_L are the temperatures on the left and right boundaries of the repeated element, respectively. In order to solve the boundary value problem in the repeated element of the composite (Figure 1) the boundary collocation method is used [Kołodziej and Zieliński 2009]. The general solution of the Laplace equation in a polar coordinate system has the form

$$T = A_0 + A_1\theta + A_2\theta \ln R + A_3 \ln R + \sum_{k=1}^{\infty} (B_k R^k + C_k R^{-k}) \cos(k\theta) + (D_k R^k + E_k R^{-k}) \sin(k\theta), \quad (2-1)$$

where A_0, A_1, \dots, E_k are integral constants.

Given the repetitive element of the square array $\Omega = \Omega_m + \Omega_f$ in the region of the fiber Ω_f and the matrix Ω_m , a solution is predicted with the form of (2-1). Some of the constants must be determined

strictly by the conditions at the bottom and on the left side of the repeated element:

$$\frac{\partial T_f}{\partial \theta} = \frac{\partial T_m}{\partial \theta} = 0 \quad \text{for } \theta = 0, \quad T_f = T_m = 1 \quad \text{for } \theta = \frac{\pi}{2}, \quad (2-2)$$

and the contact conditions of the fiber-matrix:

$$F \frac{\partial T_f}{\partial R} = \frac{\partial T_m}{\partial R} \quad \text{for } R = E, \quad T_f = T_m \quad \text{for } R = E. \quad (2-3)$$

After determining the constants from the boundary conditions (2-2) and from the contact conditions (2-3) of fiber-matrix, marking the remaining constants as w_k , and cutting off an infinite number of test functions to N expressions, we obtain a solution for the temperature field of the fiber and matrix:

$$T_f = 1 + \sum_{k=1}^N w_k R^{(2k-1)} \cos((2k-1)\theta), \quad (2-4)$$

$$T_m = 1 + \sum_{k=1}^N \frac{w_k}{2} \left[(1+F)R^{(2k-1)} + (1-F) \frac{E^{2(2k-1)}}{R^{(2k-1)}} \right] \cos((2k-1)\theta). \quad (2-5)$$

The constants w_k are determined by fulfillment of the condition on the collocation points on the upper Γ_2 and on the right Γ_1 edges of the concerned region (Figure 2):

$$T_m = 0 \quad \text{for } X = 1, \quad (2-6)$$

$$\frac{\partial T_m}{\partial Y} = 0 \quad \text{for } Y = 1. \quad (2-7)$$

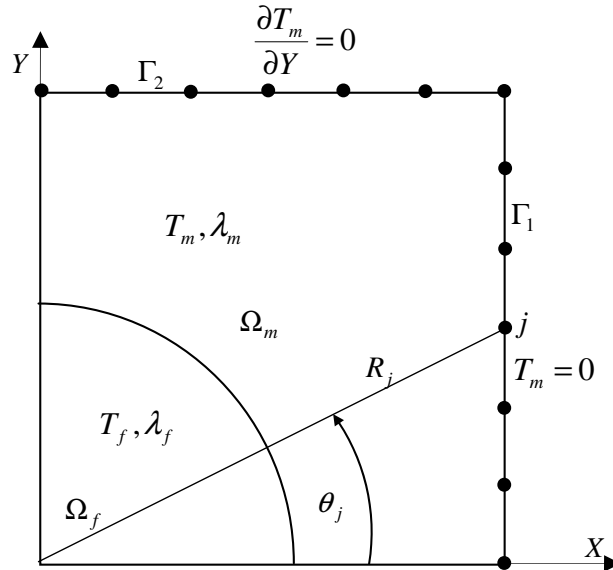


Figure 2. The collocation points at the upper and right boundaries of the matrix in a repeated element in which the boundary conditions are collocated.

The condition (2-7) can be written for polar coordinates:

$$\frac{\partial T_m}{\partial Y} = \frac{\partial T_m}{\partial R} \sin(\theta) + \frac{1}{R} \frac{\partial T_m}{\partial \theta} \cos(\theta). \quad (2-8)$$

Choosing N_1 points on the right boundary Γ_1 and N_2 points on the upper boundary Γ_2 and collocating the conditions (2-6) and (2-8) we obtain the system of $N_1 + N_2$ linear equations with N unknown coefficients $w_k, k = 1, \dots, N$:

$$\mathbf{A} \mathbf{w} = \mathbf{b}, \quad (2-9)$$

$$\begin{aligned} \sum_{k=1}^N w_k \left[(1+F) R_j^{(2k-1)} + (1-F) \frac{E^{2(2k-1)}}{R_j^{(2k-1)}} \right] \cos((2k-1)\theta_j) &= -2, \quad (R_j, \theta_j) \in \Gamma_1, \quad j = 1, \dots, N_1, \\ \sum_{k=1}^N w_k (2k-1) \left[(1+F) R_j^{(2k-1)} \sin((2k-1)\theta_j) + (1-F) \frac{E^{2(2k-1)}}{R_j^{2k}} \cos(2k\theta_j) \right] &= 0, \\ & (R_j, \theta_j) \in \Gamma_2, \quad j = N_1 + 1, \dots, N_1 + N_2. \end{aligned}$$

The constants w_k obtained by the Gaussian elimination method provide estimates of the value of the global heat flux through the unit region of the considered element:

$$q = \frac{1}{b} \left[-\lambda_f \int_0^a \frac{\partial \hat{T}_f}{\partial x} \Big|_{x=0} dy + \lambda_m \int_a^b \frac{\partial \hat{T}_m}{\partial x} \Big|_{x=0} dy \right]. \quad (2-10)$$

The transverse effective thermal conductivity is defined by the formula

$$\lambda_z = \frac{qb}{\Delta \hat{T}}, \quad (2-11)$$

where b is the distance between the isothermal boundaries and $\Delta \hat{T} = \hat{T}_L - \hat{T}_R$ is the difference of the temperatures at the isothermal edges. After taking into consideration in formula (2-11) the definition of the nondimensional temperature and coordinates, the value of the effective thermal conductivity in relation to the thermal conductivity of the matrix can be calculated from the relationship:

$$\frac{\lambda_z}{\lambda_m} = -F \int_0^E \frac{1}{R} \frac{\partial T_f}{\partial \theta} \Big|_{\theta=\frac{\pi}{2}} dR + \int_E^1 \frac{1}{R} \frac{\partial T_m}{\partial \theta} \Big|_{\theta=\frac{\pi}{2}} dR, \quad (2-12)$$

or

$$\frac{\lambda_z}{\lambda_m} = \sum_{k=1}^N \frac{w_k}{2} (-1)^k [(F+1) + (F-1)E^{2(2k-1)}]. \quad (2-13)$$

3. The results of the numerical experiment

The results of the calculations of the effective thermal conductivity of the fibrous composite are shown in Figure 3. The value of the effective thermal conductivity in relation to the thermal conductivity of the matrix $\lambda_z/\lambda_m = (\lambda_z/\lambda_m)(\varphi)|_F$ is presented as a function of the volume fraction of fibers φ for the desired value of thermal conductivity ratio F of the fiber λ_f to the matrix λ_m , with $F \in \{0.5, 2, 10, 20\}$. In order to compare the results, for a flat layer composite consisting of two components with different

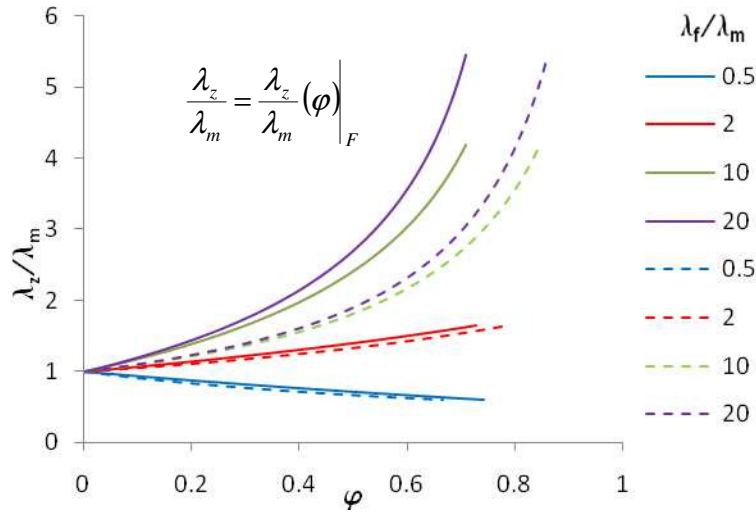


Figure 3. The effective thermal conductivity as a function of the volume fraction of the fibers in the matrix for different values of the ratio of thermal conductivity of the fibers to the matrix.

coefficients of thermal conductivity we calculate the effective thermal conductivity coefficient in relation to the thermal conductivity of the matrix for an ideal contact of the components from the formula

$$\frac{\lambda_z}{\lambda_m} = \left((1 - \varphi) + \frac{\varphi}{F} \right)^{-1}.$$

The comparative results for a flat layer of composite are shown in Figure 3 by the dotted line. The value of the effective thermal conductivity λ_z depends not only on the constants characterizing the composite, F and E , but also on the coefficients w_k involved in fulfilling the boundary conditions at the $N_1 + N_2$ collocation points. Table 1 shows the influence of the number of collocation points on the maximum error fulfilling the collocation boundary conditions calculated at the control points (between the collocation points). The analysis of the results shows that increase in the number of collocation points doesn't lead to an increase in the accuracy of the calculations. Increasing the number of collocation points entails a rise in the dimension of the matrix system of equations. In all four examples presented in Table 1, the smallest maximum error satisfying the boundary conditions was obtained for 7 collocation points on the right edge and for 6 points on the upper edge of the region considered.

4. Inverse problem: determination of the volume fraction of fibers in a composite for a given effective thermal conductivity

At times, when designing composites with specific properties of the fibers and matrix we must estimate the fraction of the volume of fibers to obtain effective thermal conductivity values. Assuming that $E = a/b$ is unknown, we use the known value of the effective thermal conductivity in relation to the thermal conductivity of the matrix λ_z/λ_m . From the collocation of the boundary conditions in the $N_1 + N_2$ points on the right and upper edges of the considered region and from condition (2-11) we obtain a system of $N_1 + N_2 + 1$ nonlinear equations with the $N + 1$ unknowns w_k and E :

$E = 0.5, F = 10$					$E = 0.9, F = 10$		
N_1	N_2	λ_z/λ_m	$\delta_{\max} _{T_m=0}$	$\delta_{\max} _{\partial T_m/\partial Y=0}$	λ_z/λ_m	$\delta_{\max} _{T_m=0}$	$\delta_{\max} _{\partial T_m/\partial Y=0}$
5	4	1.3829	1.13×10^{-4}	1.33×10^{-3}	3.3401	0.004232	0.004027
6	5	1.3829	2.42×10^{-5}	3.83×10^{-4}	3.3408	2.61×10^{-3}	1.12×10^{-2}
7	6	1.3829	6.20×10^{-7}	8.38×10^{-5}	3.3405	5.48×10^{-4}	1.63×10^{-2}
8	7	1.3829	9.35×10^{-6}	3.85×10^{-4}	3.3413	1.55×10^{-3}	8.48×10^{-2}
9	8	1.3829	1.97×10^{-5}	8.77×10^{-4}	3.3396	4.25×10^{-3}	2.02×10^{-1}
10	9	1.3829	4.96×10^{-5}	2.47×10^{-3}	3.3431	1.14×10^{-2}	0.578786
11	10	1.3829	7.29×10^{-5}	3.98×10^{-3}	3.3372	1.72×10^{-2}	0.943426
12	11	1.3829	2.26×10^{-4}	0.013628	3.3502	0.053729	3.235684
13	12	1.3829	1.87×10^{-4}	0.012135	3.3328	4.46×10^{-2}	2.895936
14	13	1.3831	1.98×10^{-3}	0.139725	3.4128	0.463741	32.72905
15	14	1.3829	4.42×10^{-4}	0.033299	3.3242	1.06×10^{-1}	7.967415
$E = 0.5, F = 0.5$					$E = 0.9, F = 0.5$		
N_1	N_2	λ_z/λ_m	$\delta_{\max} _{T_m=0}$	$\delta_{\max} _{\partial T_m/\partial Y=0}$	λ_z/λ_m	$\delta_{\max} _{T_m=0}$	$\delta_{\max} _{\partial T_m/\partial Y=0}$
5	4	0.87713	3.73×10^{-5}	0.000484	0.64835	4.10×10^{-4}	0.010038
6	5	0.87714	8.21×10^{-6}	1.46×10^{-4}	0.64849	2.28×10^{-4}	6.92×10^{-3}
7	6	0.87714	1.14×10^{-7}	2.17×10^{-5}	0.64844	6.26×10^{-5}	2.18×10^{-3}
8	7	0.87714	2.96×10^{-6}	1.21×10^{-4}	0.64845	4.66×10^{-6}	2.22×10^{-4}
9	8	0.87714	6.31×10^{-6}	2.81×10^{-4}	0.64846	9.55×10^{-5}	4.29×10^{-3}
10	9	0.87713	1.59×10^{-5}	0.000792	0.64842	2.96×10^{-4}	0.014795
11	10	0.87714	2.34×10^{-5}	0.001275	0.64849	4.58×10^{-4}	0.025030
12	11	0.87713	7.26×10^{-5}	0.00437	0.64834	1.44×10^{-3}	0.086817
13	12	0.87714	6.00×10^{-5}	0.003891	0.64855	1.20×10^{-3}	0.077723
14	13	0.87708	6.35×10^{-4}	0.044798	0.64758	0.012614	0.890239
15	14	0.87715	1.42×10^{-4}	0.010678	0.64865	2.84×10^{-3}	0.213776

Table 1. The impact of the number of collocation points on the value of the effective thermal conductivity of the composite and the maximum error of fulfilling the boundary conditions at control points.

$$f_j = 1 + \sum_{k=1}^N \frac{w_k}{2} \left[(1+F)R_j^{(2k-1)} + (1-F)\frac{E^{2(2k-1)}}{R_j^{(2k-1)}} + \right] \cos((2k-1)\theta_j) = 0, \quad (R_j, \theta_j) \in \Gamma_1 \quad j = 1, \dots, N_1,$$

$$f_j = \sum_{k=1}^N w_k(2k-1) \left[(1+F)R_j^{(2k-1)} \sin((2k-1)\theta_j) + (1-F)\frac{E^{2(2k-1)}}{R_j^{(2k-1)}} \cos(2k\theta_j) \right] = 0, \quad (R_j, \theta_j) \in \Gamma_2 \quad j = N_1 + 1, \dots, N_1 + N_2,$$

$$f_{N_1+N_2+1} = \sum_{k=1}^N \frac{w_k}{2} (-1)^k \left[(1+F) + (F-1)E^{2(2k-1)} \right] - \frac{\lambda_z}{\lambda_m} = 0. \quad (4-1)$$

The nonlinear system of $N_1 + N_2 + 1$ equations f with $N + 1$ unknowns $W = [w_1, \dots, w_N, E]^T$ is solved by using Newton's iterative method:

$$\begin{bmatrix} w_1 \\ \vdots \\ w_N \\ E \end{bmatrix}^{(i+1)} = \begin{bmatrix} w_1 \\ \vdots \\ w_N \\ E \end{bmatrix}^{(i)} - \begin{bmatrix} f_1^{(i)} \\ \vdots \\ f_{N_1+N_2}^{(i)} \\ f_{N_1+N_2+1}^{(i)} \end{bmatrix} \begin{bmatrix} J_{1,1}^{(i)} & \cdots & J_{1,N+1}^{(i)} \\ \vdots & \ddots & \vdots \\ J_{N_1+N_2,1}^{(i)} & \cdots & \vdots \\ J_{N_1+N_2+1,1}^{(i)} & \cdots & J_{N_1+N_2+1,N+1}^{(i)} \end{bmatrix}^{-1}, \quad (4-2)$$

$$\begin{aligned} W^{(i+1)} &= W^{(i)} - f(W^{(i)})J(W^{(i)})^{-1} \rightarrow W^{(i+1)} = W^{(i)} - Y(W^{(i)}), \\ Y(W^{(i)}) &= f(W^{(i)})J(W^{(i)})^{-1} \rightarrow J(W^{(i)})^{-1}Y(W^{(i)}) = f(W^{(i)}). \end{aligned}$$

The functions f_i are described by (4-1), while the Jacobi elements have the following form:

$$\begin{aligned} J_{j,k} &= \frac{\partial f_j}{\partial w_k} = \frac{1}{2} \left[(1+F)R_j^{(2k-1)} + (1-F)\frac{E^{2(2k-1)}}{R_j^{(2k-1)}} + \right] \cos((2k-1)\theta_j), \\ & \qquad \qquad \qquad j = 1, \dots, N_1, \quad k = 1, \dots, N, \\ J_{j,N+1} &= \frac{\partial f_j}{\partial E} = \sum_{k=1}^N w_k (2k-1)(1-F)\frac{E^{(4k-3)}}{R_j^{(2k-1)}} \cos((2k-1)\theta_j), \quad j = 1, \dots, N_1, \\ J_{j,k} &= \frac{\partial f_j}{\partial w_k} = \frac{(2k-1)}{2} \left[(1+F)R_j^{2(k-1)} \sin(2(k-1)\theta_j) + (1-F)\frac{E^{2(2k-1)}}{R_j^{(2k)}} \sin(2k\theta_j) \right], \\ & \qquad \qquad \qquad j = N_1 + 1, \dots, N_1 + N_2, \quad k = 1, \dots, N, \quad (4-3) \\ J_{j,N+1} &= \frac{\partial f_j}{\partial E} = \sum_{k=1}^N w_k (2k-1)^2 \left[(1-F)\frac{E^{(4k-3)}}{R_j^{(2k)}} \sin(2k\theta_j) \right], \quad j = N_1 + 1, \dots, N_1 + N_2, \\ J_{j,k} &= \frac{\partial f_j}{\partial w_k} = \frac{(-1)^k}{2} [(1+F) + (F-1)E^{2(2k-1)}], \quad j = N_1 + N_2 + 1, \quad k = 1, \dots, N, \\ J_{j,N+1} &= \frac{\partial f_j}{\partial E} = \sum_{k=1}^N w_k (2k-1)(-1)^k (F-1)E^{(4k-3)}, \quad j = N_1 + N_2 + 1. \end{aligned}$$

To start the Newton's iteration we need to know $W^{(0)} = [w_1^{(0)}, \dots, w_N^{(0)}, E^{(0)}]^T$ as an initial condition. As an initial value of the constants $w_k^{(0)}$, $k = 1, \dots, n$, the solution of the linear problem for $E = 0.1$ has been adopted. The condition for the end of the iteration was adopted at $\delta_{\text{Newton}} = \|W^{(i+1)} - W^{(i)}\|_{\text{max}} \leq 10^{-7}$, where $\| \cdot \|_{\text{max}}$ means the maximum norm.

5. The results of the numerical experiment

The results of the iterative calculation of the volume fraction of fibers for a composite are shown in Figure 4. The value of the volume fraction of fibers in a composite ϕ is presented as a function $\varphi = \varphi(\lambda_z/\lambda_m)|_F$ of the effective thermal conductivity in relation to the thermal conductivity of the matrix

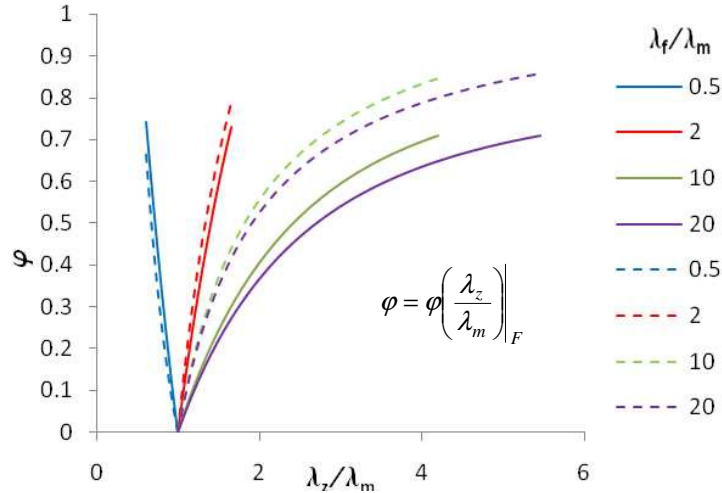


Figure 4. The volume fraction of fibers in the matrix as a function of the effective thermal conductivity of the composite for different relative values of thermal conductivity of the fiber and matrix.

λ_z/λ_m for the assumed value of the thermal conductivity ratio of the fiber to the matrix, $F = \lambda_f/\lambda_m \in \{0.5, 2, 10, 20\}$. In order to compare the results for a flat composite layer consisting of two components with different thermal conductivities, the volume fraction of the fibers for a known value of the effective thermal conductivity for an ideal contact with the components can be calculated from

$$\varphi = \left(\left(\frac{\lambda_z}{\lambda_m} \right)^{-1} - 1 \right) \frac{F}{1 - F}.$$

		$\lambda_z/\lambda_m = 1.4, F = 10$				$\lambda_z/\lambda_m = 3.35, F = 10$			
N_1	N_2	φ	E	$\delta_{\max} _{T_m=0}$	$\delta_{\max} _{\partial T_m/\partial Y=0}$	φ	E	$\delta_{\max} _{T_m=0}$	$\delta_{\max} _{\partial T_m/\partial Y=0}$
5	4	0.1904	0.4924	$5.82 \cdot 10^{-5}$	0.100879	0.5013	0.7989	$1.74 \cdot 10^{-3}$	2.688120
6	5	0.2036	0.5092	$4.99 \cdot 10^{-5}$	0.000256	0.6362	0.9	$2.05 \cdot 10^{-2}$	0.059686
7	6	0.2036	0.5092	$6.72 \cdot 10^{-7}$	$8.91 \cdot 10^{-5}$	0.6372	0.9007	$5.68 \cdot 10^{-4}$	0.016511
8	7	—	—	—	—	—	—	—	—
		$\lambda_z/\lambda_m = 0.88, F = 0.5$				$\lambda_z/\lambda_m = 0.65, F = 0.5$			
N_1	N_2	φ	E	$\delta_{\max} _{T_m=0}$	$\delta_{\max} _{\partial T_m/\partial Y=0}$	φ	E	$\delta_{\max} _{T_m=0}$	$\delta_{\max} _{\partial T_m/\partial Y=0}$
5	4	0.1790	0.4774	$1.49 \cdot 10^{-5}$	0.026341	0.7876	1.0014	0.00025	0.32083
6	5	0.1915	0.4937	$1.18 \cdot 10^{-5}$	$7.26 \cdot 10^{-5}$	0.6327	0.8976	0.00025	0.0005
7	6	0.1915	0.4938	$1.13 \cdot 10^{-7}$	$2.13 \cdot 10^{-5}$	0.6328	0.8976	$5.84 \cdot 10^{-5}$	0.00204
8	7	—	—	—	—	—	—	—	—

Table 2. The impact of the number of collocation points on the value of the volumetric fraction of the fibers in the composite and the maximal error fulfillment of the boundary conditions at checkpoints.

$F = 10$				
λ_z/λ_m	$\lambda_z/\lambda_m = 1.4$		$\lambda_z/\lambda_m = 3.35$	
Iter.	δ_{Newton}	E	δ_{Newton}	E
1	0.456063	0.5439	0.265565	0.7344
2	0.032858	0.5111	0.179407	0.9138
3	1.89×10^{-3}	0.5092	0.013073	0.9008
4	3.41×10^{-6}	0.5092	4.17×10^{-5}	0.9007
5	1.13×10^{-11}	0.5092	2.71×10^{-9}	0.9007
$F = 0.5$				
λ_z/λ_m	$\lambda_z/\lambda_m = 0.88$		$\lambda_z/\lambda_m = 0.65$	
Iter.	δ_{Newton}	E	δ_{Newton}	E
1	0.357932	0.6421	0.217974	0.9164
2	1.31×10^{-1}	0.5113	0.018393	0.8980
3	1.72×10^{-2}	0.4941	0.000336	0.8976
4	2.99×10^{-4}	0.4938	3.61×10^{-8}	0.8976
5	9.05×10^{-8}	0.4938	—	—

Table 3. Convergence of Newton's method for the test examples, with $N_1 = 7$ and $N_2 = 8$.

The results for a flat composite layer are presented by the dotted lines in Figure 4. As with the problem of identification of λ_z/λ_m , so also for the iterative identification of the volume fraction of fibers φ in a composite; the number of collocation points $N_1 + N_2$ where the boundary condition is approximately fulfilled affects the accuracy of the calculations. Table 2 shows the impact of the number of collocation points on the value of the volumetric fraction of fibers φ in the composite and the maximum error of fulfillment of boundary conditions at the checkpoints (between collocation points). As in the case of the direct problem, we obtain the best results for 7 collocation points at the right edge Γ_1 of a large finite element and 6 points at the upper edge Γ_2 . In the case of the inverse problem for a large number of collocation points (greater than 7) the convergence of the algorithm is lost. Table 3 presents the convergence of the used Newton's iterative method for four test examples. The method proves to be convergent very quickly, and just after five iterations we get the correct result of the iteration with an error of less than 10^{-7} .

6. Conclusions

The presented method of determining the volume fraction of fibers of a composite or the effective thermal conductivity except in the cases of maximal fiber density is easy to implement and efficient. It can be easily applied to other configurations of regular arrangement of fibers in the matrix, for example to a triangular or hexagonal mesh. This study compared the influence of the ratio of the thermal conductivity of fibers to the thermal conductivity of matrix F on the value of the volumetric fraction of the fibers and the value of the effective thermal conductivity of the composite. It was also shown that increasing the number of collocation points doesn't reduce the error of the approximation of the boundary conditions; it leads to the ill-conditioning of the system of equations.

References

- [Chantasiriwan 2002] S. Chantasiriwan, “Steady-state determination of temperature-dependent thermal conductivity”, *Int. Commun. Heat Mass* **29**:6 (2002), 811–819.
- [Han and Cosner 1981] L. S. Han and A. A. Cosner, “Effective thermal conductivities of fibrous composites”, *J. Heat Transf. (ASME)* **103**:2 (1981), 387–392.
- [Hon and Wei 2004] Y. C. Hon and T. Wei, “A fundamental solution method for inverse heat conduction problem”, *Eng. Anal. Bound. Elem.* **28**:5 (2004), 489–495.
- [Kołodziej and Zieliński 2009] J. A. Kołodziej and A. P. Zieliński, *Boundary collocation techniques and their application in engineering*, WIT Press, Southampton, 2009.
- [Marin 2005] L. Marin, “Numerical solution of the Cauchy problem for steady-state heat transfer in two-dimensional functionally graded materials”, *Int. J. Solids Struct.* **42**:15 (2005), 4338–4351.
- [Yan et al. 2008] L. Yan, C.-L. Fu, and F.-L. Yang, “The method of fundamental solutions for the inverse heat source problem”, *Eng. Anal. Bound. Elem.* **32**:3 (2008), 216–222.

Received 29 Sep 2010. Revised 5 Jun 2011. Accepted 15 Dec 2011.

MAGDALENA MIERZWICZAK: magdalena.mierzwiczak@wp.pl

Institute of Applied Mechanics, Poznan University of Technology, ul. Jana Pawla II 24, 60-965 Poznan, Poland

JAN ADAM KOŁODZIEJ: jan.kolodziej@put.poznan.pl

Institute of Applied Mechanics, Poznan University of Technology, ul. Jana Pawla II 24, 60-965 Poznan, Poland

ANALYTICAL-NUMERICAL SOLUTION OF THE INVERSE PROBLEM FOR THE HEAT CONDUCTION EQUATION

MICHAŁ CIAŁKOWSKI, ANDRZEJ MAĆKIEWICZ,
JAN ADAM KOŁODZIEJ, UWE GAMPE AND ANDRZEJ FRĄCKOWIAK

The solution of the inverse problem for the transient heat transfer equation is considered. The partial differential equation was discretized with respect to the space variable, and a system of ordinary differential equations of first order was obtained. The solution of the system of equations has a wave form. The numerical results obtained from the solution of the inverse problem confirm the effectiveness of the proposed method.

1. Introduction

Numerical solutions to linear partial differential equations can be obtained by different methods depending on the number of variables and the shape of the domain. When the unknown variable is a function of time, one can use the finite difference method, finite element method, boundary element method or other methods in order to conduct discretization with respect to the space variables. Consider a differential equation of heat transfer with initial and boundary conditions as follows:

$$\rho c \frac{\partial T}{\partial t} = \lambda \nabla T \quad x, y, z \in \Omega \subset R^3 \quad t \in (0, \infty), \quad (1-1)$$

with an initial and boundary condition

$$T(x, y, z, 0) = g(x, y, z) \quad T(x, y, z, t) |_{x,y,z \in \Gamma} = T_{\Gamma}(t), \quad t > 0, \quad (1-2)$$

The solution of the matrix equation using the initial condition has the form

$$\left\{ \frac{dT(t)}{dt} \right\} = [A]\{T(t)\} + [B]\{T_{\Gamma}(t)\} \quad (1-3)$$

(see [Athans and Falb 1969]), which integrates to

$$\{T(t)\} = e^{[A]t}\{g\} + \int_0^t e^{[A](t-p)}[B]\{T_{\Gamma}(p)\}dp, \quad t \geq 0. \quad (1-4)$$

The purpose of this paper is to investigate solutions to the inverse problem in the form proposed above by using the different approximation of space-dependent temperature.

The inverse problem considered in this paper is a boundary type problem, which means seeking an unknown boundary condition based on temperature measured in some chosen points inside the domain. In engineering practice, the number of measured points is limited, and in the case of turbines it is typically

The work was partially supported by Grant 3134/B/T02/2007/33 and 4917/B/T02/2010/39.

Keywords: inverse problems, stability, matrix exponential, sensitivity analysis, transient heat transfer equation.

only one or two points, as a result of the occurrence of stress concentration surrounding the thermoelement. That is why we decided to investigate the one-dimensional problem.

During the last decades, some numerical techniques have been proposed to solve a 1-D IHCP. In [Al-Khalidy 1998] the control volume algorithm has been combined with a digital filter method to estimate temperature and heat flux values on the surface of a body based on the temperature measurement inside the body. The accuracy of the method was verified by comparison with a direct analytical solution of the problem. Lesnic and Elliott [1999] have used the Adomian's decomposition approach for solving the inverse heat conduction problem in which temperature and heat flux histories on the left boundary were estimated based on temperature and heat flux on the right boundary. The mollification method was applied to deal with noisy input data and to obtain a stable approximate solution. In [Shen 1999] two kinds of boundary element method were employed to solve IHCP, namely a collocation method and a weighted method. The author has used the Tikhonov's regularization method and the truncated singular value decomposition method for stabilization results. The conjugate gradient method supported by Fourier analysis has been applied in [Prud'homme and Hguyen 1999] to solve the IHCP among others for the 1-D case. It was found that an unknown time-dependent heat flux may be recovered satisfactorily using a single sensor inside the region. A Kalman filter combined with a variable forgetting factor as a weighting function in a recursive least-squares algorithm was applied in [Lee et al. 2000] to estimate impulsive heat flux. In this method, a spatial derivative in the 1-D heat equation was approximated by finite differences. In [Jonas and Louis 2000] some versions of mollification method have been used to solve the 1-D IHCP. Usually the mollification is done in the data space, but in this paper the mollification is performed in the solution space. In [Taler and Duba 2001] the 1-D non-linear IHCP was solved by means of the method of lines. This method is based on replacing the partial differential equation of heat conduction by the system of ordinary differential equations through discretization of the space derivative or the time derivative. Instead of other optimization techniques, the maximum entropy method was used in [Kim and Lee 2002] in the solution of the IHCP. The presented results showed considerable enhancement in the resolution of the inverse problem and bias reduction in comparison with the conventional methods. One of the most popular methods for solving IHCP is a sequential function specification method proposed at first by Beck [1970]. In [Lin et al. 2004] a modification of Beck's method was presented to estimate the heat source in the 1-D case. One base of this proposition is an application of a finite difference method for approximation the spatial and time derivatives. Almost all of the methods mentioned above are mesh methods which need some kind of mesh. In [Hon and Wei 2004] the meshless method, namely the method of fundamental solution, has been used for solution the 1-D IHCP. For regularization of the results, the authors used Tikhonov's regularization technique equipped with the L-curve method. The IHCP in which surface heat flux is estimated based on moving measurements inside the body was presented in [Shidfar and Karamali 2005]. The authors use an integral equation method and a linear least-squares method. The sequential function specification method supported by singular value decomposition was discussed in [Cabeza et al. 2005]. In [Shidfar and Pourgholi 2006; Pourgholi et al. 2009], the ill-posed IHCP is transformed to Cauchy's problem by means of a linear transformation. Next, Cauchy's problem is solved successfully by applying Legendre polynomials. The numerical approach combining the use of the finite difference method with the solution of ordinary differential equations has been proposed in [Ebrahimian et al. 2007] for solving the 1-D IHCP. The least-squares method has been used to determine the unknown boundary condition [Cabeza et al. 2005]. Four different versions of the variable metric

method for solving the 1-D IHCP [Luksan and Spedicato 2000] with a symmetric rank-one update are compared in [Pourshaghaghly et al. 2007]. The results indicate that the accuracy of these versions do not differ significantly from each other. In [Deng and Hwang 2007] the 1-D IHCP is solved by means of a Kalman filter-enhanced Bayesian back propagation neural network. The results show that the proposed method can predict the unknown parameters in inverse problems with acceptable error.

In [Grysa 2010] an application of the Trefftz function for solving the inverse heat conduction problem is considered for 1-D problems, among others.

The use of hyperbolic spline functions to approximate the solution with respect to the space variable is novel in our paper. Thanks to it, the second derivative of the approximate solution is continuous.

2. Formulation of the problem

The linear equation of heat conduction has the form

$$\frac{\rho c}{\lambda} \frac{\partial T}{\partial t} = \frac{\partial^2 T}{\partial r^2} + \frac{1 - 2\gamma}{r} \frac{\partial T}{\partial r}, \quad R_i < r < R_a, \tag{2-1}$$

where

$$\gamma = \begin{cases} -\frac{1}{2} & \text{for a spherical layer,} \\ 0 & \text{for a cylindrical layer,} \\ \frac{1}{2} & \text{for a plane layer,} \end{cases}$$

is a parameter describing the shape of the domain (see Figure 1). The following conditions are imposed:

- The initial condition,

$$T(r, 0) = T_0(r), \quad R_i \leq r \leq R_a. \tag{2-2}$$

- The boundary condition at the surface $r = R_a$,

$$-\lambda \frac{\partial T}{\partial r} \Big|_{r=R_a} = \alpha(T - T_{\text{fluid}}). \tag{2-3}$$

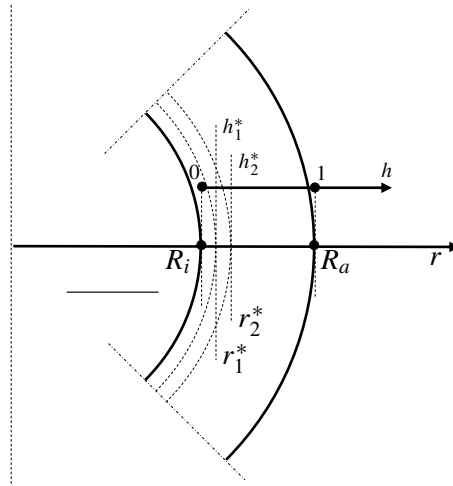


Figure 1. Notation.

- Additional conditions resulting from the measurement of temperature at the inner points of the region r_k^* , $k = 1, 2, \dots, M$:

$$T(r_k^*, t) = f_k(t). \quad (2-4)$$

We will apply the substitutions

$$r = R_i + \eta(R_a - R_i), \quad 0 \leq \eta \leq 1, \quad (2-5)$$

$$\vartheta = \frac{T}{T_m}, \quad T_m = \max(T_0(r), T_{\text{fluid}}), \quad \tau = \frac{\lambda}{\rho c} \frac{t}{(R_a - R_i)^2}, \quad a = \frac{R_i}{R_a - R_i}$$

to obtain the nondimensional counterparts of (2-1)–(2-4):

- The equation of heat transfer,

$$\frac{\partial \vartheta}{\partial \tau} = \frac{\partial^2 \vartheta}{\partial \eta^2} + \frac{1 - 2\gamma}{\eta + a} \frac{\partial \vartheta}{\partial \eta}, \quad \eta \in (0, 1), \quad \tau > 0. \quad (2-6)$$

- The initial condition,

$$\vartheta(\eta, 0) = \frac{T_0(r, \eta)}{T_m} = g(\eta), \quad \eta \in [0, 1]. \quad (2-7)$$

- The boundary condition at surface $r = R_a$,

$$\frac{\partial \vartheta}{\partial \eta} \Big|_{\eta=1} = \frac{\alpha(R_a - R_i)}{\lambda} (\vartheta - \vartheta_{\text{fluid}}) = Bi_a (\vartheta - \vartheta_{\text{fluid}}), \quad \tau > 0. \quad (2-8)$$

- The additional conditions in inner points η_k^* , $k = 1, \dots, M$:

$$\vartheta(\eta_k^*, \tau) = f_k(\tau), \quad \tau > 0. \quad (2-9)$$

The solution of (2-6) can be expressed as

$$\vartheta(\eta, \tau) = \sum_{i=0}^N \vartheta_i(\tau) \varphi_i(\eta) \quad (2-10)$$

where the interpolation basis functions $\varphi_i(\eta)$ are specified on a grid of points (see Figure 2).

Taking into consideration the character of the temperature function in r direction (the character of a hyperbolic function), the spline hyperbolic function is chosen as a base function. The unknown functions $\vartheta_i(\tau)$, $i = 0, \dots, N$ are sought by solving (2-6) in the interior marked points of the segment $[0, 1]$; that

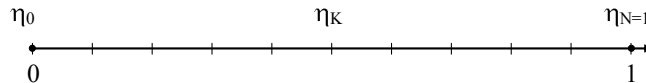


Figure 2. Grid of points for interpolation of spline function.

is, we substitute (2-10) into (2-6) to obtain $N - 1$ equations:

$$\sum_{i=0}^N \frac{\vartheta_i(\tau)}{d\tau} \varphi_i(\eta_k) = \sum_{i=0}^N \vartheta_i(\tau) \left(\frac{d^2 \varphi_i(\eta)}{d\eta^2} + \frac{1 - 2\gamma}{\eta_k + a} \frac{d\varphi_i(\eta)}{d\eta} \right) = \sum_{i=0}^N \vartheta_i(\tau) \psi_i(\eta_k), \quad k = 1, \dots, N-1. \quad (2-11)$$

The successive equations result from the conditions (2-8) and (2-9); that is, by substituting the solution (2-10) to the condition (2-8) we obtain

$$- \sum_{i=0}^N \vartheta_i(\tau) \varphi_i'(1) = Bi_a \left(\sum_{i=0}^N \vartheta_i(\tau) \varphi_i(1) - \vartheta_{\text{fluid}} \right) = Bi_a (\vartheta_N(\tau) - \vartheta_{\text{fluid}}),$$

which we rewrite in the form

$$- \sum_{i=0}^{N-1} \vartheta_i(\tau) \varphi_i'(1) - \vartheta_N(\tau) (\varphi_N'(1) + Bi_a) = -Bi_a \vartheta_{\text{fluid}}(\tau). \quad (2-12)$$

Introducing

$$b_i = \varphi_i'(1), \quad i = 0, 1, \dots, N - 1,$$

and

$$b_N = \varphi_N'(1) + Bi_a,$$

Equation (2-12) becomes

$$\sum_{i=0}^N \vartheta_i(\tau) b_i = Bi_a \vartheta_{\text{fluid}}(\tau). \quad (2-13)$$

The additional conditions for the temperature function result from condition (2-9) and have the form

$$\sum_{i=0}^N \vartheta_i(\tau) \varphi_i(\eta_k^*) = f_k(\tau), \quad i = 1, 2, \dots, M. \quad (2-14)$$

3. The solution of the direct problem

The idea for solving the inverse problem is based on the ability to express the solution of the direct problem in parametric form with the boundary conditions attached. Equation (2-11) leads to the following system of equations:

$$\begin{bmatrix} \varphi_0(\eta_1) & \cdots & \varphi_N(\eta_1) \\ \vdots & & \vdots \\ \varphi_0(\eta_k) & \cdots & \varphi_N(\eta_k) \\ \vdots & & \vdots \\ \varphi_0(\eta_{N-1}) & \cdots & \varphi_N(\eta_{N-1}) \end{bmatrix} \begin{bmatrix} \frac{d\vartheta_0}{d\tau} \\ \vdots \\ \frac{d\vartheta_{N-1}}{d\tau} \\ \frac{d\vartheta_N}{d\tau} \end{bmatrix} = \begin{bmatrix} \psi_0(\eta_1) & \cdots & \psi_N(\eta_1) \\ \vdots & & \vdots \\ \psi_0(\eta_k) & \cdots & \psi_N(\eta_k) \\ \vdots & & \vdots \\ \psi_0(\eta_{N-1}) & \cdots & \psi_N(\eta_{N-1}) \end{bmatrix} \begin{bmatrix} \vartheta_0 \\ \vdots \\ \vartheta_{N-1} \\ \vartheta_N \end{bmatrix} \quad (3-1)$$

The system (3-1) has dimension $(N - 1) * (N + 1)$. In the direct problem, a boundary condition in point $\eta = 1$ is attached, which leads to an equation involving an $(N - 1) \times (N - 1)$ matrix:

$$\begin{bmatrix} \varphi_1(\eta_1) & \cdots & \varphi_{N-1}(\eta_1) \\ \vdots & & \vdots \\ \varphi_1(\eta_k) & \cdots & \varphi_{N-1}(\eta_k) \\ \vdots & & \vdots \\ \varphi_1(\eta_{N-1}) & \cdots & \varphi_{N-1}(\eta_{N-1}) \end{bmatrix} \begin{bmatrix} \frac{d\vartheta_1}{d\tau} \\ \vdots \\ \frac{d\vartheta_{N-1}}{d\tau} \end{bmatrix} = \begin{bmatrix} \psi_1(\eta_1) & \cdots & \psi_{N-1}(\eta_1) \\ \vdots & & \vdots \\ \psi_1(\eta_k) & \cdots & \psi_{N-1}(\eta_k) \\ \vdots & & \vdots \\ \psi_1(\eta_{N-1}) & \cdots & \psi_{N-1}(\eta_{N-1}) \end{bmatrix} \begin{bmatrix} \vartheta_0 \\ \vdots \\ \vartheta_{N-1} \end{bmatrix} - \begin{bmatrix} \varphi_0(\eta_1) \\ \vdots \\ \varphi(\eta_{N-1}) \end{bmatrix} \cdot \frac{d\vartheta_0(\tau)}{d\tau} + \begin{bmatrix} \psi_0(\eta_1) \\ \vdots \\ \psi(\eta_{N-1}) \end{bmatrix} \cdot \psi_0(\tau) - \begin{bmatrix} \varphi_N(\eta_1) \\ \vdots \\ \varphi(\eta_{N-1}) \end{bmatrix} \cdot \frac{d\vartheta_N(\tau)}{d\tau} + \begin{bmatrix} \psi_N(\eta_1) \\ \vdots \\ \psi(\eta_{N-1}) \end{bmatrix} \cdot \psi_N(\tau). \quad (3-2)$$

The base functions φ_i , $i = 0, 1, \dots, N$, are interpolation functions with the property

$$\varphi_i(\eta_k) = \begin{cases} 0 & \text{if } i \neq k, \\ 1 & \text{if } i = k, \end{cases}$$

so the vectors $d\vartheta_0/d\tau$ and $d\vartheta_N/d\tau$ on the right-hand side of the (3-2) disappear, and the matrix of coefficients matching vector $\{d\vartheta/d\tau\}$ is diagonal. Equation (3-2) can be then written as

$$\left\{ \frac{d\vartheta(\tau)}{d\tau} \right\} = [\psi] \{ \vartheta(\tau) \} + \{ \psi_0 \} \cdot \vartheta_0(\tau) + \{ \psi_N \} \cdot \vartheta_N(\tau). \quad (3-3)$$

The solution of (3-3) is equal to (see for example [Athans and Falb 1969])

$$\{ \vartheta(\tau) \} = e^{[\psi]\tau} \cdot \{ g \} + \int_0^\tau e^{[\psi](\tau-p)} [\{ \psi_0 \} \vartheta_0(p) + \{ \psi_N \} \vartheta_N(p)] dp. \quad (3-4)$$

The diagonalizable matrix $e^{[\psi]}$ takes the form

$$e^{[\psi]} = [Z] \cdot [\text{diag}(e^\lambda)] [Z]^{-1} \quad (3-5)$$

where $[\text{diag}(e^\lambda)]$ is the diagonal matrix with elements e^{λ_i} , $i = 1, \dots, N - 1$ on the main diagonal and the numbers λ_i are eigenvalues of the matrix [Shen 1999]. Determining the integral in expression (3-4) for any moment of time τ requires each time the integration over the whole interval $[0, \tau]$. Determining the temperature $\vartheta(\tau)$ in subsequent moments of time τ and $\tau + \Delta\tau$ based on the dependence (3-4) we

get

$$\begin{aligned}
& \{\vartheta(\tau + \Delta\tau)\} \\
&= e^{[\psi](\tau + \Delta\tau)} \cdot \{g\} + \int_0^{\tau + \Delta\tau} e^{[\psi](\tau + \Delta\tau - p)} [\{\psi_0\}\vartheta_0(p) + \{\psi_N\}\vartheta_N(p)] dp \\
&= e^{[\psi](\Delta\tau)} \cdot \left(e^{[\psi](\tau + \Delta\tau)} \cdot \{g\} + \int_0^{\tau} e^{[\psi](\tau - p)} [\{\psi_0\}\vartheta_0(p) + \{\psi_N\}\vartheta_N(p)] dp \right) \\
&\quad + \int_{\tau}^{\tau + \Delta\tau} e^{[\psi](\tau + \Delta\tau - p)} [\{\psi_0\}\vartheta_0(p) + \{\psi_N\}\vartheta_N(p)] dp \\
&= e^{[\psi](\Delta\tau)} \cdot \{\vartheta(\tau)\} + \int_{\tau}^{\tau + \Delta\tau} e^{[\psi](\tau + \Delta\tau - p)} [\{\psi_0\}\vartheta_0(p) + \{\psi_N\}\vartheta_N(p)] dp \\
&= e^{[\psi](\Delta\tau)} \cdot \{\vartheta(\tau)\} + \Delta t \int_0^1 e^{[\psi]\Delta(1-t)} \{\psi_0\}\vartheta_0(\tau + \Delta\tau t) dt \cdot \int_0^1 e^{[\psi]\Delta(1-t)} \{\psi_N\}\vartheta_N(\tau + \Delta\tau t) dt. \quad (3-6)
\end{aligned}$$

In engineering practice the measurement of temperature is usually done with constant time steps $\Delta\tau$. Taking $\tau = \tau_m = n \cdot \Delta\tau$ and $\tau + \Delta\tau = \tau_{n+1}$, then ϑ_0 and ϑ_N are known at the measured points $\vartheta_0(\tau + \Delta\tau) = \vartheta_0(\tau_{n+1}) = \vartheta_0^{n+1}$, $\vartheta_0(\tau) = \vartheta_0^n$ and similarly for $\vartheta_N(\tau)$. How to calculate the integral in (3-6) is an important problem. We propose three ways to do this:

(a) Approximate the function ϑ by its average value (depending on the parameter ξ):

$$\begin{aligned}
\Delta\tau \cdot \int_0^1 e^{[\psi]\Delta\tau(1-t)} \cdot w(\tau_n + \Delta\tau \cdot t) dt &= \Delta\tau \cdot \int_0^1 e^{[\psi]\Delta\tau(1-t)} \cdot dt [w^n \xi + w^{n+1}(1 - \xi)] \\
&= w^n [S(\Theta)] + w^{n+1} [T(\Theta)]. \quad (3-7)
\end{aligned}$$

(b) Use the mean value theorem for definite integrals:

$$\begin{aligned}
\Delta\tau \cdot \int_0^1 e^{[\psi]\Delta\tau(1-t)} \cdot w(\tau_n + \Delta\tau \cdot t) dt &= \Delta\tau \cdot \int_0^{\xi} e^{[\psi]\Delta\tau(1-t)} \cdot dt \cdot w^n + \Delta\tau \cdot \int_{\xi}^1 e^{[\psi]\Delta\tau(1-t)} \cdot dt \cdot w^{n+1} \\
&= w^n [S(\xi)] + w^{n+1} [T(\xi)], \quad 0 < \xi < 1, \quad (3-8)
\end{aligned}$$

(c) Approximate the function ϑ by its asymptotic expansion [Ciałkowski 2008]:

$$\begin{aligned}
\Delta\tau \cdot \int_0^1 e^{[\psi]\Delta\tau(1-t)} \cdot w(\tau_n + \Delta\tau \cdot t) dt &= \Delta\tau \cdot \int_0^1 e^{[\psi]\Delta\tau(1-t)} \cdot [w^n(1 - t^\xi) + w^{n+1}t^\xi] dt \\
&= w^n [S] + w^{n+1} [T], \quad 0 < \xi < 1. \quad (3-9)
\end{aligned}$$

The function in these equations is replaced with ϑ_0 or ϑ_N . In the integration process the matrix $\exp([\psi] \cdot \Delta\tau)$ expressed in the form (3-5) is used. The choices (3-7) and (3-9) guarantee that the solution of the inverse problem is stable. After this operation the expressions (3-7) and (3-9) take on the form

$$\begin{aligned}
\{\vartheta^{n+1}\} &= e^{[\psi]\Delta\tau} \cdot \{\vartheta^n\} + (\vartheta_0^n [S] + \vartheta_0^{n+1} [T]) \{\psi_0\} + (\vartheta_N^n [S] + \vartheta_N^{n+1} [T]) \{\psi_N\} \\
&= e^{[\psi]\Delta\tau} \cdot \{\vartheta^n\} + \{S0\} \cdot \vartheta_0^n + \{T0\} \cdot \vartheta_0^{n+1} + \{SN\} \cdot \vartheta_N^n + \{TN\} \cdot \vartheta_N^{n+1}. \quad (3-10)
\end{aligned}$$

The matrix $\exp([\psi] \cdot \Delta\tau)$ is a matrix of stability for the direct problem with a boundary condition of the first type at the point $\eta = 0$ and $\eta = 1$. The dependence (3-10) can be written more compactly as

$$\begin{aligned} \{\vartheta^{n+1}\} &= [\{S\}, e^{[\psi]\Delta\tau}, \{SN\}]\{\bar{\vartheta}_n\} + \{T0\}\vartheta_0^{n+1} + \{TN\}\vartheta_N^{n+1} \\ &= [S\psi]\{\bar{\vartheta}_n\} + \{T0\}\vartheta_0^{n+1} + \{TN\}\vartheta_N^{n+1}, \quad \{\bar{\vartheta}\} = \{\vartheta_0, \vartheta_1, \dots, \vartheta_N\}, \end{aligned} \quad (3-11)$$

where $\dim[S\psi] = (N-1) * (N+1)$. Supplementing the vector (ϑ^{n+1}) with the elements ϑ_0^{n+1} and ϑ_N^{n+1} we obtain

$$\begin{aligned} \{\bar{\vartheta}^{n+1}\} &= \begin{bmatrix} \{0\}^T \\ [S\psi] \\ \{0\}^T \end{bmatrix} \{\bar{\vartheta}^n\} + \begin{bmatrix} 1 \\ \{T0\} \\ 0 \end{bmatrix} \{\vartheta_0^{n+1}\} + \begin{bmatrix} 0 \\ \{TN\} \\ 1 \end{bmatrix} \{\vartheta_N^{n+1}\} \\ &= [S\bar{\psi}]\{\bar{\vartheta}^n\} + \{P0\}\vartheta_0^{n+1} + \{PN\}\vartheta_N^{n+1} = [S\bar{\psi}]\{\bar{\vartheta}^n\} + [TT] \cdot \{\vartheta_0^{n+1}, \vartheta_N^{n+1}\}^T, \end{aligned} \quad (3-12)$$

for $n = 0, 1, \dots$, or, in a form which takes into account the values of temperature ϑ_0^{n+1} , ϑ_N^{n+1} at the boundary in the subsequent moments of time:

$$\{\bar{\vartheta}^{n+1}\} = [\psi]^{n+1} \cdot \sum_{k=0}^{n-1} [\psi]^{n-1+k} \cdot \{P0\}\vartheta_0^{n+k} + \sum_{k=0}^{n-1} [\psi]^{n-1+k} \cdot \{PN\}\vartheta_N^{k+1} \quad (3-13)$$

This gives the solution of the direct problem with a boundary condition of the first type. This series is convergent, if the spectral radius of matrix ψ , fulfills condition $\rho_s[\psi] < 1$. The dependence (3-13) gives a convenient method for solving the global inverse problem [Ciałkowski and Grysa 2010].

4. The solution of the inverse problem

In many practical situations it is impossible to determine temperature ϑ at the surface $\eta = 0$. However, it is possible to measure the temperature $\vartheta(\eta, \tau)$ at points $\eta = \eta_k^*$, $0 < \eta_k^* < 1$, $k = 1, \dots, M_{\text{stern}}$, $\tau = \tau_{n+1}$, $n = 0, 1, 2, \dots$. The dependence (2-9) takes the form

$$\vartheta(\eta_k^*, \tau_{n+1}) = \vartheta^{n+1}(\eta_k^*) = \sum_{i=0}^N \varphi_i(\eta_k^*) \vartheta_i^{n+1} = f_k^{n+1}, \quad k = 1, 2, \dots, M_{\text{stern}} \quad (4-1)$$

or separate in (4-1) temperatures ϑ_0^{n+1} and ϑ_N^{n+1} at the ends of a segment $[0, 1]$ we have

$$\varphi_0(\eta_k^*) \vartheta_0^{n+1} + \sum_{i=1}^{N-1} \varphi_i(\eta_k^*) \vartheta_i^{n+1} + \varphi_N(\eta_k^*) \vartheta_N^{n+1} = f_k^{n+1}$$

or

$$\varphi_0(\eta_k^*) \vartheta_0^{n+1} + \{\varphi(\eta_k^*)\}^T \{\vartheta^{n+1}\} + \varphi_N(\eta_k^*) \vartheta_N^{n+1} = f_k^{n+1}. \quad (4-2)$$

Substituting relationship (3-11) into (4-2) we obtain

$$\varphi_0(\eta_k^*) \vartheta_0^{n+1} + \{\varphi(\eta_k^*)\}^T \cdot ([S\psi]\{\bar{\vartheta}_n\} + \{T0\}\vartheta_0^{n+1} + \{TN\}\vartheta_N^{n+1}) + \varphi_N(\eta_k^*) \vartheta_N^{n+1} = f_k^{n+1}$$

or

$$(\varphi_0(\eta_k^*) + \{\varphi(\eta_k^*)\}^T \{T0\}) \cdot \vartheta_0^{n+1} + (\varphi_n(\eta_k^*) + \{\varphi(\eta_k^*)\}^T \{TN\}) \cdot \vartheta_N^{n+1} = f_k^{n+1} - \{\varphi(\eta_k^*)\}^T [S\psi] \cdot \{\bar{\vartheta}^n\}, \quad (4-3)$$

for $k = 1, 2, \dots, M_{\text{stern}}$. The boundary condition (2-13) is simplified to a similar form:

$$b_0 \cdot \vartheta_0^{n+1} + \{b\}^T \{\vartheta^{n+1}\} + b_N \cdot \vartheta_N^{n+1} = Bi_a \cdot \vartheta_{f_a}^{n+1} \quad (4-4)$$

and after introducing the dependence (3-11) we have:

$$b_0 \cdot \vartheta_0^{n+1} + \{b\}^T ([S\psi]\{\bar{\vartheta}^n\} + \{T0\}\vartheta_0^{n+1} + \{TN\}\vartheta_N^{n+1}) + b_N \cdot \vartheta_N^{n+1} = Bi_a \cdot \vartheta_{f_a}^{n+1},$$

or

$$(b_0 + \{b\}^T \{T0\}) \cdot \vartheta_0^{n+1} + (b_N + \{b\}^T \{TN\}) \cdot \vartheta_N^{n+1} = Bi_a \cdot \vartheta_{f_a}^{n+1} - \{b\}^T [S\psi] \cdot \{\bar{\vartheta}^n\}. \quad (4-5)$$

Equations (4-3) and (4-4) create a system of equations with the unknowns ϑ_0^{n+1} and ϑ_N^{n+1} which can be written as follows:

$$\begin{aligned} & \begin{bmatrix} \varphi_0(\eta_1^*) + \{\varphi(\eta_1^*)\}^T \{T0\} & \cdots & \varphi_N(\eta_1^*) + \{\varphi(\eta_1^*)\}^T \{TN\} \\ \vdots & & \vdots \\ \varphi_0(\eta_M^*) + \{\varphi(\eta_M^*)\}^T \{T0\} & \cdots & \varphi_N(\eta_M^*) + \{\varphi(\eta_M^*)\}^T \{TN\} \\ b_0 + \{b\}^T \{T0\} & \cdots & b_N + \{b\}^T \{TN\} \end{bmatrix} \cdot \begin{bmatrix} \vartheta_0^{n+1} \\ \vdots \\ \vartheta_N^{n+1} \end{bmatrix} \\ & = \begin{bmatrix} f_1^{n+1} \\ \vdots \\ f_M^{n+1} \\ Bi_a \cdot \vartheta_{f_n}^{n+1} \end{bmatrix} - \begin{bmatrix} \{\varphi(\eta_1^*)\}^T [S\psi] \\ \vdots \\ \{\varphi(\eta_M^*)\}^T [S\psi] \\ \{b\}^T [S\psi] \end{bmatrix} \cdot \{\bar{\vartheta}^n\}, \quad M = M_{\text{stern}}, \end{aligned}$$

or

$$[FIB] \begin{bmatrix} \vartheta_0^{n+1} \\ \vartheta_N^{n+1} \end{bmatrix} = \{FBiot^{n+1}\} - [SB]\{\bar{\vartheta}^n\}, \quad \dim[FIB] = \dim[SB] = 2(M_{\text{stern}} + 1), \quad (4-6)$$

and finally

$$\begin{bmatrix} \vartheta_0^{n+1} \\ \vartheta_N^{n+1} \end{bmatrix} = [FIB]^+ \{FBiot^{n+1}\} - [FIB]^+ [SB] \{\bar{\vartheta}^n\}. \quad (4-7)$$

The solution (3-13) takes the form:

$$\begin{aligned} \{\bar{\vartheta}^{n+1}\} &= [S\bar{\psi}]\{\bar{\vartheta}^n\} + [TT]([FIB]^+ \{FBiot^{n+1}\} - [FIB]^+ [SB]\{\bar{\vartheta}^n\}) \\ &= ([S\bar{\psi}] - [TT][FIB]^+ [SB])\{\bar{\vartheta}^n\} + [TT][FIB]^+ \{FBiot^{n+1}\} \\ &= [\psi_{int}]\{\bar{\vartheta}^n\} + [TF]\{FBiot^{n+1}\}, \quad n = 1, 2, \dots, \end{aligned} \quad (4-8)$$

where

$$\{FBiot^{n+1}\} = \{f^{n+1}(\eta_1^*), \dots, f^{n+1}(\eta_M^*), Bi_a \cdot \vartheta_{f_n}^{n+1}\}^T, \quad f^{n+1} = f(\tau_{n+1}).$$

5. The stability of the inverse problem

For the subsequent time steps $\tau = \tau_n$, $n = 0, 1, 2, \dots$ we write (4-8) as

$$\begin{aligned}\{\bar{\vartheta}^1\} &= [\psi_{\text{inv}}]\{\bar{\vartheta}^0\} + [FIB]^+ \{FBiot^1\}, \\ \{\bar{\vartheta}^2\} &= [\psi_{\text{inv}}]\{\bar{\vartheta}^1\} + [FIB]^+ \{FBiot^2\}, \\ \{\bar{\vartheta}^3\} &= [\psi_{\text{inv}}]\{\bar{\vartheta}^2\} + [FIB]^+ \{FBiot^3\}, \\ \{\bar{\vartheta}^n\} &= [\psi_{\text{inv}}]^n \{\bar{\vartheta}^0\} + \sum_{k=0}^{n-1} [\psi_{\text{inv}}]^k \cdot [FIB]^+ \{FBiot^{n-k}\}.\end{aligned}\tag{5-1}$$

If the spectral radius ρ_s of the matrix $[\psi_{\text{inv}}]$ satisfies $\rho_s([\psi_{\text{inv}}]) < 1$, the Neumann series is convergent and the solution of the inverse Equation (4-8) is stable. For the initial temperature vector $\{\bar{\vartheta}_0\}$ disturbed by $\{\delta\bar{\vartheta}_0\}$ and the data vector $\{FBiot^n\}$ disturbed by value $\{\delta FBiot^n\}$, the value of disturbance $\{\delta\bar{\vartheta}\}$ of temperature by $\{\bar{\vartheta}^n\}$ is determined from the dependence (5-1), namely

$$\{\bar{\vartheta}^n + \delta\bar{\vartheta}^n\} = [\psi_{\text{inv}}]^n \{\bar{\vartheta}^0 + \delta\bar{\vartheta}^0\} + \sum_{k=0}^{n-1} [\psi_{\text{inv}}]^k \cdot [TF]\{FBiot^{n-k} + \delta FBiot^{n-k}\}.\tag{5-2}$$

Subtracting (5-2) from the dependence (5-1), we have:

$$\{\delta\bar{\vartheta}^n\} = [\psi_{\text{inv}}]\{\delta\bar{\vartheta}^0\} + \sum_{k=0}^{n-1} [\psi_{\text{inv}}]^k \cdot [TF]\{\delta FBiot^{n-k}\}, \quad n = 1, 2, \dots\tag{5-3}$$

The dependence (5-3) determines the propagation of the measurement errors of the initial temperature and of the vector of measured temperatures in points $\eta_1^*, \dots, \eta_M^*$, $M = M_{\text{stern}}$. The distance between the first thermoelement and the boundary $\eta = 0$ has an essential influence on the value of the spectral radius ρ_s , and so does the method of determining the integral — (3-7), (3-8), or (3-9).

6. Numerical calculation

To investigate the numerical properties of the proposed method, the calculation was carried out for a circular ring with inner radius $R_i = 0.1$ m and outer radius $R_a = 0.209$ m. We further took $r_1^* = 0.108$ m and $r_2^* = 0.157$ m. The thermophysical properties were chosen as $c = 500$ J/(kg K), $\rho = 7800$ kg/m³, and $\lambda = 47.76$ W/mK. For test values, we took temperatures in cylindrical ring with different heat transfer coefficient at inner surface of ring $\alpha_i = \{5000, 2500, 1000, 500, 100\}$ W/m²K, outer surface isolation $q = 0$ and the temperature $T_{f_i} = 535^\circ\text{C}$, initial temperature $T_0 = 0^\circ\text{C}$. Figure 3 presents the distribution of heat transfer coefficient α_I obtained from the solution of the inverse problem for the data mentioned above.

The distribution of heat transfer coefficient is obtained from the solution of the inverse problem by means of a different way of calculating the integral in (3-6). Integration according to the method expressed by the formula (3-8) or (3-9) leads to a nonoscillating solution of the inverse problem.

For $\zeta = 0.75$ and method of integration (3-7), the spectral radius of the matrix is given in Figure 4 for positions of thermoelements at $s_1 = 8$ mm and $s_2 = 57$ mm from the inner surface. The influence the number of spline functions on the heat transfer coefficient is given in Figure 5. Figure 6 presents inverse

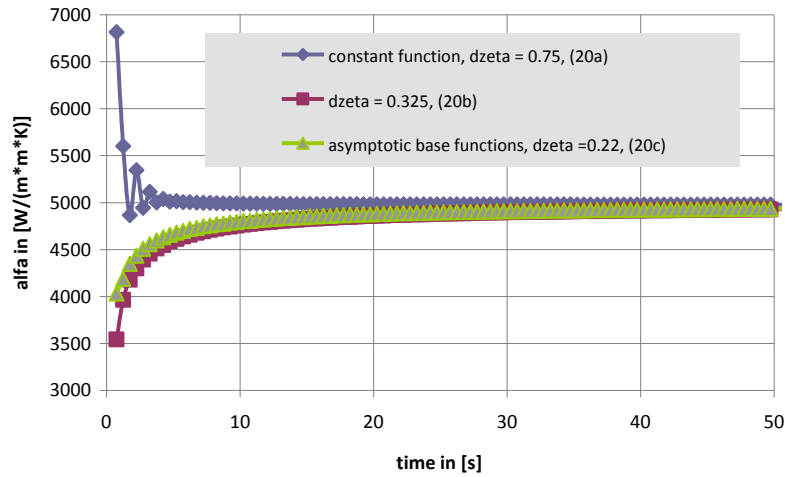


Figure 3. Comparison of methods of calculating the integral in formula (3-6).

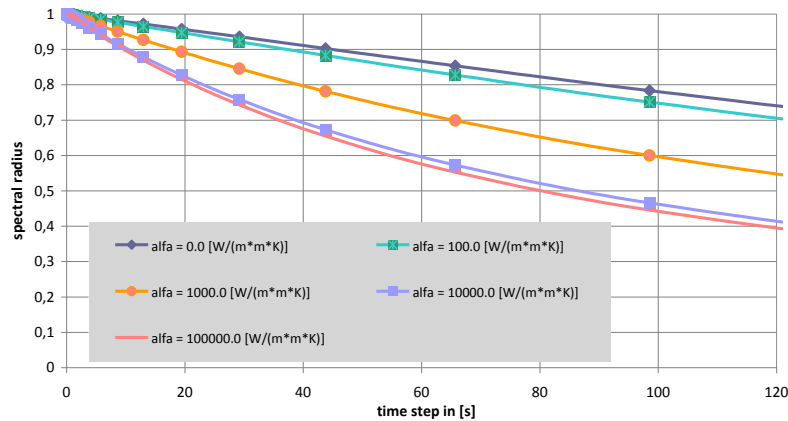


Figure 4. Influence of time step on the spectral radius of the stability matrix of the inverse problem ($\zeta = 0.75$) for given values of heat transfer coefficient at the outer surface.

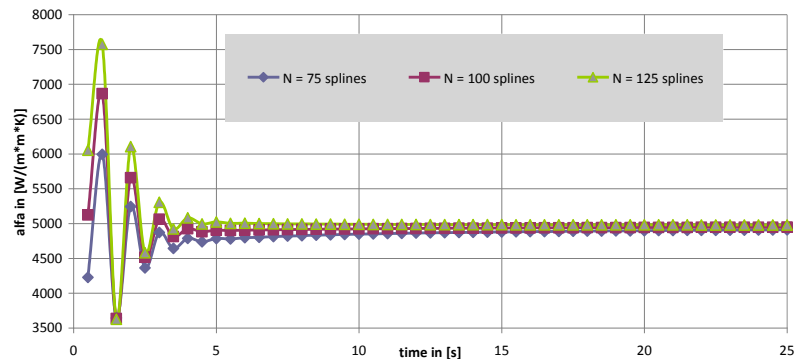


Figure 5. Influence of spline number on the calculation of heat transfer coefficient. All curves tend asymptotically to the exact value. ($\zeta = 0.75$.)

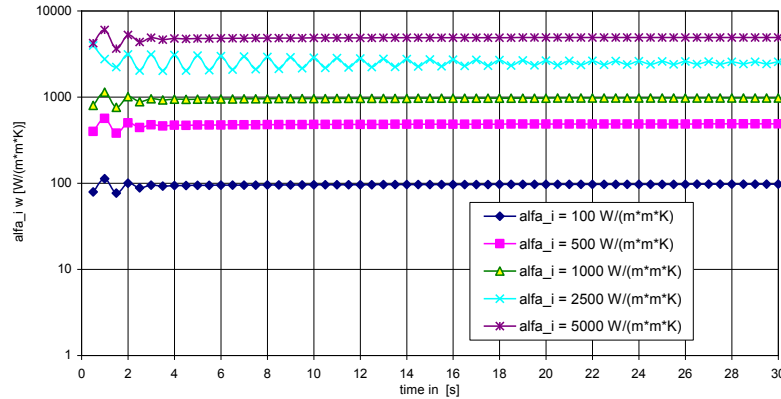


Figure 6. Solution of the inverse problem for different measurements (analytical values). ($\zeta = 0.75$.)

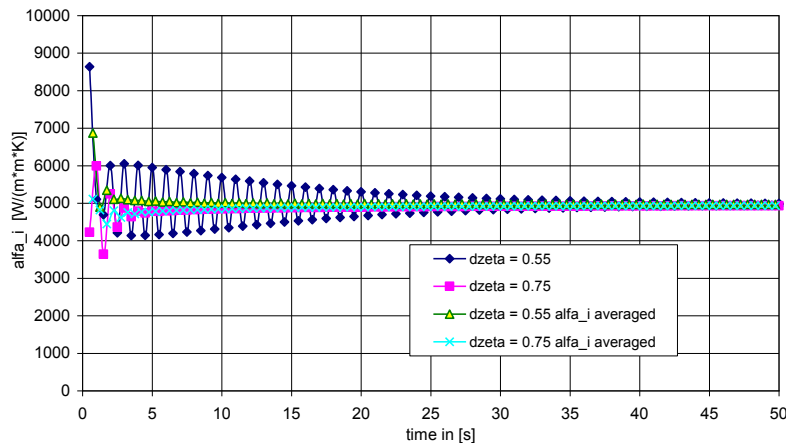


Figure 7. Solution of the inverse problem for different values of parameter ζ in (3-7).

problem solution for the data taken from the exact solution. Stability of the inverse problem depends on a length of time interval, a way of integration and the value of heat transfer coefficient on the outer side of cylinder. The time step was equal to 0.5 s. The use of (3-7) with parameter $\zeta = 0.75$ in our calculations guarantees the stability of the inverse problem while at the same time identifying the value of the heat transfer coefficient with high precision in a large time interval. Decreasing the value of parameter ζ leads to oscillation of the heat transfer coefficient obtained from the solution of the inverse problem, Figure 7. The arithmetic average of the subsequent values for $\zeta = 0.55$ brings the results very near to the values for parameter $\zeta = 0.75$. It can then be concluded that the interval of appropriate values for the parameter ζ is relatively broad and allows one to obtain stable results for the solution of the inverse problem using the arithmetic average. Figure 8 demonstrates the distribution of the measured temperature in a fluid at two inner points of a ring with radius $R_i = 0.1\text{m}$ placed $s_1 = 8\text{mm}$ and $s_2 = 57\text{mm}$ from the inner surface.

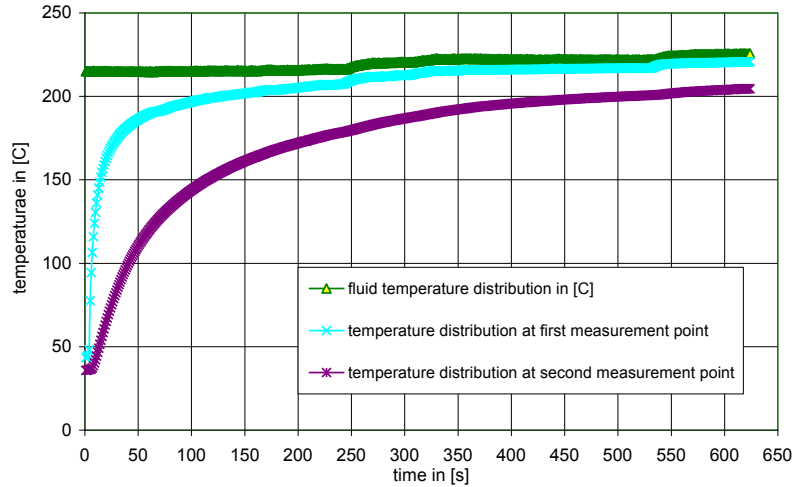


Figure 8. Distribution of measured temperature.

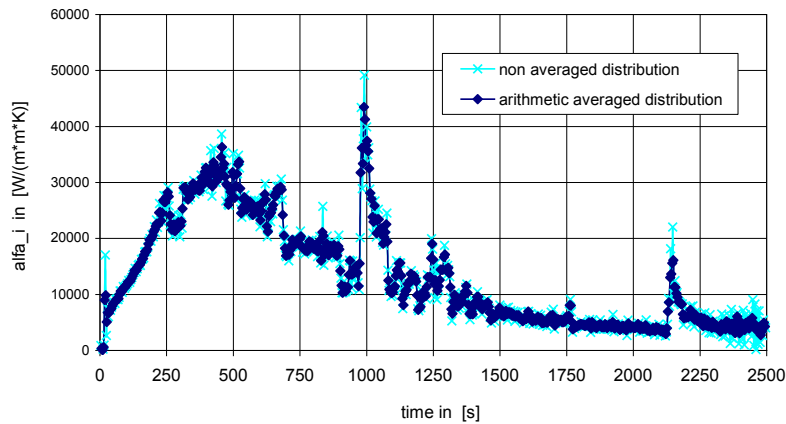


Figure 9. Solution to the inverse problem for real measurement. The thermocouples were placed at $s_1 = 8 \text{ mm}$ and $s_2 = 57 \text{ mm}$ from the inner surface.

These distributions are used to solve the inverse problem and to determine the heat transfer coefficient at the surface $r = R_i$. The values of the heat transfer coefficient are shown on Figure 9, where the time step is equal to $\Delta t = 4 \text{ s}$.

7. Conclusions

We have presented a method for solving the inverse problem for the transient linear heat transfer equation by approximating the solution with respect to the space variable with hyperbolic spline functions. The unknown coefficients of the linear combination of spline functions were determined by fulfilling the differential equation in the points of the net (Figure 2).

The essence of the proposed method is based on the approximation of the solution of differential equations with respect to the space variable by a twice-differentiable function. Hyperbolic spline functions

were chosen because using a backward quotient difference for the time variable transforms the heat transfer to Helmholtz's equation with source function, the solution of which contains a hyperbolic function. The smoothness of spline functions guarantees continuity of heat flux in each point of region which do not have place in the finite element method (there are jumps of flux between elements). The proposed method is appropriate for continuous temperature monitoring of casings with cylindrical or spherical geometries. This assumption usually follows from the lack of possibility of placing a large number of thermoelements because each hole leads to greater thermal stress.

References

- [Al-Khalidy 1998] N. Al-Khalidy, "On the solution of parabolic and hyperbolic inverse heat conduction problems", *Int. J. Heat Mass Transf.* **41** (1998), 3731–3740.
- [Athans and Falb 1969] M. Athans and P. L. Falb, *Sterownie optymalne*, Wydawnictwa Naukowo-Techniczne, Warsaw, 1969.
- [Beck 1970] J. V. Beck, "Nonlinear estimation applied to the nonlinear inverse heat conduction problem", *Int. J. Heat Mass Transf.* **13** (1970), 703–716.
- [Cabeza et al. 2005] J. M. G. Cabeza, J. A. M. Garcia, and A. C. Rodriguez, "A sequential algorithm of inverse heat conduction problems using singular value decomposition", *Int. J. Thermal Sci.* **44** (2005), 235–244.
- [Ciałkowski 2008] M. Ciałkowski, "Zastosowanie asymptotycznych funkcji bazowych do aproksymacji niestacjonarnych przebiegów temperatur", *Zeszyty Nauk. Politech. Poznań. Maszyny Robocze i Transport* **63** (2008), 27–43.
- [Ciałkowski and Grysa 2010] M. Ciałkowski and K. Grysa, "A sequential and global method of solving an inverse problem of heat conduction equation", *J. Theor. Appl. Mech. (Warsaw)* **48**:1 (2010), 111–134.
- [Deng and Hwang 2007] S. Deng and Y. Hwang, "Solution of inverse heat conduction problems using Kalman filter-enhanced Bayesian back propagation neural network data fusion", *Int. J. Heat Mass Transf.* **50** (2007), 2089–2100.
- [Ebrahimian et al. 2007] M. Ebrahimian, R. Pourgholi, M. Emamjome, and P. Reihani, "A numerical solution of an inverse parabolic problem with unknown boundary conditions", *Appl. Math. Comput.* **189** (2007), 228–234.
- [Grysa 2010] K. Grysa, *Funkcje Treffitza i ich zastosowania w rozwiązywaniu zagadnień odwrotnych*, Monografie, Studia, Rozprawy **M13**, Politechnika Świętokrzyska, Kielce, 2010.
- [Hon and Wei 2004] Y. C. Hon and T. Wei, "A fundamental solution method for inverse heat conduction problem", *Eng. Anal. Bound. Elem.* **28** (2004), 489–495.
- [Jonas and Louis 2000] P. Jonas and A. K. Louis, "Approximate inverse for a one-dimensional inverse heat conduction problem", *Inverse Problems* **16** (2000), 175–185.
- [Kim and Lee 2002] S. K. Kim and W. I. Lee, "Solution of inverse heat conduction problems using maximum entropy method", *Int. J. Heat Mass Transf.* **45** (2002), 381–391.
- [Lee et al. 2000] W.-S. Lee, Y.-H. Ko, and C.-C. Ji, "A study of an inverse method for the estimation of impulsive heat flux", *J. Franklin Inst.* **337** (2000), 661–671.
- [Lesnic and Elliot 1999] D. Lesnic and L. Elliot, "The decomposition approach to inverse heat conduction", *J. Math. Anal. Appl.* **232** (1999), 82–98.
- [Lin et al. 2004] S.-M. Lin, C.-K. Chen, and Y.-T. Yang, "A modified sequential approach for solving inverse heat conduction problems", *Int. J. Heat Mass Transf.* **47** (2004), 2669–2680.
- [Luksan and Spedicato 2000] L. Luksan and E. Spedicato, "Variable metric methods for unconstrained optimisation and nonlinear least squares", *J. Comput. Appl. Math.* **124** (2000), 61–95.
- [Pourgholi et al. 2009] R. Pourgholi, N. Azizi, Y. S. Gasimov, F. Aliev, and H. K. Khalafi, "Removal of numerical instability in the solution of an inverse heat conduction problem", *Comm. Nonlin. Sci. Numer. Simul.* **14** (2009), 2664–2669.
- [Pourshaghaghay et al. 2007] A. Pourshaghaghay, F. Kowsary, and A. Behbahaninia, "Comparison of four different versions of the variable metric method for solving inverse heat conduction problems", *Heat Mass Transf.* **43** (2007), 285–294.

- [Prud'homme and Hguyen 1999] M. Prud'homme and T. H. Hguyen, "Fourier analysis of conjugate gradient method applied to inverse heat conduction problems", *Int. J. Heat Mass Transf.* **42** (1999), 4447–4460.
- [Shen 1999] S.-Y. Shen, "A numerical study of inverse heat conduction problems", *Comput. Math. Appl.* **38** (1999), 173–188.
- [Shidfar and Karamali 2005] A. Shidfar and G. R. Karamali, "Numerical solution of inverse heat conduction problem with nonstationary measurements", *Appl. Math. Comput.* **168** (2005), 540–548.
- [Shidfar and Pourgholi 2006] A. Shidfar and R. Pourgholi, "Numerical approximation of solution of an inverse heat conduction problem based on Legendre polynomials", *Appl. Math. Comput.* **175** (2006), 1366–1374.
- [Taler and Duba 2001] J. Taler and P. Duba, "Solution of non-linear inverse heat conduction problems using the method of lines", *Heat Mass Transf.* **37** (2001), 147–155.

Received 14 Oct 2010. Revised 16 Jan 2012. Accepted 3 Apr 2012.

MICHAŁ CIAŁKOWSKI: michal.cialkowski@put.poznan.pl

Chair of Thermal Engineering, Poznan University of Technology, ul. Jana Pawla II 24, 60-965 Poznan, Poland

ANDRZEJ MAĆKIEWICZ: andrzej.mackiewicz@put.poznan.pl

Institute of Mathematics, Poznan University of Technology, ul. Jana Pawla II 24, 60-965 Poznan, Poland

JAN ADAM KOŁODZIEJ: jan.kolodziej@put.poznan.pl

Institute of Applied Mechanics, Poznan University of Technology, ul. Jana Pawla II 24, 60-965 Poznan, Poland

UWE GAMPE: uwe.gampe@tu-dresden.de

Institut für Energietechnik, Technische Universität Dresden, Helmholtzstraße 14, 01069 Dresden, Germany

ANDRZEJ FRACKOWIAK: andrzej.frackowiak@put.poznan.pl

Chair of Thermal Engineering, Poznan University of Technology, 60-965 Poznan, Poland

ANALYSIS OF STRESS-STRAIN DISTRIBUTION WITHIN A SPINAL SEGMENT

ZDENKA SANT, MARIJA CAUCHI AND MICHELLE SPITERI

The biomechanical feedback of biological tissue is difficult to measure. A spinal segment model can be used to obtain fundamental information by means of a computer simulation using finite element analysis.

1. Introduction

Interest in spine research has changed its focus from military-based tasks to problems related to the treatment of various spinal disorders, degenerative diseases, or traumas. Various studies have listed pain related to spinal structures as constituting the majority of health problems. A recent EU Commission study [EC 2007] also suggests that 67 million people suffered pain in their lower or upper back in the week previous to the survey.

The degenerative process accompanying aging causes changes in the form and composition of spinal tissues. This results in back pain particularly in cases such as internal disruption of the intervertebral disc (IVD) or stress shielding. In the case of stress shielding the damaged tissue has decreased ability to resist loading, and tends to be protected by adjacent healthy tissue, as occurs in the lumbar spine [Adams and Dolan 2005; Benzel 2005]. A healthy spine has nonlinear, elastic behavior and thus under lower loads provides little resistance while under increased loads it responds with augmented resistance. The stability of the spine provided by the IVD, the surrounding ligaments, and the muscles together with the geometry of the vertebral body must be preserved in any situation; thus in some cases a degenerated disc has to be replaced by an implant. Implant selection is usually based on the surgeon's own experience with particular implants and the results of tests carried out by the manufacturer in compliance with available standards. Unfortunately these results do not provide information about the biomechanical feedback which gives valuable insight for the surgeon. At the same time there is also a lack of information about the effect of degenerated components on the mechanical behavior of the entire IVD. Once the degenerative process alters the mechanical response, the whole complex structure of the segment is affected due to an adjustment of the load transfer trajectory that might affect as well the process of bone remodeling. All this might ultimately lead to undesirable performance of the IVD implant.

The goal of this work is to study the biomechanical behavior of a spinal segment under varying conditions related to the deterioration of the material properties of the IVD. Decisions about the methodology of this research and get satisfactory answers had to be made in the very early stages of the project. Since it is very difficult, if not impossible, to obtain the complete complex data about the response of different components of the system by means of measurements in vivo, and in the view that measurements in vitro

This research project was supported by grant 'R29' No. 31-329 obtained from the Research Fund Committee, University of Malta.

Keywords: spinal segment, finite element analysis, intervertebral disc.

are not feasible due to the lack of available spinal segments as well as economic and time constraints, the situation called for the development of a reliable computational model. Such a model would allow the investigation of biomechanical deficiencies within a geometrically identical pathological spinal segment and assist the proper understanding of the role played by each anatomical structure of the system.

2. Modeling

The pathophysiology of intervertebral disc degeneration is multifactorial [Hadjipavlou et al. 2008]. Mechanical factors have a significant effect, as excessive mechanical loading can cause disc structural disruption [Adams and Roughley 2006]. Disc degeneration impairs the shock-dissipating capacity of the vertebral column, thus a greater portion of the axial load is transmitted directly to the endplates of the lower adjacent vertebra [Norkin and Levangie 1992]. To provide a computational simulation of the desired situation, the creation of a computational model suitable for finite element analysis (FEA) was required.

The motion segment generated in this work consists of two adjacent vertebrae, L3 and L4, and an IVD modeled as a two-phase structure while the cartilages at the contact regions of the facet joints were simplified to a single-phase connective tissue. The material properties of the IVD, consisting of the annulus fibrosus (AF) and the nucleus pulposus (NP), distinguish the three different scenarios that simulate the physiological, the mildly degenerated IVD, and the fully degenerated IVD. Thus three spinal segments with different material properties simulated load transfer through a healthy IVD, a mildly degenerated IVD, and a severely degenerated IVD.

The two vertebrae were digitized using a reverse engineering approach applied to images in DICOM format, obtained from a computer tomography (CT) helical scan at Mater Dei Hospital. Each CT scan slide was processed by means of drawing software, capturing the real surface of the vertebrae with all anomalies, and the recreated vertebrae were then transported into the FEA package. To create the intervertebral disc we had to take into consideration the complexity of the real disc, the computational power required to sustain the simulation for such a complex structure, and the material data of [Acaroglu et al. 1995] based on an experimental investigation of the mechanical properties of anterior and posterior segments cut from the inner and outer layers of an AF. In the median plane, the lamellae reveal the major difference in their properties related to the posterior-anterior direction of their position. The collagenous fibers at the anterior median location are much stiffer than the lamellae found at the posterior side of the annulus, and both cases exhibit a nonlinear, axial stress-strain relation at low strains in “toe” region

	Young's modulus E (MPa)			
	Anterior		Posterior	
	Outer	Inner	Outer	Inner
Healthy annulus	27.2±14.6	7.6±6.6	13.6±9.4	2.4±2.5
Mild degeneration	23.3±16.6	6.1±5.2	6.6±4.0	4.3±4.9
Severe degeneration	21.2±12.2	4.8±4.5	8.2±5.5	3.4±3.9

Table 1. Young's modulus (mean ± standard deviation) in MPa for fibers at different locations of the annulus [Acaroglu et al. 1995].

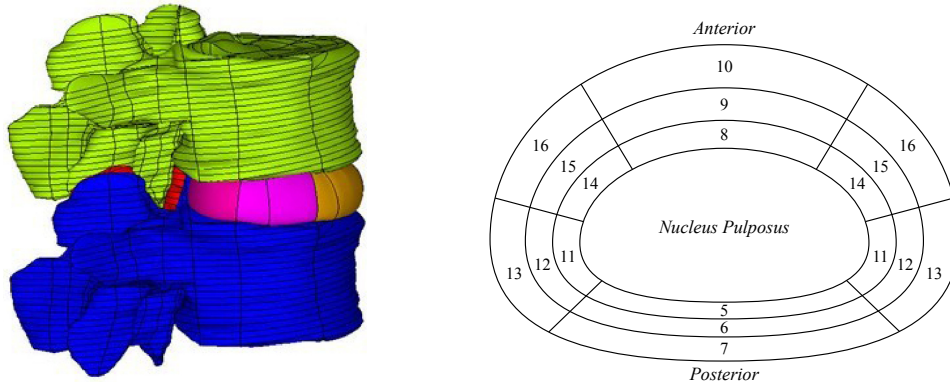


Figure 1. Spinal segment L3-L4 with detail of IVD model.

while at the region of high strains the behavior is nearly linear. The Young’s modulus, as a result of a cubic function fitted to the experimental data, is presented in Table 1 as continuously varying from the posterior to the anterior side of the annulus [Acaroglu et al. 1995].

Our model of the IVD in Figure 1 represents a simplification of an IVD that in reality has 10–20 layers of collagen fibers encapsulating the nucleus. The NP was modeled as a single volume surrounded by three lamellae divided into six segments. Further connective tissue was created at the region of the facet joints. Considering that the loads applied to the bone would result in bone response, which can be approximated by a linear function, the two types of bone tissue, cortical and cancellous, were modeled as linear isotropic material even though in reality the bone is anisotropic heterogeneous viscoelastic material. The necessity for simplification is related to the computational power and CPU time required for the simulation, together with the available geometry/material data and modeling facility. The continuously changing directions of trabeculae orientation within both types of bone tissue are compensated for by the corresponding orientation of the elements within each structure. Thus, accepting these simplifications, the verified data of the Young’s modulus for the cortical bone, the cancellous bone, and the endplates was used as listed in Table 2. The material properties of the IVD were extrapolated from available data [Acaroglu et al. 1995] and processed using (2-1) to evaluate the Young’s modulus/Poisson’s ratio at the geometrical positions of the outer and inner locations of the segment. The average value of the Young’s modulus/Poisson’s ratio was then computed using (2-2). The computation was based on the assumption of linear variation of both quantities in the sagittal and transverse directions:

$$E_{sl} = \frac{E_{jo} - E_{ji}}{d_{jl}} * d_{sl}, \tag{2-1}$$

Material properties of vertebrae			
Component	Young’s modulus (MPa)	Poisson’s ratio	Reference
Cortical bone	16000	0.25	[Sant 2007]
Cancellous bone	120	0.25	[Sant 2007]
Endplate	500	0.25	[Teo et al. 2003]

Table 2. Material properties of vertebrae.

	Material properties of IVD			
	Healthy IVD		Severely degenerated IVD	
	E (MPa)	ν	E (MPa)	ν
NP	100	0.499	1	0.499
AF 5	6.75	0.445	2.25	0.345
AF 6	9.75	0.425	3.25	0.325
AF 7	13.5	0.4	4.5	0.3
AF 8	9.5	0.415	5	0.315
AF 9	15.5	0.395	9	0.295
AF 10	23	0.37	14	0.27
AF 11	7.575	0.436	3.075	0.336
AF 12	11.475	0.416	4.975	0.316
AF 13	16.35	0.391	7.35	0.291
AF 14	8.675	0.424	4.175	0.324
AF 15	13.775	0.404	7.275	0.304
AF 16	20.15	0.379	11.15	0.279

Table 3. Computed material properties of IVD based on data from [Acaroglu et al. 1995].

where E_{jo} , E_{ji} , and E_{sl} represent the Young's moduli at the outer j position, the inner j position, and the position defined by d_{sl} , respectively, and d_{jl} and d_{sl} represent the distances l between the outer and inner j position and between the segment's position and the outer j reference position, respectively. The average value used in our simulation for segment s is computed from

$$E_{av_s} = \frac{E_{jo} + E_{sl}}{2}. \quad (2-2)$$

The material properties characterizing the healthy and degenerated states of the IVD material are listed in Table 3 according to the position of each AF segment.

Finally, the discretization of the virtual solid model was created by means of combination of free and mapped meshing using an esize of two elements. The cortical bone and endplates were meshed with shell elements having bending and membrane capabilities while the cancellous bone was meshed with a solid element type with midside nodes. The connectivity between various meshes at the contacting surfaces between the vertebrae and the IVD was secured through the use of contact elements, which were set to "always bonded contact". Another pair of contact surfaces set to "standard contact condition" were created at the facet joints to allow for flexion/extension movement and limited torsion, as well as to provide resistance to the sliding of the vertebrae against each other.

3. Simulation

In addition to the geometrical and material model, the FE model in Figure 2 also requires the load model. The latter depends on the particular activity associated with the certain position on the spine, which is in turn associated with a particular load transfer through the spinal structure. The spine undergoes a combined motion due to the fact that simple flexion is always accompanied by coupled motions, which

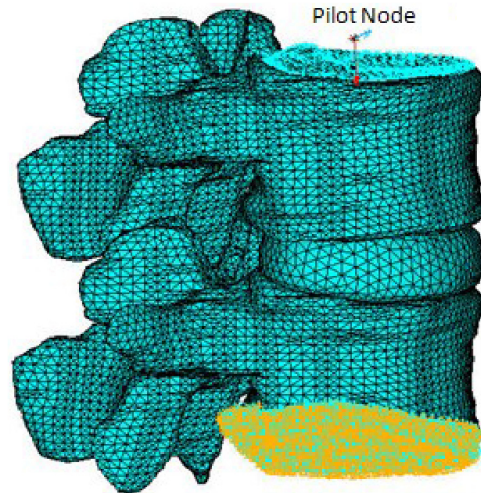


Figure 2. Finite element model of the spinal segment L3-L4.

vary in nature and magnitude according to the level of the segment within the whole spine. Thus the applied load simulating physiological activity can be either in the form of displacement and rotation or forces and moments. Due to the fact that the model in this study was simplified and therefore did not include any ligamentous structures, the exact neutral range of motion for the L3-L4 segment must be applied to simulate a real life situation without the contribution of the ligamentous structures to the load transfer. Since this data was not available, it was decided to run the simulation based on [Arjmand and Shirazi-Adl 2006], in which the authors measured and verified data for the lumbar spine at various positions without contribution from ligamentous structures. Such data was deemed suitable for the simulation in the present study. The simulated load for various positions of the patient was comprised of the compressive force, shear force, and bending moment. It was decided to simulate an upright standing position without additional external carrying load from the hands. In this situation, the sagittal moment $M = 3.9 \text{ Nm}$ is positive while the segment is in flexion, the axial compression $N = 447 \text{ N}$, and the shear force $S = -63 \text{ N}$ is positive in the anterior direction. These loads were applied by means of a pilot node positioned at the fictitious midplane in the center of the NP of the intervertebral disc L2-L3. This corresponds to the position where the data was measured and computed by Arjmand and Shirazi-Adl. By having identical geometry and loading conditions, it was possible to run a comparative analysis in order to investigate the effect of IVD degeneration on the mechanical behavior of the segment. Thus the simulation was performed for three different conditions: physiological, mildly degenerated IVD, and severely degenerated IVD.

4. Results

The comparative study presented here aims to investigate the effect of pathological deterioration of the material properties on the load transfer through the IVD and the biomechanical feedback of the adjacent structures. To be able to correctly analyze and compare the results, the necessary path passing throughout the median plane of the segment at the center of the nucleus had to be created. The results in the

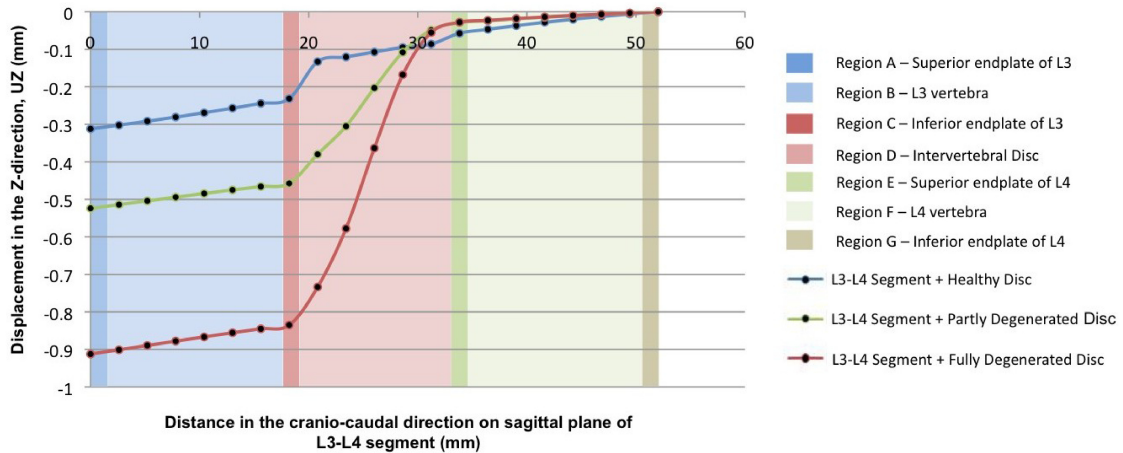


Figure 3. Variation of displacement along the craniocaudal direction for L3-L4 segment.

craniocaudal direction for both the vertebrae and the IVD were mapped onto this path. These results are visualized in Figure 3, from which the effect of degeneration on the mechanical behavior was then analyzed. The gradients in Figure 3 correspond to the relative stiffness/Young's modulus of the entity, thus the greater gradient implies a lower Young's modulus and therefore a higher deformation ability. It is the IVD that always deforms the most irrespective of the state of degeneration, as confirmed by the steeper gradients within the IVD region (region D) when compared to the gradients through the L3 and L4 vertebrae represented by regions B and F, respectively. The larger displacement of the fully degenerated IVD consequently causes the segment to undergo larger displacement. In regions C and E the gradient is shallower due to the stiffening effect of the vertebral endplates. The main biomechanical deficiency of the partly and fully degenerated IVD is the inability to properly transfer the load between adjacent vertebrae as a direct consequence of the reduced stiffness and lax behavior. Thus in the cases of the partly and fully degenerated IVD, the inferior vertebra undergoes a smaller axial displacement than in the case of the healthy disc since the degenerated NP within the degenerated IVD lacks the necessary mechanical properties to bulge into the endplate of the inferior vertebra while the spinal segment is loaded, and thus it does not transmit the load properly through the segment. The axial displacement approaches zero on proceeding along the craniocaudal direction since the bottom surface of the inferior vertebra was fully constrained to be able to run the computational task.

The cortical bone is the main bearer of the load, from where the load is subsequently redistributed to the cancellous bone which fulfils the role of a shock absorber. Thus the highest compressive stresses, represented by the third principal stress, were developed at the level of the cortical bone in the posterior region of the vertebrae mainly around the pedicles in the case of the healthy IVD, as shown in Figure 4a, while in the case of the severely degenerated IVD, shown in Figure 4b, the maximum compressive stress developed at the anterior region of the epiphyseal ring. It can be noticed that the overall compressive stresses increased from 12 MPa in the case of the healthy IVD to 22.5 MPa in the case of the degenerated IVD. The cancellous bone functioning as a shock absorber develops the highest compressive stress just beneath the vertebral endplates. It is clinically confirmed that the site of the most frequent failures due to compressive loading is the region of the endplates. The cancellous bone beneath the healthy disc in

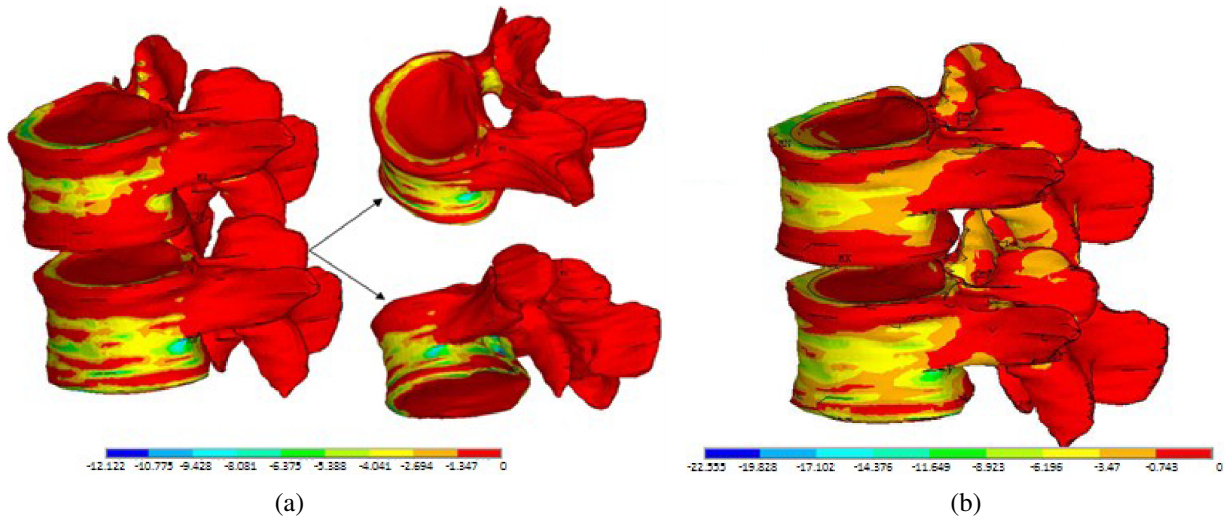


Figure 4. Variation of third principal compressive stress within the cortical bone for L3-L4 segment.

Figure 5a is subjected to larger compressive stresses than the cancellous bone beneath the severely degenerated IVD in Figure 5b, which indicates that, due to reduced stiffness, the degenerated IVD undergoes larger deformation radially, and thus reduces the load transferred through the superior endplate of the inferior vertebra. Thus the cancellous bone is characterized by lower compressive stresses, indicating a reduced magnitude of disc bulging into the endplate in the case of the severely degenerated disc, which increases the compressive stress within the cancellous bone from 1.034 MPa to 1.328 MPa for the healthy and severely degenerate IVD, respectively. The maximum tensile stress increased as well, from 0.039 MPa for the healthy IVD to 0.117 MPa for the severely degenerated IVD. The full analysis

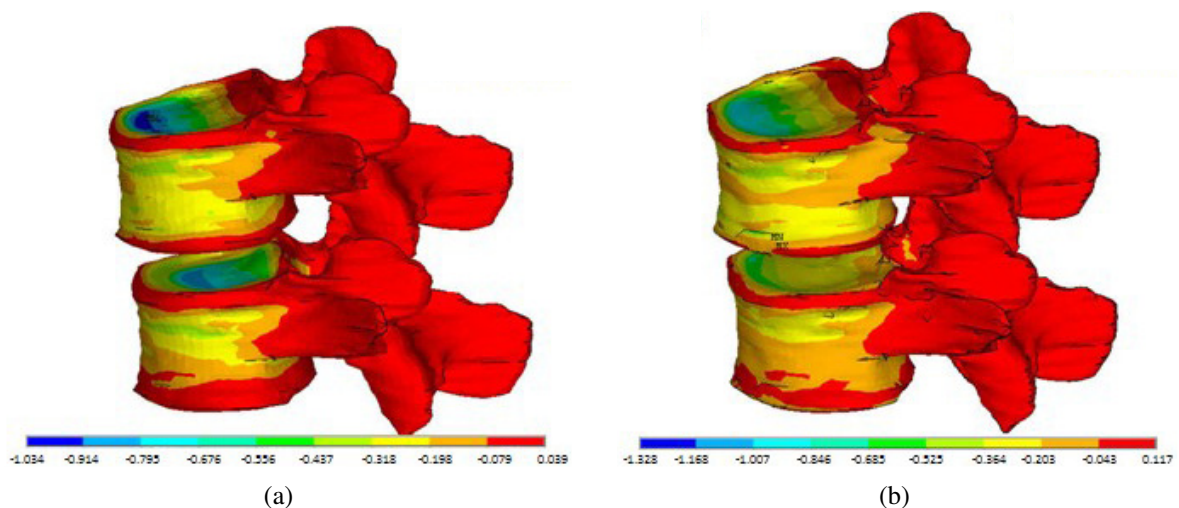


Figure 5. Variation of third principal compressive stress within the cancellous bone for L3-L4 segment.

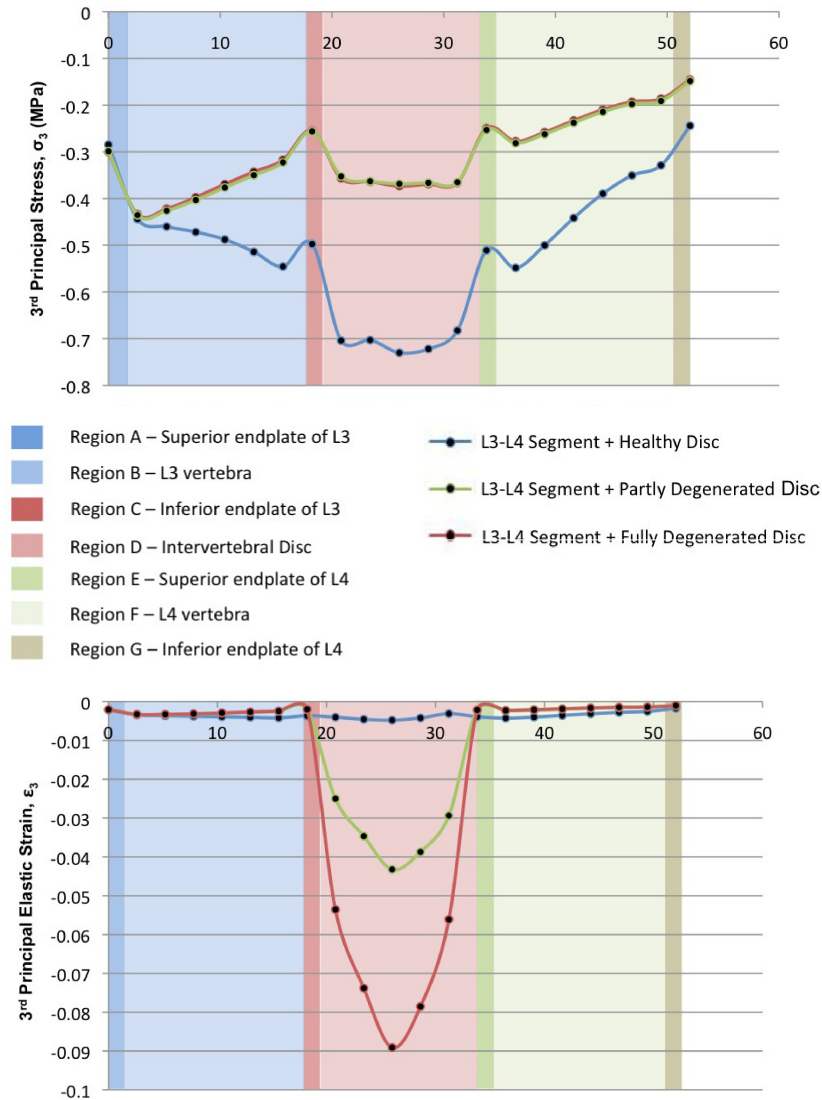


Figure 6. Variation of stress-strain along the central path in the craniocaudal direction for L3-L4 segment. The horizontal axis represents distance in mm.

of the biomechanical feedback due to the degenerative process is summarized by the graphs in Figure 6 representing the stress and strain variation along the axial craniocaudal direction through the center of the spinal segment.

5. Conclusion

These results, together with others in the posterior-anterior and lateral directions, were verified by the clinician and carefully analyzed. In all cases, the importance of the endplates and the effect of the degeneration of the nucleus were confirmed. The virtual FE model can be used for other simulations

such as the effect of loading on the biomechanical feedback of the spinal segment, in particular the structures forming the intervertebral disc, and the effect of different physical activities on load transfer through the segment.

References

- [Acaroglu et al. 1995] E. R. Acaroglu, J. C. Latridis, L. A. Setton, R. J. Foster, V. C. Mow, and M. Weidenbaum, “Degeneration and aging affect the tensile behavior of human lumbar annulus fibrosus”, *Spine* **20**:24 (1995), 2690–2701.
- [Adams and Dolan 2005] M. A. Adams and P. Dolan, “Spine biomechanics”, *J. Biomech.* **38**:10 (2005), 1972–1983.
- [Adams and Roughley 2006] M. A. Adams and P. J. Roughley, “What is intervertebral disc degeneration, and what causes it?”, *Spine* **31**:18 (2006), 2151–2161.
- [Arjmand and Shirazi-Adl 2006] N. Arjmand and A. Shirazi-Adl, “Model and in vivo studies on human trunk load partitioning and stability in isometric forward flexions”, *J. Biomech.* **39**:3 (2006), 510–521.
- [Benzel 2005] E. C. Benzel (editor), *Spine surgery: techniques, complication avoidance, and management*, Churchill Livingstone, Philadelphia, 2005.
- [EC 2007] *Health in the European Union*, Special Eurobarometer 272e, European Commission, 2007, Available at http://ec.europa.eu/health/archive/ph_publication/eb_health_en.pdf.
- [Hadjipavlou et al. 2008] A. G. Hadjipavlou, M. N. Tzermiadianos, N. Bogduk, and M. R. Zindrick, “The pathophysiology of disc degeneration: a critical review”, *J. Bone Jt. Surg. Br.* **90**:10 (2008), 1261–1270.
- [Norkin and Levangie 1992] C. C. Norkin and P. K. Levangie, *Joint structure and function: a comprehensive analysis*, 2nd ed., Davis, Philadelphia, 1992.
- [Sant 2007] Z. Sant, *Mechanické vlastnosti hrudního a bederního páteřního fixátoru*, Ph.D. thesis, University of Technology, Brno, 2007. Scientific Writings of the Technical University in Brno **446**.
- [Teo et al. 2003] E. C. Teo, K. K. Lee, H. W. Ng, T. X. Qui, and K. Yang, “Determination of load transmission and contact force at facet joints of L2–L3 motion segment using FE method”, *J. Musculoskelet. Res.* **7**:2 (2003), 97–109.

Received 14 Oct 2010. Revised 20 Jul 2011. Accepted 15 Dec 2011.

ZDENKA SANT: zdenka.sant@um.edu.mt

Mechanical Engineering Department, University of Malta, Tal Qroqq, Msida MSD 2080, Malta

MARIJA CAUCHI: mcau0010@um.edu.mt

Mechanical Engineering Department, University of Malta, Tal Qroqq, Msida MSD 2080, Malta

MICHELLE SPITERI: michespi@gmail.com

Mater Dei Hospital, Tal Qroqq, Msida MSD 2080, Malta

A MESH-FREE NUMERICAL METHOD FOR THE ESTIMATION OF THE TORSIONAL STIFFNESS OF LONG BONES

ANITA USCILOWSKA AND AGNIESZKA FRASKA

This paper considers the torsional stiffness of long bones. The phenomenon of long-bone twisting is a boundary value problem. We propose to solve the problem by a numerical procedure based on a mesh-free method, the method of fundamental solutions.

1. Introduction

External loads acting on long bones can cause fractures. A fracture is any break in a bone or cartilage. It usually is a result of trauma but can be due to an acquired disease of the bone such as osteoporosis or abnormal formation of the bone due to a congenital disease of the bone such as osteogenesis imperfecta. Fractures are classified by their character and location. Examples of classifications include “spiral fracture of the femur,” “greenstick fracture of the radius,” “impacted fracture of the humerus,” “linear fracture of the ulna,” “oblique fracture of the metatarsal,” “compression fracture of the vertebrae,” and “depressed fracture of the skull.” A “comminuted fracture” is a fracture in which the bone is broken into a number of pieces, as distinguished from a “compound fracture” in which the bone sticks through the skin. The problem addressed in this paper is the twisting of a lone bone, which can cause spiral fracture of a long bone (Figure 1).



Figure 1. Spiral fracture [Pierce et al. 2004].

This paper was financially supported by Grant 21-339/2010 DS at Poznan University of Technology.

Keywords: method of fundamental solutions, mesh-free method, torsional stiffness, long bone.

There are some papers in the literature treating problem of the torsional stiffness of a long bone. Comparative studies of long-bone biomechanics in primates frequently use the polar moment of inertia as a variable reflecting overall mechanical rigidity, average bending rigidity, or resistance to torsional shear stresses. Daegling [2002] showed that while the use of this variable for characterizing the first two properties is appropriate, it is potentially a highly misleading measure of torsional resistance. Indeed, theoretical and experimental research has shown that the use of the polar moment of inertia for estimating long-bone torsional rigidity should be restricted to samples of relatively invariant or cylindrical geometry.

The open section effect in a long bone with a longitudinal defect is the subject of [Elias et al. 2000], where it was found that a longitudinal defect dramatically alters the stress distribution within a long bone. For applied torsion, the defect interrupts the normal shear flow around the bone. The problem is solved by the finite element method (FEM).

Bone material properties. Bone in a living animal consists of both living tissue and nonliving substances. Within live bone are blood vessels, nerves, collagen, and living cells, including osteoblasts (cells that help form bone), and osteoclasts (cells that help eat away old bone). In addition, bone contains cells called osteocytes, which are mature osteoblasts that have ended their bone-forming careers. The nonliving, but very important, substances in bone are minerals and salts. Besides the metabolically active cellular portion of bone tissue, bone is also made up of a matrix (a bonding of multiple fibers and chemicals) of different materials, including primarily collagen fibers and crystalline salts. The crystalline salts deposited in the matrix of bone are composed principally of calcium and phosphate, which are combined to form hydroxyapatite crystals. In particular, it is the collagen fibers and calcium salts that help to strengthen bone. In fact, the collagen fibers of bone have great tensile strength (the strength to endure stretching forces), while the calcium salts, which are similar in physical properties to marble, have great compressional strength (the strength to endure squeezing forces). These combined properties, plus the degree of bondage between the collagen fibers and the crystals, provide a bony structure that has both extreme tensile and compressional strengths. Due to such a complicated structure the bone is treated as a object made with functionally graded material (FGM) [Pompe et al. 2003]. FGMs are materials with continuously varying material properties designed for specific engineering and bioengineering applications. Although the torsion problem for homogeneous linearly elastic bars is a classical one in elasticity, there has been relatively little attention paid to the case when material is inhomogeneous.

Recently, research activity on functionally graded materials has also stimulated investigation on the torsion problem for inhomogeneous material. Chen [1964] studied the torsion of inhomogeneous bars. He presented governing equations and boundary conditions for the torsion problem of inhomogeneous bars in terms of a stress function. Then, he applied a semiinverse method and found a specific distribution for the shear modulus of rigidity in a specific geometry of cross-section. By this method, he could find simple solutions for the stress function and torsional stiffness of circular and elliptical shafts. An analytical formulation for torsional analysis of functionally graded elastic bars with circular cross-sections was presented by Horgan and Chan [1999]. They supposed the shear modulus of rigidity to be a function of radius. Using the axisymmetric geometry of the cross-section of the circular bar, they found an exact analytical solution. They used governing equations and boundary conditions in terms of Prandtl's stress function. Saint-Venant's torsion problem for linearly elastic, isotropic, nonhomogeneous cylindrical bars was considered in [Ecsedi 2009].

The novelty of this paper is that the shear modulus of the investigated nonhomogeneous bar is a given function of the Prandtl stress function of a homogeneous bar, which has the same cross-sections as the nonhomogeneous bar considered. The main result of the present paper is a contribution to the existing exact benchmark solutions for functionally graded twisted elastic cylinders. Five examples (a hollow elliptical cylinder, a solid equilateral triangle cross-section, an approximate solution for a thin-walled tube, a rectangular cross-section, and a narrow rectangular cross-section) illustrate the application of the proposed method. In [Arghavan and Hematiyan 2009] an analytical formulation was presented for the torsion of functionally graded hollow tubes of arbitrary shape. The authors assumed that the thicknesses of all segments of the cross-section were the same and the shear modulus of rigidity changed continuously across the thickness. In this way the simple but relatively accurate formulas for the stresses and torsional stiffness were obtained on the basis of analytical integration of the governing equation for the stress function.

As this short review shows, the uniform torsion problem for functionally graded materials has been solved primarily by analytical methods and traditional mesh methods such as FEM [Arghavan and Hematiyan 2009] and FED [Ely and Zienkiewicz 1960]. The purpose of this paper is the application of the method of fundamental solutions (MFS) to the torsion problem of functionally graded materials. This method belongs to the so-called meshless methods which have become more and more popular in the two last decades. The MFS was first proposed in [Kupradze and Aleksidze 1964]. Its numerical implementation was carried out in [Mathon and Johnston 1977]. Comprehensive reviews of the MFS for various applications can be found in [Fairweather and Karageorghis 1998; Golberg and Chen 1999]. Here, based on the Saint-Venant displacement assumption, the boundary-value linear problem for the stress function is formulated. For isotropic materials the governing equation is linear with constant coefficients. The torsion problem for rods made with isotropic materials is solved by the MFS. For FGM the governing equation is a linear one with variable coefficients. The torsion problem for rods made with FGMs is solved by means of Picard iteration. The proposed algorithm is based on the solution of a linear Poisson equation at each iteration step. The mentioned boundary value problem is solved by the MFS with interpolation of the right-hand side by a radial basis function.

2. Problem description

The following assumptions about bone characteristics are made:

- Nonuniform bone geometry is analyzed as a tube with a constant cross-section (circular), neglecting lengthwise variations in bone geometry.
- The areal properties of the smallest bone section are taken into account.
- The bone material is considered as a functionally graded material (FGM) (the shear modulus is a function of geometrical variables).

The steady-state problem of the torsion of a long bone is modeled as the torsion of a bar with circular cross-section with a circular hollow. It is assumed that the bar is made of FGM, that is, the shear modulus is a function of geometric variables. The cross-section of the region of the bar under consideration is presented in Figure 2. The Oz -axis is directed parallel to the generators of the cylindrical surface. There are no normal stresses on the end cross-section. The applied tangential forces on the end cross-section

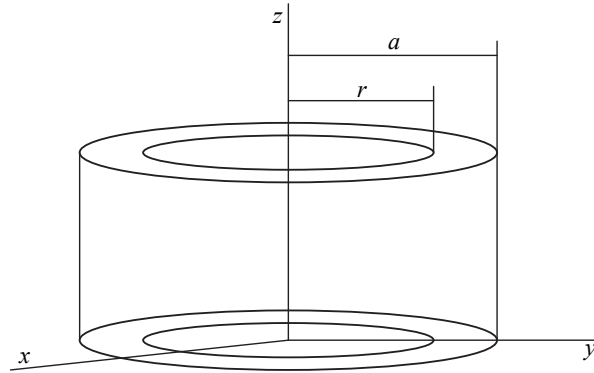


Figure 2. Geometry of the porous medium.

are equivalent to two couples whose magnitudes are the same and whose moments are directed along the z -axis in opposite directions.

3. The equations of strength theory

To introduce the equations governing the torsion of a bar with circular cross-section, general strength theory is applied. The geometry of the bar is presented in Figure 2. The displacement components in cylindrical coordinates are

$$u_x(x, y, z), \quad u_y(x, y, z), \quad u_z(x, y, z). \quad (3-1)$$

As in homogeneous Saint-Venant theory, let us assume that all the stress components are zero except for τ_{xz} and τ_{yz} . The assumption of strength theory allows the introduction of the Prandtl stress function ψ , which is defined by the stresses as follows:

$$\tau_{xz} = \omega \frac{\partial \psi}{\partial y}, \quad \tau_{yz} = -\omega \frac{\partial \psi}{\partial x}, \quad (3-2)$$

where ψ is the Prandtl stress function, τ_{xz} and τ_{yz} are stress tensor components, and ω is the twist angle. The equilibrium equation is automatically satisfied by (3-2) and the resulting compatibility equations are

$$\frac{\partial}{\partial x} \left(\frac{1}{G(x, y)} \frac{\partial \psi}{\partial x} \right) + \frac{\partial}{\partial y} \left(\frac{1}{G(x, y)} \frac{\partial \psi}{\partial y} \right) = -2\omega \quad \text{for } (x, y) \in \Omega, \quad (3-3)$$

where Ω is the area of the bar cross-section and $G(x, y)$ is a function defining the shear modulus of the FGM which is assumed to be a continuously differentiable positive function on Ω . The boundary conditions for the problem are described below.

The traction-free boundary condition on the lateral surface is fulfilled if

$$\psi = 0 \quad \text{for } (x, y) \in \Gamma. \quad (3-4)$$

In the case of a bar with a multiconnected cross-section we get the condition

$$\psi = \psi_0 \quad \text{for } (x, y) \in \Gamma_1, \quad (3-5)$$

where ψ_0 is an unknown constant on the inner contour Γ_I , which is determined from

$$\oint_{\Gamma_I} \frac{\partial \psi}{\partial n} ds = - \oint_{\Gamma_I} \frac{1}{f(x, y)} (x dy - y dx) - \oint_{\Gamma_I} \frac{1}{f(x, y)} du_z, \tag{3-6}$$

where Γ and Γ_I are respectively the outer and inner boundaries of the bar cross-section, Ω_I is the area of the hollow, and du_z is the deflection along the z -axis. The stiffness of the bar is defined by

$$S = 2 \iint_{\Omega} \psi(x, y) dx dy. \tag{3-7}$$

Thus the torsion problem of the inhomogeneous bar reduces to solving (3-3) on the domain Ω subjected to the boundary conditions (3-4)–(3-6). The corresponding stresses are given by (3-2).

To make numerical calculations more convenient dimensionless variables are introduced:

$$X = \frac{x}{a}, \quad Y = \frac{y}{a}, \quad E = \frac{r}{a}, \quad \Psi(x, y) = \frac{\psi(x, y)}{a^2 G_0}, \quad f(x, y) = \frac{G_0}{G(x, y)}, \tag{3-8}$$

where G_0 is constant which has dimension of the shear modulus and a is a characteristic dimension.

Considering the problem for dimensionless variables and using the symmetry of the region $\tilde{\Omega}$ presented in Figure 3 gives the equation

$$\frac{\partial}{\partial X} \left(f(X, Y) \frac{\partial \Psi}{\partial X} \right) + \frac{\partial}{\partial Y} \left(f(X, Y) \frac{\partial \Psi}{\partial Y} \right) = -2 \quad \text{for } (X, Y) \in \tilde{\Omega}. \tag{3-9}$$

The boundary conditions after introducing the dimensionless variables are:

- for the outer boundary:

$$\Psi = 0 \quad \text{for } (x, y) \in \tilde{\Gamma}; \tag{3-10}$$

- for the hollow boundary:

$$\Psi = \Psi_0 \quad \text{for } (x, y) \in \tilde{\Gamma}_I; \tag{3-11}$$

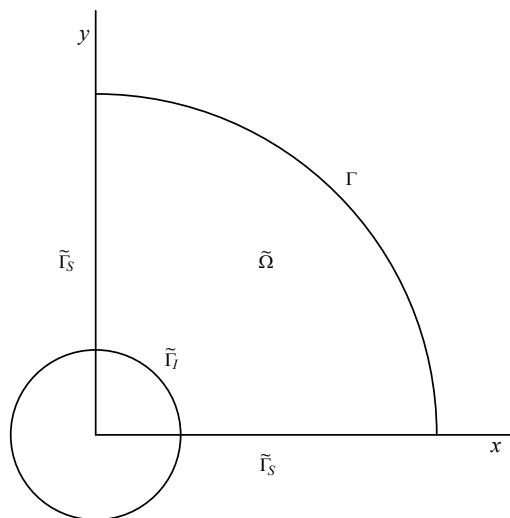


Figure 3. The region under consideration in dimensionless form.

and

$$\oint_{\tilde{\Gamma}_1} \frac{\partial \Psi}{\partial n} ds = - \oint_{\tilde{\Gamma}_1} \frac{1}{f(X, Y)} (X dY - Y dX) - \oint_{\tilde{\Gamma}_1} \frac{1}{f(X, Y)} d\tilde{u}_z, \quad (3-12)$$

where $\tilde{\Gamma}$ is the outer boundary of the bar cross-section, $\tilde{\Gamma}_1$ is the inner boundary of the bar cross-section, $\tilde{\Omega}_I$ is the area of the hollow, and $\tilde{u}_z = u_z/a$ is the dimensionless deflection along the z -axis. The extra condition appears for the symmetry of the region considered:

$$\frac{\partial \Psi}{\partial n} = 0 \quad \text{for } (x, y) \in \tilde{\Gamma}_S. \quad (3-13)$$

4. The numerical method for solving the boundary value problem

The proposal of this paper is to solve the boundary value problem given above by a mesh-free method, the method of fundamental solutions (MFS). The differential equation (3-9) is of the second order with variable coefficients. A procedure based on Picard iteration is proposed to solve the problem of such an equation. Equation (3-9) is rewritten in iterative fashion:

$$\frac{\partial^2 \Psi^{(i)}}{\partial X^2} + \frac{\partial^2 \Psi^{(i)}}{\partial Y^2} = - \frac{1}{f(X, Y)} \left(2 + \frac{\partial f}{\partial X} \frac{\partial \Psi^{(i-1)}}{\partial X} + \frac{\partial f}{\partial Y} \frac{\partial \Psi^{(i-1)}}{\partial Y} \right) \quad \text{for } (X, Y) \in \tilde{\Omega}, \quad (4-1)$$

for $i = 1, 2, \dots$. The boundary conditions have the form

$$\Psi^{(i)} = 0 \quad \text{for } (X, Y) \in \tilde{\Gamma}, \quad (4-2)$$

$$\Psi^{(i)} = \Psi_0 \quad \text{for } (X, Y) \in \tilde{\Gamma}_I, \quad (4-3)$$

$$\oint_{\tilde{\Gamma}_I} \frac{\partial \Psi^{(i)}}{\partial n} ds = - \oint_{\tilde{\Gamma}_I} \frac{1}{f(X, Y)} (X dY - Y dX) - \oint_{\tilde{\Gamma}_I} \frac{1}{f(X, Y)} d\tilde{u}_z, \quad (4-4)$$

$$\frac{\partial \Psi^{(i)}}{\partial n} = 0 \quad \text{for } (X, Y) \in \tilde{\Gamma}_S. \quad (4-5)$$

At each iteration step, the boundary value problem with the Poisson-like equation (4-1) and the boundary conditions (4-2)–(4-5) is to be solved. The governing equation is rewritten in a very general form:

$$L\Psi^{(i)}(X, Y) = F(X, Y, \Psi^{(i-1)}(X, Y)) \quad \text{for } (X, Y) \in \tilde{\Omega}, \quad (4-6)$$

where L is the Laplace operator. The function on the right-hand side of the equation is

$$F(X, Y, \Psi^{(i-1)}(X, Y)) = - \frac{1}{f(X, Y)} \left(2 + \frac{\partial f}{\partial X} \frac{\partial \Psi^{(i-1)}}{\partial X} + \frac{\partial f}{\partial Y} \frac{\partial \Psi^{(i-1)}}{\partial Y} \right). \quad (4-7)$$

The boundary conditions (4-2)–(4-5) are still valid. It is assumed that the solution of the problem is a sum of particular and homogeneous solutions:

$$\Psi^{(i)}(X, Y) = \Psi_p^{(i)}(X, Y) + \Psi_h^{(i)}(X, Y). \quad (4-8)$$

The particular solution is related to the right-hand-side function of the inhomogeneous equation (4-6). The function (4-7) is interpolated by means of radial basis functions (RBFs) in the following manner:

$$F(X, Y, \Psi^{(i-1)}(X, Y)) = \sum_{k=1}^{Na} a_k^{(i)} \varphi_k(X, Y) + \sum_{l=1}^{Nl} b_l^{(i)} p_l(X, Y), \quad (4-9)$$

where $\varphi_k(X, Y) = \varphi(X, Y, X_k^{(a)}, Y_k^{(a)})$ is a RBF, $\{X_k^{(a)}, Y_k^{(a)}\}_{k=1}^{Na}$ is the set of approximation points (see Figure 4) in the region $\tilde{\Omega}$, N_a is the number of approximation points, and $p_l(X, Y)$ for $l = 1, 2, \dots, N_l$ are monomials. Moreover, $\{a_k^{(i)}\}_{k=1}^{Na}$ and $\{b_l^{(i)}\}_{l=1}^{Nl}$ are sets of real numbers, which are determined in each iterative step. The approximated particular solution has the form

$$\Psi^{(i)}(X, Y) = \sum_{k=1}^{Na} a_k^{(i)} \phi_k(X, Y) + \sum_{l=1}^{Nl} b_l^{(i)} P_l(X, Y), \quad (4-10)$$

where $\phi_k(X, Y)$ and $P_l(X, Y)$ functions are particular solutions of the equations

$$L\phi_k(X, X) = \varphi_k(X, X) \quad \text{for } k = 1, 2, \dots, N_a, \quad (4-11)$$

$$LP_l(X, Y) = p_l(X, Y) \quad \text{for } l = 1, 2, \dots, N_l. \quad (4-12)$$

The approximation formula at the i -th iterative step ($i = 1, 2, \dots$) is written for every approximation point chosen in the domain

$$F(X_j^{(a)}, Y_j^{(a)}, \Psi^{(i-1)}(X_j^{(a)}, Y_j^{(a)})) = \sum_{k=1}^{Na} a_k^{(i)} \varphi_k(X_j^{(a)}, Y_j^{(a)}) + \sum_{l=1}^{Nl} b_l^{(i)} p_l(X_j^{(a)}, Y_j^{(a)}) \quad \text{for } j = 1, 2, \dots, N_a, \quad (4-13)$$

$$\sum_{k=1}^{Na} a_k^{(i)} p_l(X_k^{(a)}, Y_k^{(a)}) = 0 \quad \text{for } l = 1, 2, \dots, N_l. \quad (4-14)$$

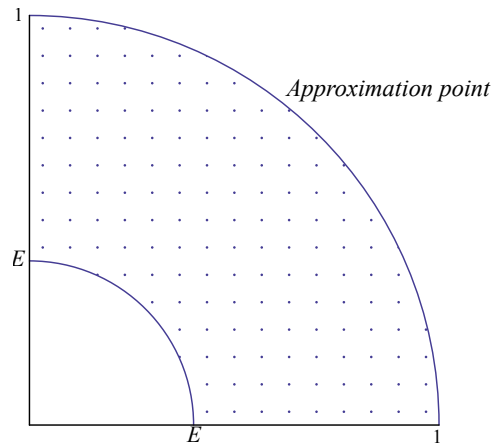


Figure 4. Approximation points.

Once the real coefficients $\{a_k^{(i)}\}_{k=1}^{Na}$ and $\{b_l^{(i)}\}_{l=1}^{Nl}$ are calculated the particular solution of form (4-10) is obtained. In the MFS the approximate homogeneous solution is a linear combination of fundamental solutions:

$$\Psi_h^{(i)}(X, Y) = \sum_{n=1}^{N_s} c_n^{(i)} f_{s_n}(X, Y), \tag{4-15}$$

where $f_{s_n}(X, Y) = f_s(X, Y, X_n^{(s)}, Y_n^{(s)})$ is the fundamental solution defined at the n -th source point. Moreover, $\{X_n^{(s)}, Y_n^{(s)}\}_{n=1}^{N_s}$ is a set of source points, placed outside the region considered (the set of source points is presented in Figure 5), and N_s is the number of source points. The coefficients $c_n^{(i)}$ for $n = 1, 2, \dots, N_s$ are real numbers. These coefficients are to be calculated by solving the linear algebraic equations, which are obtained by introducing (4-8) and (4-15) into the boundary conditions (4-2)–(4-5):

$$\sum_{n=1}^{N_s} c_n^{(i)} f_{s_n}(X_m^{(b)}, Y_m^{(b)}) = -\Psi_p^{(i)}(X_m^{(b)}, Y_m^{(b)}) \quad \text{for } (X_m^{(b)}, Y_m^{(b)}) \in \tilde{\Gamma}_0, \tag{4-16}$$

$$\sum_{n=1}^{N_s} c_n^{(i)} f_{s_n}(X_m^{(b)}, Y_m^{(b)}) = \Psi_0 - \Psi_p^{(i)}(X_m^{(b)}, Y_m^{(b)}) \quad \text{for } (X_m^{(b)}, Y_m^{(b)}) \in \tilde{\Gamma}_1, \tag{4-17}$$

$$\sum_{n=1}^{N_s} c_n^{(i)} \oint_{\tilde{\Gamma}_1} \frac{\partial f_{s_n}(X, Y)}{\partial n} ds = -\oint_{\tilde{\Gamma}_1} \frac{1}{f(X, Y)} (X dY - Y dX) - \oint_{\tilde{\Gamma}_1} \frac{1}{f(X, Y)} d\tilde{u}_z - \oint_{\tilde{\Gamma}_1} \frac{\partial \Psi_p^{(i)}(X, Y)}{\partial n} ds, \tag{4-18}$$

$$\sum_{n=1}^{N_s} c_n^{(i)} \frac{\partial f_{s_n}(X_m^{(b)}, Y_m^{(b)})}{\partial n} = -\frac{\partial \Psi_p^{(i)}(X_m^{(b)}, Y_m^{(b)})}{\partial n} \quad \text{for } (X_m^{(b)}, Y_m^{(b)}) \in \tilde{\Gamma}_s, \tag{4-19}$$

where $\{X_m^{(b)}, Y_m^{(b)}\}_{m=1}^{N_b}$ is a set of boundary points (see Figure 5) and N_b is the number of boundary points.

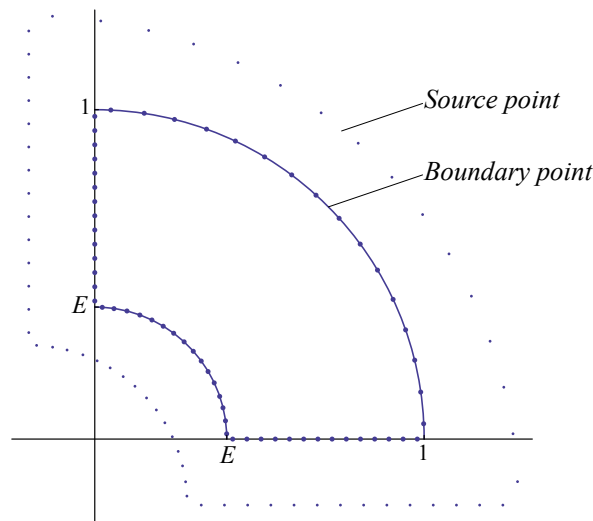


Figure 5. The boundary and source points.

Solution of the system of equations (4-16)–(4-19) introduced to the form of the homogeneous solution (4-15) and to (4-8) gives the approximate solution of the problem. The iteration procedure is stopped if the control parameter defined by the formula

$$d_i = \frac{\sqrt{\sum_{k=1}^{N_t} (\Psi^{(i)}(X_k^t, Y_k^t) - \Psi^{(i-1)}(X_k^t, Y_k^t))^2}}{N_t} \quad \text{for } i = 1, 2, \dots \quad (4-20)$$

is a small number. The formula (4-20) is written for N_t trail points (X_k^t, y_k^t) for $k = 1, 2, \dots, N_t$.

5. Numerical experiment

The numerical experiment has been performed to show the accuracy of the proposed algorithm. The MFS has been implemented with the following parameters. The number of approximation points is 100, the number of source points is 40, and the number of boundary points is 30. The distance between the contour of the region under consideration and the contour with the set of source points is chosen as 0.2.

The calculations are performed for the multiquadric RBF given by

$$\varphi(X, Y, X_j^{(a)}, Y_j^{(a)}) = \sqrt{c^2 + r(X, Y, X_j^{(a)}, Y_j^{(a)})}, \quad (5-1)$$

where

$$r(X, Y, X_j^{(a)}, Y_j^{(a)}) = \sqrt{(X - X_j^{(a)})^2 + (Y - Y_j^{(a)})^2}.$$

The particular solution for the RBF in the form (5-1) is

$$\begin{aligned} \phi(X, Y, X_j^{(a)}, Y_j^{(a)}) = & -\frac{1}{3}c^3 \ln\left(c\sqrt{c^2 + r^2(X, Y, X_j^{(a)}, Y_j^{(a)})} + c^2\right) \\ & + \frac{1}{9}(4c^2 + r^2(X, Y, X_j^{(a)}, Y_j^{(a)}))\sqrt{c^2 + r^2(X, Y, X_j^{(a)}, Y_j^{(a)})}. \end{aligned} \quad (5-2)$$

The parameter of the chosen RBF (5-1) is $c = 0.1$. The monomials $p_l(X, Y)$ and their corresponding particular integrals $P_l(X, Y)$ are as follows:

l	p_l	P_l	l	p_l	P_l
1	1	$\frac{1}{4}(X^2 + Y^2)$	4	XY	$\frac{1}{12}XY(X^2 + Y^2)$
2	X	$\frac{1}{8}X(X^2 + Y^2)$	5	X ²	$\frac{1}{14}(X^4 + X^2y^2 - \frac{1}{6}Y^4)$
3	Y	$\frac{1}{8}Y(X^2 + Y^2)$	6	Y ²	$\frac{1}{14}(Y^4 + X^2y^2 - \frac{1}{6}X^4)$

In the example the torsion of a circular bar (with radius in nondimensional form equal to 1) with a circular centered hollow of radius equal to E is considered. The function related to the shear modulus is defined as

$$\frac{1}{f(X, Y)} = 1 + 5.25\sqrt{X^2 + Y^2}. \quad (5-3)$$

The results for $E = 0.4$ are presented below. The Prandtl function is presented in Figure 6. The unknown value of the Prandtl function on the inner boundary has been calculated. It should have a constant value on the inner boundary. In Table 1 the calculated values of Ψ_0 at some trial points chosen on the inner

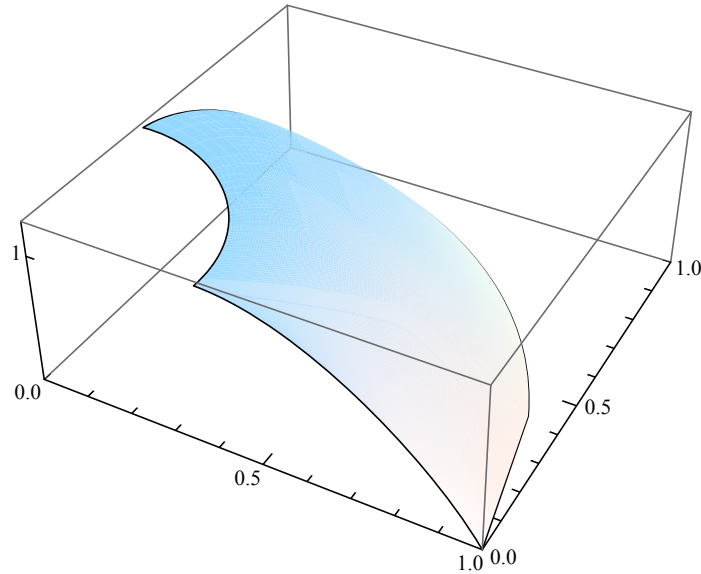


Figure 6. The Prandtl function for a bar with hollow of radius $E = 0.4$.

boundary are presented. The values of Ψ_0 on the boundary are very close to each other. It is correct to take with demanded accuracy Ψ_0 equal to 1.42605.

The accuracy of the obtained result can be confirmed by checking the boundary condition (3-12). The value on the right-hand side of (3-12) is equal to

$$-\oint_{\tilde{\Gamma}_1} \frac{1}{f(X, Y)} (X dY - Y dX) - \oint_{\tilde{\Gamma}_1} \frac{1}{f(X, Y)} d\tilde{u}_z = -0.5026548245743669.$$

X	Y	Ψ_0
0.398766933	0.0313836383	1.426047729150132
0.388947968	0.0933781455	1.426051497720865
0.369551813	0.153073373	1.426050691973953
0.341056066	0.208999426	1.426050690505380
0.3041623862	0.259779219	1.426050814325789
0.2597792193	0.304162386	1.426050908371237
0.208999426	0.341056066	1.426050402589498
0.153073373	0.369551813	1.426051442033329
0.0933781455	0.388947968	1.426049341092722
0.0313836383	0.398766933	1.426054977550235

Table 1. The values of the Prandtl function on the inner boundary for $E = 0.4$.

E	Ψ_0	$\oint_{\Gamma_1} (\partial\Psi/\partial n) ds$	$I(E)$
0.1	1.931868393966856	-0.031415926344492	-0.031415926535898
0.2	1.803559095926270	-0.125663706148103	-0.125663706143592
0.3	1.632842169956845	-0.282743338761668	-0.282743338823081
0.4	1.426050772804763	-0.502654824541456	-0.502654824574367
0.5	1.195205510255710	-0.785398163408337	-0.785398163397448
0.6	0.949110141725394	-1.130973355347243	-1.130973355292326
0.7	0.698569048610646	-1.539380400193735	-1.539380400258998

Table 2. The values of the Prandtl function on the inner boundary and checking boundary condition (3-12).

On the other side, the left-hand side of (3-6) is an integral of the normal derivative of the numerically calculated Prandtl function and it equals

$$\oint_{\Gamma_1} \frac{\partial\Psi}{\partial n} ds = -0.5026548245414568.$$

It is easy to observe that the difference between both values is 3.29101^{-11} . So, the calculated results are obtained with a very high accuracy.

The problem is solved for a rod with hollow radius $E_i = 0.1i$ for $i = 1, 2, \dots, 7$. The values of Ψ_0 and the fulfillment of the boundary condition (3-12) are presented in Table 2. It is observed that the difference

$$I(E) = \oint_{\Gamma_1} \frac{\partial\Psi}{\partial n} ds - \left(-\oint_{\bar{\Gamma}_1} \frac{1}{f(X, Y)} (X dY - Y dX) - \oint_{\bar{\Gamma}_1} \frac{1}{f(X, Y)} d\tilde{u}_z \right)$$

for all cases of E presented in Table 2 are of order 10^{-11} or 10^{-10} . This confirms that the numerical method based on the proposed algorithm is of very high accuracy and gives very good results. It is a suitable tool for solving the problem.

6. Conclusions

In this paper the torsion of a long bone is considered. The long bone is modeled as a bar with circular cross-section with a circular hollow. The proper assumption about the material of the bone have been made. The bone material is treated as a functionally graded material. This paper implements the method of fundamental solutions to solve the problem of long-bone torsion modeled by a boundary value problem with a linear partial differential equation with variable coefficients and boundary conditions. The results of the numerical experiment show that the proposed method gives results with the demanded accuracy. The presented algorithm is a self-validating one. It is possible to prove the high precision of the obtained numerical results by checking the fulfillment of the boundary conditions. The analysis of the numerical results shown in Section 5 confirms that the numerical method based on the proposed algorithm is of very high accuracy and gives very good results. It is a suitable tool to solve the problem.

References

- [Arghavan and Hematiyan 2009] S. Arghavan and M. R. Hematiyan, “Torsion of functionally graded hollow tubes”, *Eur. J. Mech. A Solids* **28**:3 (2009), 551–559.
- [Chen 1964] Y. Chen, “Torsion of nonhomogeneous bars”, *J. Franklin Inst.* **277**:1 (1964), 50–54.
- [Daegling 2002] D. J. Daegling, “Estimation of torsional rigidity in primate long bones”, *J. Hum. Evol.* **43**:2 (2002), 229–239.
- [Ecsedi 2009] I. Ecsedi, “Some analytical solutions for Saint-Venant torsion of non-homogeneous cylindrical bars”, *Eur. J. Mech. A Solids* **28**:5 (2009), 985–990.
- [Elias et al. 2000] J. J. Elias, F. J. Frassica, and E. Y. S. Chao, “The open section effect in a long bone with a longitudinal defect: a theoretical modeling study”, *J. Biomech.* **33**:11 (2000), 1517–1522.
- [Ely and Zienkiewicz 1960] J. F. Ely and O. C. Zienkiewicz, “Torsion of compound bars: a relaxation solution”, *Int. J. Mech. Sci.* **1**:4 (1960), 356–365.
- [Fairweather and Karageorghis 1998] G. Fairweather and A. Karageorghis, “The method of fundamental solutions for elliptic boundary value problems”, *Adv. Comput. Math.* **9**:1-2 (1998), 69–95.
- [Golberg and Chen 1999] M. A. Golberg and C. S. Chen, “The method of fundamental solutions for potential, Helmholtz and diffusion problems”, pp. 103–176 in *Boundary integral methods: numerical and mathematical aspects*, edited by M. A. Golberg, Comput. Eng. **1**, WIT Press, Boston, 1999.
- [Horgan and Chan 1999] C. O. Horgan and A. M. Chan, “Torsion of functionally graded isotropic linearly elastic bars”, *J. Elasticity* **52**:2 (1999), 181–199.
- [Kupradze and Aleksidze 1964] V. D. Kupradze and M. A. Aleksidze, “The method of functional equations for the approximate solution of certain boundary value problems”, *Ž. Vyčisl. Mat. i Mat. Fiz.* **4**:4 (1964), 683–715. In Russian; translated in *USSR Comput. Math. Math. Phys.* **4**:4 (1964), 82–126.
- [Mathon and Johnston 1977] R. Mathon and R. L. Johnston, “The approximate solution of elliptic boundary-value problems by fundamental solutions”, *SIAM J. Numer. Anal.* **14**:4 (1977), 638–650.
- [Pierce et al. 2004] M. C. Pierce, G. E. Bertocci, E. Vogeley, and M. S. Moreland, “Evaluating long bone fractures in children: a biomechanical approach with illustrative cases”, *Child Abus. Negl.* **28**:5 (2004), 505–524.
- [Pompe et al. 2003] W. Pompe, H. Worch, M. Epple, W. Friess, M. Gelinsky, P. Greil, U. Hempel, D. Scharnweber, and K. Schulte, “Functionally graded materials for biomedical applications”, *Mater. Sci. Eng. A* **362**:1–2 (2003), 40–60.

Received 3 Nov 2010. Revised 8 Aug 2011. Accepted 15 Dec 2011.

ANITA USCILOWSKA: anita.uscilowska@put.poznan.pl
Institute of Applied Mechanics, Poznan University of Technology, ul. Jana Pawla II 24, 60-965 Poznan, Poland

AGNIESZKA FRASKA: agnieszka.fraska@put.poznan.pl
Institute of Applied Mechanics, Poznan University of Technology, ul. Jana Pawla II 24, 60-965 Poznan, Poland

RAYLEIGH-TYPE WAVE PROPAGATION IN AN AUXETIC DIELECTRIC

ANDRZEJ DRZEWIECKI

The propagation of Rayleigh-type waves in an elastic, isotropic, dielectric half-space for some orientation of the external electric field is considered, with Poisson's ratio in the range $-1 < \nu < 0.5$.

1. Introduction

Auxetics are materials that have a negative Poisson's ratio [Stręk et al. 2008; 2009; 2010; Poźniak et al. 2010]. The earliest publications providing information on the unusual auxetic properties of certain natural materials appeared almost a hundred years ago, but they did not arouse great interest because of the low reproducibility of the reported experimental results. Physicists and engineers were also convinced for a long time that there are no materials with negative Poisson's ratio in nature, despite the fact that their existence was known to be thermodynamically possible (see, for example, [Landau and Lifshits 1954]). The possible applications of materials having this property were also overlooked at the time.

Contemporary studies of auxetics were started after the publication of [Lakes 1987]. Soon, numerous possible applications of these materials were identified, such as body armor, packing material, knee and elbow pads, robust shock absorbing material, sponge mops and many others. This is the reason for the dynamic development of these materials research in recent years (see [Friis et al. 1988; Lakes and Wineman 2006], for example).

A few articles have considered the dynamic behavior of auxetics materials in the framework of coupled field theory. Here we discuss the problem of propagation of the Rayleigh-type waves in such media. Specifically, we consider elastic, isotropic, and dielectric half-space with Poisson's ratio in the range $(-1; 0.5)$, subject to an external electric field in some fixed orientation. We derive the propagation equation and solve it numerically in special cases.

We adopt a statistical model (according to the classification by K. Hutter and A. A. F. van de Ven) for the interaction between electromagnetic and mechanical fields. To render the basic equations amenable to direct analysis, they are linearized with respect to some average state, referred to as the ξ state. The problem at hand suggests a natural definition of this state. It is assumed that ξ state is known or at least determinable. All physical fields may be decomposed into two parts: the tensor fields in the ξ state and tensor fields correction expressing the difference between the ξ state and the real state, in the framework of the model. In this paper they are denoted by ${}^0\varphi$ and ${}^*\varphi$ respectively, where φ is the tensor field in question. Because the perturbations ${}^*\varphi$ are assumed to be small, the governing equations can be linearized.

Partially supported by Poland's Ministry of Science and Higher Education (MNiSzW), grant 2363/B/TO2/2010/39.

Keywords: auxetics, Rayleigh wave, dielectric.

2. Setting up the equations

The specific version of the basic equations derived in [Hutter and van de Ven 1978] that is presented below corresponds with the problem under consideration. This specification is confined to the choice of free energy form and proper definition of some average state. It is assumed that the ξ state is a motionless, rigid body state and the electric field in this state is static and homogeneous. These assumptions are not contradictory, but in general a stress vector acting at the surface that bounds a dielectric is needed.

The free energy is postulated in the form (material description):

$$F = -\frac{1}{2\mu_0\rho_0} \frac{\kappa'}{1+\kappa'} B_\alpha B_\alpha + \frac{1}{2\rho_0\epsilon_0\kappa} P_\alpha P_\alpha - \frac{1}{2}n(\Theta - \Theta_0)^2 - \gamma(\Theta - \Theta_0)E_{\gamma\gamma} + \frac{1}{\rho_0}\mu' E_{\alpha\beta} E_{\alpha\beta} + \frac{1}{2\rho_0}\lambda' E_{\alpha\alpha} E_{\beta\beta}, \quad (1)$$

where κ' is the magnetic susceptibility, κ the electric susceptibility, λ' , μ' are the elastic constants, ρ_0 the mass density, B_α the magnetic induction, P_α the magnetic induction, Θ the absolute temperature, γ , n the material constants, $C_{\alpha\beta}$ Green's deformation tensor, $E_{\alpha\beta} = \frac{1}{2}(C_{\alpha\beta} - \delta_{\alpha\beta})$ the Lagrangian strain tensor, ϵ_0 the electric permeability of vacuum and μ_0 the magnetic permeability of vacuum.

With this choice, the constitutive equations read:

$$\begin{aligned} S &= -\frac{\partial F}{\partial \Theta} = n(\Theta - \Theta_0) + \delta E_{\alpha\alpha}, & E_\alpha &= \frac{\partial F}{\partial (P_\alpha/\rho_0)} = \frac{1}{\epsilon_0\kappa} P_\alpha, & M_\alpha &= -\rho_0 \frac{\partial F}{\partial B_\alpha} = \frac{\kappa'}{\mu_0(1+\kappa')} B_\alpha, \\ T_{\alpha\beta} &= T_{i\alpha} F_{\beta i}^{-1} = 2\rho_0 \frac{\partial F}{\partial C_{\alpha\beta}} - (P_\alpha E_\gamma - B_\alpha M_\gamma) C_{\beta\gamma}^{-1} - M_\gamma B_\gamma C_{\alpha\beta}^{-1} \\ &= 2\mu' E_{\alpha\beta} + \lambda' \delta_{\alpha\beta} E_{\gamma\gamma} - \rho_0 \gamma \delta_{\alpha\beta} (\Theta - \Theta_0) \\ &\quad - \left(\frac{1}{\epsilon_0\kappa} P_\alpha P_\gamma - \frac{\kappa'}{\mu_0(1+\kappa')} B_\alpha B_\gamma \right) C_{\beta\gamma}^{-1} - \frac{\kappa'}{\mu_0(1+\kappa')} B_\gamma B_\gamma C_{\alpha\beta}^{-1}, \end{aligned} \quad (2)$$

where S is the entropy density, E_α the electric field intensity, M_α the magnetization, $T_{i\alpha}$ the Piola–Kirchhoff stress tensor, $F_{i\alpha}$ the material deformation gradient, $F_{\alpha i}^{-1}$ the spatial deformation gradient and $C_{\alpha\beta}^{-1}$ Cauchy's deformation tensor.

For an adiabatic process one obtains

$$\Theta - \Theta_0 = -\frac{\delta}{n} E_{\alpha\alpha} \quad (3)$$

and the constitutive relation (2) can be replaced by

$$T_{\alpha\beta} = 2\mu E_{\alpha\beta} + \lambda \delta_{\alpha\beta} E_{\gamma\gamma} - \left(\frac{1}{\epsilon_0\kappa} P_\alpha P_\gamma - \frac{\kappa'}{\mu_0(1+\kappa')} B_\alpha B_\gamma \right) C_{\beta\gamma}^{-1} - \frac{\kappa'}{\mu_0(1+\kappa')} B_\gamma B_\gamma C_{\alpha\beta}^{-1}, \quad (4)$$

where

$$\lambda = \lambda' + \rho_0 \frac{\gamma^2}{n}, \quad \mu = \mu' \quad (5)$$

are the adiabatic elastic constants.

As a result of the linearizing procedure one reaches the equations of motion

$$\rho_0 \ddot{u}_\alpha = \mu u_{\alpha,\beta\beta} + (\lambda + \mu) u_{\beta,\beta\alpha} - \frac{1}{\epsilon_0\kappa} P_\alpha^* P_{\beta,\beta} \quad (6)$$

(u_α stands for the displacement), the Maxwell equations

$$\begin{aligned} {}^*B_{\alpha,\alpha} = 0, \quad {}^*\dot{B}_\alpha + \frac{1}{\epsilon_0\kappa} e_{\alpha\beta\gamma} {}^*P_{\gamma,\beta} = 0, \quad \left(\frac{1}{\kappa} + 1\right) {}^*P_{\alpha,\alpha} - \frac{1}{\kappa} {}^0P_\beta u_{\beta,\alpha\alpha} = 0, \\ -\left(\frac{1}{\kappa} + 1\right) {}^*\dot{P}_\alpha + \frac{1}{\kappa} {}^0P_\gamma \dot{u}_{\gamma,\alpha} + \frac{1}{\mu_0(1+\kappa')} e_{\alpha\beta\gamma} {}^*B_{\gamma,\beta} = 0, \end{aligned} \quad (7)$$

$$e_{\alpha\beta\gamma} {}^0P_{\gamma,\beta} = 0, \quad {}^0P_{\alpha,\alpha} = 0, \quad (8)$$

and the jump conditions

$$\left[\epsilon_0 {}^0E_\alpha^+ - \left(1 + \frac{1}{\kappa}\right) {}^0P_\alpha^- \right] N_\alpha = 0, \quad e_{\alpha\beta\gamma} \left({}^0E_\alpha^+ - \frac{1}{\epsilon_0\kappa} {}^0P_\beta^- \right) N_\gamma = 0, \quad ({}^*B_\alpha^+ - {}^*B_\alpha^-) N_\alpha = 0, \quad (9a)$$

$$T_i^+ = \frac{1}{2} \delta_{i\beta} {}^0P_\alpha^- {}^0E_\beta^+ N_\alpha - \frac{1}{2\epsilon_0\kappa} \delta_{i\beta} {}^0P_\alpha^- {}^0P_\beta^- N_\alpha, \quad e_{\alpha\beta\gamma} \left({}^*E_\beta^+ - \frac{1}{\epsilon_0\kappa} {}^*P_\beta^- \right) N_\gamma = 0, \quad (9b)$$

$$\left[\epsilon_0 {}^*E_\alpha^+ - \left(1 + \frac{1}{\kappa}\right) {}^*P_\alpha^- \right] N_\alpha + {}^0P_\alpha^- u_{\gamma,\gamma} N_\alpha - \left(\epsilon_0 {}^0E_\gamma^+ - \frac{1}{\kappa} {}^0P_\gamma^- \right) (u_{\gamma,\alpha} - u_{\alpha,\gamma}) N_\alpha = 0, \quad (9c)$$

$$\frac{1}{\mu_0} e_{\alpha\beta\gamma} \left({}^*B_\beta^+ - \frac{1}{1+\kappa'} {}^*B_\beta^- \right) N_\gamma + {}^0P_\gamma^- \dot{u}_\alpha N_\gamma - \left(\epsilon_0 {}^0E_\alpha^+ - \frac{1}{\kappa} {}^0P_\alpha^- \right) \dot{u}_\gamma N_\gamma = 0, \quad (9d)$$

$$\begin{aligned} [\mu(u_{\omega,\beta} + u_{\beta,\omega}) - \delta_{\omega\beta} \lambda u_{\gamma,\gamma}] N_\beta = \frac{1}{2} u_{\alpha,\omega} {}^0P_\beta^- \left({}^0E_\alpha^+ + \frac{1}{\epsilon_0\kappa} {}^0P_\alpha^- \right) N_\beta \\ - \frac{1}{2} {}^0P_\beta^- \left({}^*E_\omega^+ + \frac{1}{\epsilon_0\kappa} {}^*P_\omega^- \right) N_\beta - \frac{1}{2} {}^*P_\beta^- \left({}^0E_\omega^+ + \frac{1}{\epsilon_0\kappa} {}^0P_\omega^- \right) N_\beta. \end{aligned} \quad (9e)$$

The elastic dielectric is placed on the “-” side of the surface (see Figure 1). It is assumed that T_i^+ (needed for the mechanical equilibrium of motionless rigid body placed in the electric field) is the only surface traction of the other than electromagnetic origin. The quantities ${}^0E_\alpha^+$, ${}^*E_\alpha^+$ and ${}^*B_\alpha^+$ are defined by

$${}^0E_\alpha^+ = \delta_{i\alpha} {}^0e_i^+, \quad {}^*E_\alpha^+ = \delta_{i\alpha} {}^*e_i^+ + \delta_{i\beta} {}^0e_i^+ u_{\beta,\alpha}, \quad {}^*B_\alpha^+ = \delta_{i\alpha} {}^*b_i^+, \quad (10)$$

where ${}^0e_i^+$, ${}^*e_i^+$, ${}^*b_i^+$ are the limits to which tend the decomposed fields e_i , b_i on the surface. The latter vector fields are the electric field intensity and the magnetic induction in vacuum.

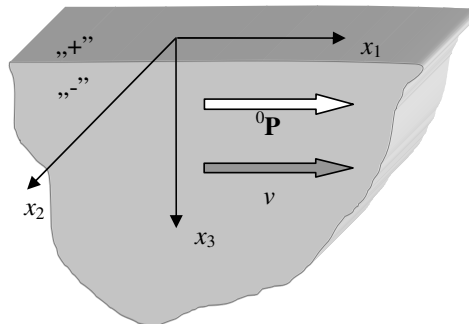


Figure 1. The geometry of the problem.

The vectors of electromagnetic field in vacuum satisfy the following equations:

$$e_{ijk}e_{k,j} = -\dot{b}_i, \quad e_{i,i} = 0, \quad \frac{1}{\mu_0}e_{ijk}b_{k,j} = \epsilon_0\dot{e}_i, \quad b_{i,i} = 0, \quad (11)$$

$$e_{ijk}{}^0e_{k,j} = 0, \quad {}^0e_{i,i} = 0, \quad e_{ijk}{}^*e_{k,j} = -{}^*b_i, \quad {}^*e_{i,i} = 0, \quad \frac{1}{\mu_0}e_{ijk}{}^*b_{k,j} = \epsilon_0{}^*\dot{e}_i, \quad {}^*b_{i,i} = 0. \quad (12)$$

3. Rayleigh-type wave

The geometry of the problem is shown in Figure 1. The initial uniform electric polarization 0P has the direction of x_1 axis. Consider the propagation equations of a Rayleigh-type surface wave [Eringen and Suhubi 1975; Nowacki 1970; Miklowitz 1978] in the same direction:

$$\begin{aligned} \{u_1, u_3, P_1, P_3, B_2\} &= \{\tilde{u}_1(x_3), \tilde{u}_3(x_3), \tilde{P}_1(x_3), \tilde{P}_3(x_3), \tilde{B}_2(x_3)\} \exp[i\gamma(vt - x_1)], \\ \{e_1, e_3, b_2\} &= \{\tilde{e}_1(x_3), \tilde{e}_3(x_3), \tilde{b}_2(x_3)\} \exp[i\gamma(vt - x_1)]. \end{aligned} \quad (13)$$

In the above equations and in the further considerations the following description (which should not lead to failures) is introduced:

$${}^*P_\alpha = P_\alpha, \quad {}^*B_\alpha = B_\alpha, \quad {}^*e_i = e_i, \quad {}^*b_i = b_i, \quad {}^0P_\alpha = \delta_{\alpha 1}P. \quad (14)$$

After simply calculations one obtains the following system of the ordinary differential equations valid in the half space $x_3 > 0$.

$$\begin{aligned} c_2^2\tilde{u}_1'' + \gamma^2(v^2 - c_1^2)\tilde{u}_1 - i\gamma(c_1^2 - c_2^2)\tilde{u}_3' + i\frac{\gamma P}{\rho_0\epsilon_0\kappa}\tilde{P}_1 - \frac{P}{\rho_0\epsilon_0\kappa}\tilde{P}_3' &= 0, \\ c_1^2\tilde{u}_3'' + \gamma^2(v^2 - c_2^2)\tilde{u}_3 - i\gamma(c_1^2 - c_2^2)\tilde{u}_1' &= 0, \\ \tilde{P}_1'' - \gamma^2\alpha\tilde{P}_1 - i\frac{\gamma^3\alpha}{1+\kappa}P\tilde{u}_1 + i\frac{\gamma}{1+\kappa}P\tilde{u}_1'' &= 0, \\ \tilde{P}_3'' - \gamma^2\alpha\tilde{P}_3 + \frac{\gamma^2\alpha}{1+\kappa}P\tilde{u}_1' - \frac{1}{1+\kappa}P\tilde{u}_1''' &= 0. \end{aligned} \quad (15)$$

The amplitude \tilde{B}_2 satisfies the equation

$$\tilde{B}_2'' - \gamma^2\alpha\tilde{B}_2 = 0. \quad (16)$$

In (15) and (16) the following notation has been introduced:

$$\alpha = 1 - (1 + \kappa)(1 + \kappa')\frac{v^2}{c_0^2}, \quad c_1^2 = \frac{\lambda + 2\mu}{\rho_0}, \quad c_2^2 = \frac{\mu}{\rho_0}, \quad (17)$$

$$\frac{d\tilde{\phi}}{dx_3} = \tilde{\phi}', \quad \frac{d^2\tilde{\phi}}{dx_3^2} = \tilde{\phi}'', \quad \frac{d^3\tilde{\phi}}{dx_3^3} = \tilde{\phi}'''. \quad (18)$$

The characteristic equation of the system (15) is

$$\epsilon(\epsilon^2 - \gamma^2\alpha)^2 \{ c_1^2(c_2^2 - v^2)\epsilon^4 + [(v^2 + v^2)(c_1^2 + c_2^2) - 2c_1^2c_2^2 - v^2v^2]\gamma^2\epsilon^2 + [v^2(v^2 - c_2^2) + (v^2 - c_1^2)(v^2 - c_2^2)]\gamma^4 \} = 0, \quad (19)$$

where

$$v^2 = \frac{P^2}{\rho_0\epsilon_0\kappa(1 + \kappa)}. \quad (20)$$

The solutions of the set of (15) have finally the form

$$\begin{aligned} \tilde{u}_1 &= S_1 \exp(\epsilon_1 x_3) + S_2 \exp(\epsilon_2 x_3), \\ \tilde{u}_3 &= \frac{i\gamma\epsilon_1(c_1^2 - c_2^2)}{c_1^2\epsilon_1^2 + \gamma^2(v^2 - c_2^2)} S_1 \exp(\epsilon_1 x_3) + \frac{i\gamma\epsilon_2(c_1^2 - c_2^2)}{c_1^2\epsilon_2^2 + \gamma^2(v^2 - c_2^2)} S_2 \exp(\epsilon_2 x_3), \\ \tilde{P}_1 &= S_3 \exp(-\gamma\sqrt{\alpha}x_3) - \frac{i\gamma P}{1 + \kappa} S_1 \exp(\epsilon_1 x_3) - \frac{i\gamma P}{1 + \kappa} S_2 \exp(\epsilon_2 x_3), \\ \tilde{P}_3 &= -\frac{i}{\sqrt{\alpha}} S_3 \exp(-\gamma\sqrt{\alpha}x_3) + \frac{\epsilon_1 P}{1 + \kappa} S_1 \exp(\epsilon_1 x_3) + \frac{\epsilon_2 P}{1 + \kappa} S_2 \exp(\epsilon_2 x_3), \end{aligned} \quad (21)$$

where S_1, S_2 and S_3 are constants, and ϵ_1 and ϵ_2 are the roots of the expression in (outer) braces in (19), which satisfy the restriction $\text{Re } \epsilon < 0$. There is no physical singularity for $\epsilon_1 = \epsilon_2$ and $\epsilon_1 = \epsilon_2 = -\gamma\sqrt{\alpha}$. Similarly, the solution of the (16) is

$$\tilde{B}_2 = \frac{i}{\epsilon_0\kappa v} \frac{1 - \alpha}{\sqrt{\alpha}} S_3 \exp(-\gamma\sqrt{\alpha}x_3). \quad (22)$$

In the same way we obtain the following solution for the electromagnetic field in a vacuum:

$$\tilde{e}_1 = G \exp(\gamma\sqrt{\beta}x_3), \quad \tilde{e}_3 = \frac{i}{\sqrt{\beta}} G \exp(\gamma\sqrt{\beta}x_3), \quad \tilde{b}_2 = \frac{i(\beta - 1)}{v\sqrt{\beta}} G \exp(\gamma\sqrt{\beta}x_3), \quad (23)$$

where

$$\beta = 1 - \frac{v^2}{c_0^2}. \quad (24)$$

Successive relations between S_1, S_2, S_3 and G are the consequence of fact that jump conditions (9) hold true. In this case they become

$$\begin{aligned} e_1^+ + \frac{P}{\epsilon_0\kappa} u_{1,1} - \frac{1}{\epsilon_0\kappa} P_1^- = 0, \quad e_3^+ + \frac{P}{\epsilon_0\kappa} u_{1,3} - \frac{\kappa + 1}{\epsilon_0\kappa} P_3^- = 0, \quad b_2^+ - \frac{1}{1 + \kappa} B_2^- = 0, \\ u_{1,3} + u_{3,1} = 0, \quad (c_1^2 - 2c_2^2)u_{1,1} + c_1^2 u_{3,3} = 0. \end{aligned} \quad (25)$$

After substitutions it is easy to obtain that

$$G = -\sqrt{\frac{\beta}{\alpha}} \frac{1 + \kappa}{\epsilon_0\kappa} S_3. \quad (26)$$

This conclusion follows from the third equality in (25). The second equality in (25) is satisfied identically. Finally the following set of equations has to be considered:

$$R_1 S_1 + R_2 S_2 + R_3 S_3 = 0, \quad Q_1 S_1 + Q_2 S_2 = 0, \quad W_1 S_1 + W_2 S_2 = 0, \quad (27)$$

where

$$R_1 = R_2 = i\gamma\sqrt{\alpha}\frac{\kappa P}{1+\kappa}, \quad R_3 = \sqrt{\beta}(1+\kappa) + \sqrt{\alpha}, \quad k = 1, 2$$

$$Q_k = \left[1 + \frac{\gamma^2(c_1^2 - c_2^2)}{c_1^2\epsilon_k^2 + \gamma^2(v^2 - c_2^2)}\right]\epsilon_k, \quad W_k = \frac{\epsilon_k^2 c_1^2 (c_1^2 - c_2^2)}{c_1^2 \epsilon_k^2 + \gamma^2 (v^2 - c_2^2)} - c_1^2 + 2c_2^2. \quad (28)$$

Then in the case under consideration, the propagation condition of the Rayleigh-type wave has the form

$$\begin{vmatrix} R_1 & R_2 & R_3 \\ Q_1 & Q_2 & 0 \\ W_1 & W_2 & 0 \end{vmatrix} = 0. \quad (29)$$

If the condition (29) holds true, it is possible to solve the system (27) with the respect of S_1 and S_2 :

$$S_1 = -\frac{R_3 Q_2}{R_1 Q_2 - R_2 Q_1} S_3, \quad S_2 = \frac{R_3 Q_1}{R_1 Q_2 - R_2 Q_1} S_3. \quad (30)$$

For the analysis in the sequel it is convenient to use some dimensionless quantities

$$a = \frac{c_1^2}{c_2^2}, \quad g = \frac{v^2}{c_2^2}, \quad f = \frac{\nu^2}{c_2^2}, \quad \tilde{\epsilon} = \frac{\epsilon}{\gamma}. \quad (31)$$

The substitutions (31), applied to (29), yield

$$[a(\tilde{\epsilon}_1^2 + 1) + f - 2][a(\tilde{\epsilon}_2^2 + 1) + 2f - 2 - fa]\tilde{\epsilon}_1 - [a(\tilde{\epsilon}_2^2 + 1) + f - 2][a(\tilde{\epsilon}_1^2 + 1) + 2f - 2 - fa]\tilde{\epsilon}_2 = 0. \quad (32)$$

Similarly, writing explicitly the equation from which the roots ϵ_1 and ϵ_2 are determined (see (19)), the following expression has been obtained:

$$a(1-g)\tilde{\epsilon}^4 + [(f+g)(a+1) - 2a - fg]\tilde{\epsilon}^2 + [(f-1)(g+f-a)] = 0. \quad (33)$$

The root of (33) do not depend on γ . They are the functions of material constants, P and ν only. Then, from the propagation condition follows that ν does not depend on γ , too (it is convenient to consider this condition in the form (32)). There is no dispersion comparing to in the classical case [Stręk et al. 2010].

4. Some results for classical and auxetic materials

The propagation condition (32) can only be examined numerically. The only exception is the case $a = 2$ (Poisson ratio $\nu = 0$), for which analytical analysis is possible. The results obtained in this case are similar (though not identical) to results which are in force for auxetic materials. These results have not been presented in the paper.

In Figure 2 the dependence of dimensionless phase velocity f on dimensionless (low) external electric field strength g (see (20) and (31)) for conventional material is presented in two scales. In the area bounded by the curve in the shape of a loop, the roots of (33) are complex. There is an interval of values of parameter g for which the wave does not propagate ($g \in (g_B, g_C)$).

In Figure 3 the same dependence for strong external electric field is presented.

For the auxetic [Stręk et al. 2009] material and for the weak external electric field, character of examined dependence is similar to presented above (Figure 2). Significant differences become apparent in the case of strong external electric field ($g \geq g_C$). In this case two extra modes (rapidly vanishing

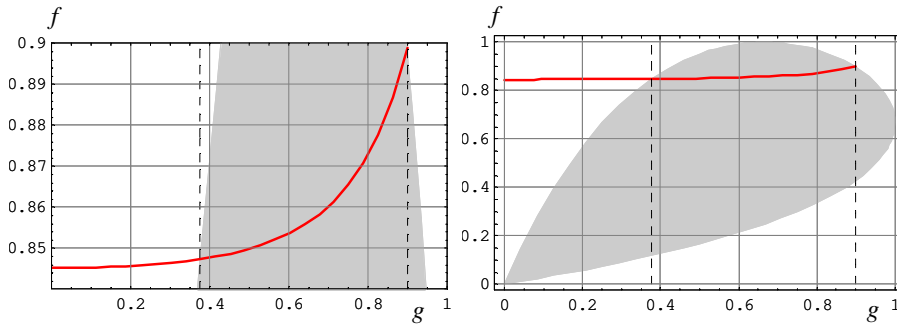


Figure 2. The case $a = 3$ (conventional material, $\nu = 0.25$); $g \leq g_B \approx 0.8990$.

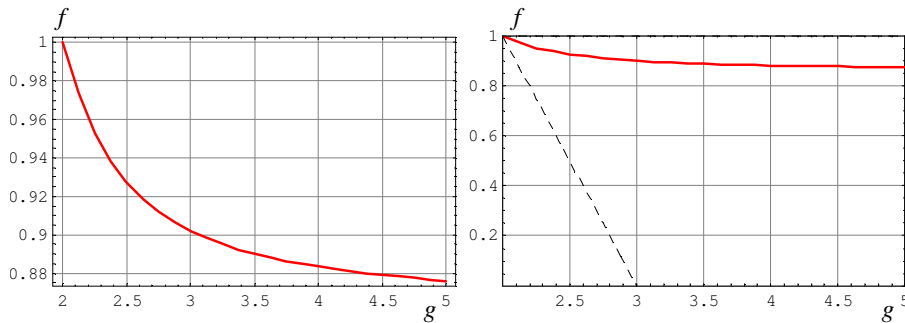


Figure 3. The case $a = 3$ (conventional material, $\nu = 0.25$); $g \geq g_C = 1$.

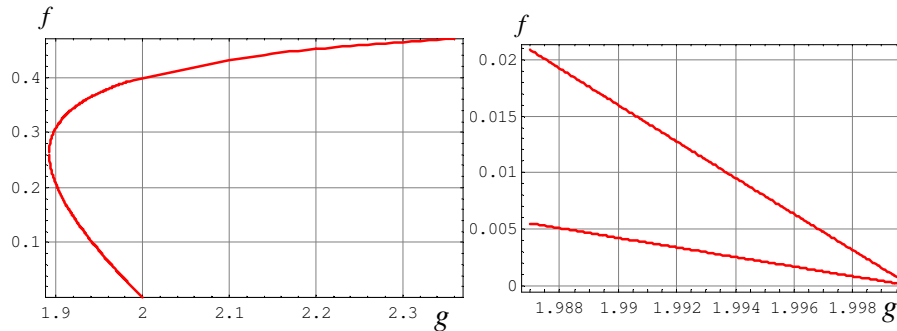


Figure 4. The case $a = 1.5$ (auxetic, $\nu = -0.25$), $g \geq g_C \approx 1.8925$.

with increasing of g) of the wave appear. In the previously reported case, f decreased with increasing g (Figure 3). The other situation is for the “fast”, not disappearing mode of the wave in the auxetic. The increase in g results in an increase of f . Similar results were obtained in the previously mentioned case $\nu = 0$. In this case for strong external electric field only two modes of the wave appear.

In Figure 4 the dependence of dimensionless phase velocity f on dimensionless (strong) external electric field g for the auxetic material is presented in two scales. Lowest mode fades so quickly that it was necessary to present it choosing a different scale (Figure 4, right).

References

- [Eringen and Suhubi 1975] A. C. Eringen and E. S. Suhubi, *Elastodynamics, II: Linear theory*, Academic Press, New York, 1975.
- [Friis et al. 1988] E. A. Friis, R. S. Lakes, and J. B. Park, “Negative Poisson’s ratio polymeric and metallic foams”, *J. Mater. Sci.* **23**:12 (1988), 4406–4414.
- [Hutter and van de Ven 1978] K. Hutter and A. A. F. van de Ven, *Field matter interactions in thermoelastic solids: unification of existing theories of electro-magneto-mechanical interactions*, Lecture Notes in Physics **88**, Springer, Berlin, 1978.
- [Lakes 1987] R. S. Lakes, “Foam structures with a negative Poisson’s ratio”, *Science* **235**:4792 (1987), 1038–1040.
- [Lakes and Wineman 2006] R. S. Lakes and A. Wineman, “On Poisson’s ratio in linearly viscoelastic solids”, *J. Elasticity* **85**:1 (2006), 45–63.
- [Landau and Lifshits 1954] L. D. Landau and E. M. Lifshits, *Механика сплошных сред*, Gos. Izd. tekhn.-teoret. lit., Moscow, 1954. Translated as *Fluid mechanics*, Pergamon, London, 1959.
- [Miklowitz 1978] J. Miklowitz, *The theory of elastic waves and waveguides*, Series in Applied Mathematics and Mechanics **22**, North-Holland, Amsterdam, 1978.
- [Nowacki 1970] W. Nowacki, *Teoria sprężystości*, PWN, Warsaw, 1970.
- [Poźniak et al. 2010] A. A. Poźniak, H. Kamiński, P. Kędziora, B. Maruszewski, T. Stręk, and K. W. Wojciechowski, “Anomalous deformation of constrained auxetic square”, *Rev. Adv. Mater. Sci.* **23**:2 (2010), 169–174.
- [Stręk et al. 2008] T. Stręk, B. Maruszewski, J. W. Narojczyk, and K. W. Wojciechowski, “Finite element analysis of auxetic plate deformation”, *J. Non-Cryst. Solids* **354**:35–39 (2008), 4475–4480.
- [Stręk et al. 2009] T. Stręk, P. Kędziora, B. Maruszewski, A. A. Poźniak, K. V. Tretiakov, and K. W. Wojciechowski, “Finite element analysis of auxetic obstacle deformation and fluid flow in a channel”, *J. Non-Cryst. Solids* **355**:24–27 (2009), 1387–1392.
- [Stręk et al. 2010] T. Stręk, B. Maruszewski, A. A. Poźniak, and K. W. Wojciechowski, “Computational modelling of auxetics”, pp. 265–284 in *Finite element analysis*, edited by D. Moratal, Sciyo, Rijek, 2010.

Received 24 Jan 2011. Revised 12 Dec 2011. Accepted 29 Dec 2011.

ANDRZEJ DRZEWIECKI: andrzej.drzewiecki@put.poznan.pl

Poznań University of Technology, Institute of Applied Mechanics, ul. Jana Pawła II 24, 60-965 Poznań, Poland

LOCAL GRADIENT THEORY OF DIELECTRICS WITH POLARIZATION INERTIA AND IRREVERSIBILITY OF LOCAL MASS DISPLACEMENT

VASYL KONDRAT AND OLHA HRYTSYNA

A complete system of equations of the local gradient theory of electromagnetothermomechanics of polarized nonferromagnetic isotropic solids is obtained with regard to polarization inertia and the irreversibility of the processes of local mass displacement and polarization. It is shown that in this case the constitutive relations for specific vectors of the local mass displacement and polarization are rheological and contain time derivatives of the first and higher orders. A corresponding key system of equations for the isothermal approximation is obtained. This system is also written relatively to scalar and vector potentials of the displacement vector, vectors of the electromagnetic field, and a reduced energy measure μ'_π of the effect of the mass displacement on the internal energy. The Lorentz gauge is generalized in such a way that equations for the vector potential of the electromagnetic field and for the generalized scalar potential are not coupled and have similar structures. The effect of polarization inertia and the above-mentioned irreversibility of processes on the interaction of the fields is analyzed.

1. Introduction

In recent decades in the scientific literature there has been considerable interest in developing nonlocal theories of physical and mechanical processes in condensed matter. First of all, it is related to the need to describe some of the observed effects [Mead 1961; 1962; Ma and Cross 2003; Majdoub et al. 2009] and to the intensive introduction of composite materials in various technologies, including nanomaterials, [Tauchert and Guzelsu 1972; Buryachenko and Pagano 2003; Kuno 2004; Sharma et al. 2007; Majdoub 2010] where nonlocal effects are of crucial importance. These investigations also urged the development of the principles and methods of nonlocal thermodynamics [Ván 2003; Dolfin et al. 2004; Cimmelli and Ván 2005], thermomechanics and theories of heat conduction [Papenfuss and Forest 2006; Forest and Amestoy 2008], wave theory [Erofeyev 2003; Yerofeyev and Sheshenina 2005; Papargyri-Beskou et al. 2009], etc.

Nonlocal theories of deformable dielectrics are constructed by defining the functional constitutive equations of spatial type (strongly nonlocal theories) or by means of an expansion of the space of state parameter by gradients of certain physical quantities (weakly nonlocal theories) [Maugin 1988; Yang 2006; Kondrat and Hrytsyna 2009a]. In the scientific literature theories of both the first (see for example [Eringen 1984]) and second type are well known, the latter taking into account the dependence of the body state on the strain gradients [Tagantsev 1986; Majdoub et al. 2008; 2009; Majdoub 2010], the polarization gradient [Mindlin 1972], or the electric field gradients [Kafadar 1971; Yang and Yang 2004] corresponding to internal variables and their gradients [Ciancio 1989; Dolfin et al. 2004]. Another

Keywords: coupled electromagnetothermomechanical processes, local displacement of mass, dielectrics, nonlocal theory, irreversibility, inertia of polarization.

approach to the construction of the nonlocal theory of dielectrics, proposed in [Burak et al. 2008; Kondrat and Hrytsyna 2008a], is based on considering the *process of local mass displacement*. Burak [1987] was the first to pay attention to this process. He assumed that a mass flux has a component $\partial \mathbf{\Pi}_m / \partial t$ of nonconvective and nondiffusive nature. Burak related this flux to a process referred to as the process of local mass displacement and the vector $\mathbf{\Pi}_m$ was named the vector of this displacement [Burak 1987]. Later it was shown that the equations of the local gradient electromagnetothermomechanics of polarized nonferromagnetic solids describe surface inhomogeneity in the mechanical and electromagnetic fields [Burak et al. 2008], a high-frequency dispersion of elastic waves [Kondrat and Hrytsyna 2009b], and the Mead anomaly [Chapla et al. 2009]. It should be noted that the relations of the theory obtained in [Burak et al. 2008] are based on the assumption of reversibility of the polarization process; local mass displacement and polarization inertia is not taken into account. However, such an approximation may be insufficient and unacceptable for the study of transitional processes of the formation of near-surface inhomogeneities and the perturbation of electromagnetomechanical processes by shock loads, as well as for the description of acoustic and electromagnetic emission caused by the formation of surfaces, etc.

In this article a complete system of equations of the local gradient electromagnetothermomechanics of polarized nonferromagnetic solids is obtained taking into account the inertia of polarization and the irreversibility of processes of polarization and local mass displacement. In order to consider the irreversibility of these processes we used the approach proposed in [Hrytsyna and Kondrat 2007; Kondrat and Hrytsyna 2008b]. Moreover, in the total energy balance equation we took into account the kinetic energy of polarization [Maugin 1988] that enables us to describe the inertia of polarization. The key system of equations is obtained in isothermal approximation for isotropic solids. This system is also written relative to the scalar and vector potentials of the displacement vector and the vectors of the electromagnetic field. In order to arrive at the potential description, the Lorentz gauge had to be generalized. Based on this, the interaction of the electromagnetic processes, deformation, and local mass displacement is discussed.

2. The balance equations

We consider an isotropic thermoelastic polarized nonferromagnetic body that occupies the domain (V) of Euclidean space and is bounded by the smooth surface (Σ) with unit exterior normal \mathbf{n} . The body is subjected to the action of an external load, which induces the mechanical, thermal, and electromagnetic processes, and the process of local displacement of mass. The polarization inertia as well as the irreversibility of processes of polarization and local mass displacement are taken into account.

Taking into account the process of local displacement of mass we represent the mass flux \mathbf{J}_{m*} as the sum of the convective term $\mathbf{J}_{mc} = \rho \mathbf{v}_*$ and the term $\mathbf{J}_{ms} = \partial \mathbf{\Pi}_m / \partial t$, which is caused by structural changes of the fixed body element, namely $\mathbf{J}_{m*} = \mathbf{J}_{mc} + \mathbf{J}_{ms}$ [Burak et al. 2008]. Here \mathbf{v}_* is a velocity of the convective displacement of the fixed body element and ρ is the mass density.

Let us define the vector of the velocity of the continuum center of mass \mathbf{v} by the relation

$$\mathbf{v} = \mathbf{v}_* + \frac{1}{\rho} \frac{\partial \mathbf{\Pi}_m}{\partial t}.$$

Then, the equation of mass balance takes the standard form

$$\frac{\partial \rho}{\partial t} + \nabla \cdot (\rho \mathbf{v}) = 0. \quad (2-1)$$

Let us introduce the quantity $\rho_{m\pi}$, which has dimension of mass density. We assume that, for an arbitrary body of finite size that occupies the domain (V), the vector of local displacement of mass and the density of the induced mass are such that [Burak et al. 2008]

$$\int_{(V)} \mathbf{\Pi}_m dV = \int_{(V)} \rho_{m\pi} \mathbf{r} dV. \quad (2-2)$$

Here \mathbf{r} is the position vector. By analogy with an induced electric charge [Landau and Lifshitz 1982], we refer to the quantity $\rho_{m\pi}$ as a density of the induced mass [Burak et al. 2008].

The consequence of relation (2-2) is [Kondrat and Hrytsyna 2008a]

$$\rho_{m\pi} = -\nabla \cdot \mathbf{\Pi}_m. \quad (2-3)$$

By differentiating (2-3) with respect to time and taking into account that $\partial \mathbf{\Pi}_m / \partial t = \mathbf{J}_{ms}$, we obtain the equation

$$\frac{\partial \rho_{m\pi}}{\partial t} + \nabla \cdot \mathbf{J}_{ms} = 0,$$

which can be interpreted as the balance equation of induced mass.

We also write the entropy balance equation, which is of the form [de Groot and Mazur 1962]

$$\rho T \frac{ds}{dt} = -\nabla \cdot \mathbf{J}_q + \frac{1}{T} \mathbf{J}_q \cdot \nabla T + T \sigma_s + \rho \mathfrak{R}, \quad (2-4)$$

where s is the specific entropy, \mathbf{J}_q is the density of heat flux, σ_s is the entropy production, T is the temperature, \mathfrak{R} denotes the distributed thermal sources, and $d \dots / dt = \partial \dots / \partial t + \mathbf{v} \cdot \nabla \dots$

From Maxwell's equations,

$$\nabla \cdot \mathbf{B} = 0, \quad \nabla \cdot \mathbf{D} = \rho_e, \quad \nabla \times \mathbf{E} = -\frac{\partial \mathbf{B}}{\partial t}, \quad \nabla \times \mathbf{H} = \mathbf{J}_e + \frac{\partial \mathbf{D}}{\partial t}, \quad (2-5)$$

we obtain the electromagnetic field energy balance equation:

$$\begin{aligned} \frac{\partial U_e}{\partial t} + \nabla \cdot \mathbf{S}_e + \mathbf{J}_{e*} \cdot \mathbf{E}_* + \left[\rho_e \mathbf{E}_* + \left(\mathbf{J}_{e*} + \frac{\partial(\rho \mathbf{p})}{\partial t} \right) \times \mathbf{B} + \rho (\nabla \mathbf{E}_*) \cdot \mathbf{p} \right] \cdot \mathbf{v} \\ + \rho \mathbf{E}_* \cdot \frac{d\mathbf{p}}{dt} - \nabla \cdot [\rho (\mathbf{E}_* \cdot \mathbf{p}) \hat{\mathbf{I}} \cdot \mathbf{v}] = 0. \end{aligned} \quad (2-6)$$

Here $U_e = (\varepsilon_0 \mathbf{E}^2 + \mu_0 \mathbf{H}^2) / 2$ is the energy density of the electromagnetic field and $\mathbf{S}_e = \mathbf{E} \times \mathbf{H}$ is the flux density of its energy, \mathbf{E} and \mathbf{H} are the electric and magnetic fields, \mathbf{D} and \mathbf{B} are the electric and magnetic inductions, $\mathbf{D} = \varepsilon_0 \mathbf{E} + \rho \mathbf{p}$, \mathbf{p} is the specific vector of polarization, \mathbf{J}_e is the density of electric current (the convection and conduction currents), ρ_e is the density of free electric charge, $\mathbf{E}_* = \mathbf{E} + \mathbf{v} \times \mathbf{B}$, $\mathbf{J}_{e*} = \mathbf{J}_e - \rho_e \mathbf{v}$, ε_0 and μ_0 are the electric and magnetic constants, and $\hat{\mathbf{I}}$ is the unit tensor. For nonferromagnetic media $\mathbf{B} = \mu_0 \mathbf{H}$.

We assume that the total energy of the system "solid-electromagnetic field" is the sum of internal energy ρu , kinetic energy of mass center $\rho \mathbf{v}^2 / 2$, energy of the electromagnetic field U_e , and polarization kinetic energy $\frac{1}{2} \rho d_E (d\mathbf{p}/dt)^2$. Here d_E is the scalar related to the inertia of the polarization process [Maugin 1988]. The total energy of the system is changed due to the convective transport of energy through the surface, the flux of energy related to work $\hat{\sigma} \cdot \mathbf{v}$ of internal forces, the heat flux \mathbf{J}_q , the electromagnetic energy flux \mathbf{S}_e , the flux of energy $\mu \mathbf{J}_m$ connected to the mass transport relative to the

center of mass of the body, and the flux of energy $\mu_\pi (\partial \mathbf{\Pi}_m / \partial t)$ related to structural changes, as well as the action of mass forces \mathbf{F} and distributed thermal sources \mathfrak{R} . Thus, the total energy balance equation in integral form looks like

$$\begin{aligned} & \frac{d}{dt} \int_{(V)} \left(\rho u + U_e + \frac{1}{2} \rho \mathbf{v}^2 + \frac{1}{2} \rho d_E \left(\frac{d\mathbf{p}}{dt} \right)^2 \right) dV = \\ & - \oint_{(\Sigma)} \left[\rho \left(u + \frac{1}{2} \mathbf{v}^2 + \frac{1}{2} d_E \left(\frac{d\mathbf{p}}{dt} \right)^2 \right) \mathbf{v} - \hat{\boldsymbol{\sigma}} \cdot \mathbf{v} + \mathbf{S}_e + \mathbf{J}_q + \mu \mathbf{J}_m + \mu_\pi \frac{\partial \mathbf{\Pi}_m}{\partial t} \right] \cdot \mathbf{n} d\Sigma + \int_{(V)} (\rho \mathbf{F} \cdot \mathbf{v} + \rho \mathfrak{R}) dV. \end{aligned} \quad (2-7)$$

Here $\hat{\boldsymbol{\sigma}}$ is the Cauchy stress tensor, μ is the chemical potential, μ_π is the energy measure of the effect of the mass displacement on the internal energy [Burak et al. 2008], and $\mathbf{J}_m = \rho(\mathbf{v}_* - \mathbf{v})$.

Taking into account the energy balance equation of the electromagnetic field (2-6), the balance equations of mass and entropy, (2-1) and (2-4), relation (2-3), and formula $\mathbf{J}_m = -\partial \mathbf{\Pi}_m / \partial t$ [Burak et al. 2008], as well as introducing the specific quantities $\boldsymbol{\pi}_m = \mathbf{\Pi}_m / \rho$ and $\rho_m = \rho_m \pi / \rho$, we finally obtain from (2-7) the following balance equation of internal energy in the local form:

$$\begin{aligned} \rho \frac{du}{dt} = & \rho T \frac{ds}{dt} + \hat{\boldsymbol{\sigma}}_* : (\nabla \otimes \mathbf{v}) + \rho \mathbf{E}_* \cdot \frac{d\mathbf{p}}{dt} + \rho \mu'_\pi \frac{d\rho_m}{dt} - \rho \nabla \mu'_\pi \cdot \frac{d\boldsymbol{\pi}_m}{dt} - \rho d_E \frac{d^2 \mathbf{p}}{dt^2} \cdot \frac{d\mathbf{p}}{dt} + \\ & + \mathbf{J}_{e*} \cdot \mathbf{E}_* - \mathbf{J}_q \cdot \frac{\nabla T}{T} - T \sigma_s + \mathbf{v} \cdot \left(-\rho \frac{d\mathbf{v}}{dt} + \nabla \cdot \hat{\boldsymbol{\sigma}}_* + \rho \mathbf{F}_* + \mathbf{F}_e \right). \end{aligned} \quad (2-8)$$

Here $\mu'_\pi = \mu_\pi - \mu$, \otimes denotes the tensor product, and

$$\begin{aligned} \hat{\boldsymbol{\sigma}}_* &= \hat{\boldsymbol{\sigma}} - \rho(\mathbf{E}_* \cdot \mathbf{p} - \rho_m \mu'_\pi - \boldsymbol{\pi}_m \cdot \nabla \mu'_\pi) \hat{\mathbf{I}}, \quad \mathbf{F}_* = \mathbf{F} + \rho_m \nabla \mu'_\pi - \boldsymbol{\pi}_m \cdot \nabla \nabla \mu'_\pi, \\ \mathbf{F}_e &= \rho_e \mathbf{E}_* + \left(\mathbf{J}_{e*} + \frac{\partial(\rho \mathbf{p})}{\partial t} \right) \times \mathbf{B} + \rho(\nabla \mathbf{E}_*) \cdot \mathbf{p}. \end{aligned}$$

To take into account the irreversibility of the processes of local mass displacement and polarization we represent the vectors \mathbf{E}_* and $\nabla \mu'_\pi$ as sums of a reversible component, \mathbf{E}_*^r or $(\nabla \mu'_\pi)^r$, and an irreversible in, \mathbf{E}_*^i or $(\nabla \mu'_\pi)^i$ [Hrytsyna and Kondrat 2007; Kondrat and Hrytsyna 2008b]:

$$\mathbf{E}_* = \mathbf{E}_*^r + \mathbf{E}_*^i, \quad \nabla \mu'_\pi = (\nabla \mu'_\pi)^r + (\nabla \mu'_\pi)^i. \quad (2-9)$$

Taking into account (2-9) we rewrite (2-8) as follows:

$$\begin{aligned} \rho \frac{du}{dt} = & \rho T \frac{ds}{dt} + \hat{\boldsymbol{\sigma}}_* : (\nabla \otimes \mathbf{v}) + \rho \mathbf{E}_*^r \cdot \frac{d\mathbf{p}}{dt} + \rho \mu'_\pi \frac{d\rho_m}{dt} - \rho (\nabla \mu'_\pi)^r \cdot \frac{d\boldsymbol{\pi}_m}{dt} - \rho d_E \frac{d^2 \mathbf{p}}{dt^2} \cdot \frac{d\mathbf{p}}{dt} + \\ & + \mathbf{J}_{e*} \cdot \mathbf{E}_* - \mathbf{J}_q \cdot \frac{\nabla T}{T} + \rho \mathbf{E}_*^i \cdot \frac{d\mathbf{p}}{dt} - \rho (\nabla \mu'_\pi)^i \cdot \frac{d\boldsymbol{\pi}_m}{dt} - T \sigma_s + \mathbf{v} \cdot \left(-\rho \frac{d\mathbf{v}}{dt} + \nabla \cdot \hat{\boldsymbol{\sigma}}_* + \rho \mathbf{F}_* + \mathbf{F}_e \right). \end{aligned}$$

Let us assume that the equilibrium part of the local electric field vector \mathbf{E}_L^r is a state parameter [Maugin 1988]. This vector differs from term \mathbf{E}_*^r of the macroscopic electric field \mathbf{E}_* . Therefore we rewrite the

balance equation of internal energy as

$$\begin{aligned} \rho \frac{du}{dt} = & \rho T \frac{ds}{dt} + \hat{\sigma}_* : (\nabla \otimes \mathbf{v}) + \rho \mathbf{E}_L^r \cdot \frac{d\mathbf{p}}{dt} + \rho \mu'_\pi \frac{d\rho_m}{dt} - \rho (\nabla \mu'_\pi)^r \cdot \frac{d\boldsymbol{\pi}_m}{dt} + \rho \left(\mathbf{E}_*^r - \mathbf{E}_L^r - d_E \frac{d^2\mathbf{p}}{dt^2} \right) \cdot \frac{d\mathbf{p}}{dt} \\ & + \mathbf{J}_{e*} \cdot \mathbf{E}_* - \mathbf{J}_q \cdot \frac{\nabla T}{T} + \rho \mathbf{E}_*^i \cdot \frac{d\mathbf{p}}{dt} - \rho (\nabla \mu'_\pi)^i \cdot \frac{d\boldsymbol{\pi}_m}{dt} - T\sigma_s + \mathbf{v} \cdot \left(-\rho \frac{d\mathbf{v}}{dt} + \nabla \cdot \hat{\sigma}_* + \rho \mathbf{F}_* + \mathbf{F}_e \right). \end{aligned} \quad (2-10)$$

Using the Legendre transformation $f = u - Ts - \mathbf{E}_L^r \cdot \mathbf{p} + (\nabla \mu'_\pi)^r \cdot \boldsymbol{\pi}_m$ we pass to a new thermodynamic function f , which is interpreted as a generalized Helmholtz free energy. Then, from the balance equation of internal energy (2-10) we obtain

$$\begin{aligned} \rho \frac{df}{dt} = & -\rho s \frac{dT}{dt} + \hat{\sigma}_* : (\nabla \otimes \mathbf{v}) - \rho \mathbf{p} \cdot \frac{d\mathbf{E}_L^r}{dt} + \rho \mu'_\pi \frac{d\rho_m}{dt} + \rho \boldsymbol{\pi}_m \cdot \frac{d(\nabla \mu'_\pi)^r}{dt} + \rho \left(\mathbf{E}_*^r - \mathbf{E}_L^r - d_E \frac{d^2\mathbf{p}}{dt^2} \right) \cdot \frac{d\mathbf{p}}{dt} \\ & + \mathbf{J}_{e*} \cdot \mathbf{E}_* - \mathbf{J}_q \cdot \frac{\nabla T}{T} + \rho \mathbf{E}_*^i \cdot \frac{d\mathbf{p}}{dt} - \rho (\nabla \mu'_\pi)^i \cdot \frac{d\boldsymbol{\pi}_m}{dt} - T\sigma_s + \mathbf{v} \cdot \left(-\rho \frac{d\mathbf{v}}{dt} + \nabla \cdot \hat{\sigma}_* + \rho \mathbf{F}_* + \mathbf{F}_e \right). \end{aligned} \quad (2-11)$$

The balance equation of free energy, (2-10), should be invariant relative to spatial translation, namely, it should not change if $\mathbf{v} \rightarrow \mathbf{v} + \mathbf{a}$, where \mathbf{a} is a constant vector. As a consequence, from (2-11) we get

$$\rho \frac{d\mathbf{v}}{dt} = \nabla \cdot \hat{\sigma}_* + \mathbf{F}_e + \rho \mathbf{F}_* \quad \text{for all } \mathbf{r} \in (V), \quad (2-12)$$

$$\begin{aligned} \rho \frac{df}{dt} = & -\rho s \frac{dT}{dt} + \hat{\sigma}_* : (\nabla \otimes \mathbf{v}) - \rho \mathbf{p} \cdot \frac{d\mathbf{E}_L^r}{dt} + \rho \mu'_\pi \frac{d\rho_m}{dt} + \rho \boldsymbol{\pi}_m \cdot \frac{d(\nabla \mu'_\pi)^r}{dt} \\ & + \rho \left(\mathbf{E}_*^r - \mathbf{E}_L^r - d_E \frac{d^2\mathbf{p}}{dt^2} \right) \cdot \frac{d\mathbf{p}}{dt} + \mathbf{J}_{e*} \cdot \mathbf{E}_* - \mathbf{J}_q \cdot \frac{\nabla T}{T} + \rho \mathbf{E}_*^i \cdot \frac{d\mathbf{p}}{dt} - \rho (\nabla \mu'_\pi)^i \cdot \frac{d\boldsymbol{\pi}_m}{dt} - T\sigma_s. \end{aligned} \quad (2-13)$$

Relation (2-12) is the equation of motion. We see that the redefinition of stress tensor $\hat{\sigma}_*$ and the emergence of additional mass force \mathbf{F}_* are the result of the account of the process of the local mass displacement. Note also that the mass \mathbf{F}_* and ponderomotive \mathbf{F}_e forces have similar structure.

Equation (2-13) should remain unchanged if the body rotates with constant angular velocity $\boldsymbol{\Omega}$. In this case $\mathbf{v} \rightarrow \mathbf{v} + \boldsymbol{\Omega} \times \mathbf{r}$. As a consequence, we obtain that $\hat{\sigma}_*$ is the symmetric tensor.

Let us represent the quantity $\nabla \otimes \mathbf{v}$ in the form $\nabla \otimes \mathbf{v} = d\hat{\epsilon}/dt + d\hat{\omega}/dt$. Here $\mathbf{v} = d\mathbf{u}/dt$, \mathbf{u} is the displacement vector, $\hat{\epsilon}$ is the symmetric strain tensor, and $\hat{\omega}$ is the antisymmetric rotation tensor. These tensors are related to a displacement vector \mathbf{u} by:

$$\hat{\epsilon} = \frac{1}{2} [\nabla \otimes \mathbf{u} + (\nabla \otimes \mathbf{u})^T], \quad \hat{\omega} = \frac{1}{2} [\nabla \otimes \mathbf{u} - (\nabla \otimes \mathbf{u})^T]. \quad (2-14)$$

Since the convolution of the symmetric and antisymmetric tensors is equal to zero, then $\hat{\sigma}_* : (d\hat{\omega}/dt) = 0$. Thus, the free energy balance equation (2-13) takes the form

$$\begin{aligned} \rho \frac{df}{dt} = & -\rho s \frac{dT}{dt} + \hat{\sigma}_* : \frac{d\hat{\epsilon}}{dt} - \rho \mathbf{p} \cdot \frac{d\mathbf{E}_L^r}{dt} + \rho \mu'_\pi \frac{d\rho_m}{dt} + \rho \boldsymbol{\pi}_m \cdot \frac{d(\nabla \mu'_\pi)^r}{dt} \\ & + \rho \left(\mathbf{E}_*^r - \mathbf{E}_L^r - d_E \frac{d^2\mathbf{p}}{dt^2} \right) \cdot \frac{d\mathbf{p}}{dt} + \mathbf{J}_{e*} \cdot \mathbf{E}_* - \mathbf{J}_q \cdot \frac{\nabla T}{T} + \rho \mathbf{E}_*^i \cdot \frac{d\mathbf{p}}{dt} - \rho (\nabla \mu'_\pi)^i \cdot \frac{d\boldsymbol{\pi}_m}{dt} - T\sigma_s. \end{aligned} \quad (2-15)$$

Since the summands in the second line of (2-15) do not depend on the velocities

$$\frac{dT}{dt}, \quad \frac{d\hat{\boldsymbol{e}}}{dt}, \quad \frac{d\mathbf{E}_L^r}{dt}, \quad \frac{d\rho_m}{dt}, \quad \frac{d(\nabla\mu'_\pi)^r}{dt},$$

we get the generalized Gibbs equation

$$df = -sdT + \rho^{-1}\hat{\boldsymbol{\sigma}}_* : d\hat{\boldsymbol{e}} - \mathbf{p} \cdot d\mathbf{E}_L^r + \mu'_\pi d\rho_m + \boldsymbol{\pi}_m \cdot d(\nabla\mu'_\pi)^r, \quad (2-16)$$

the expression for the entropy production

$$\sigma_s = \mathbf{J}_{e^*} \cdot \frac{\mathbf{E}_*}{T} - \mathbf{J}_q \cdot \frac{\nabla T}{T^2} + \rho \frac{d\mathbf{p}}{dt} \cdot \frac{\mathbf{E}_*^i}{T} - \rho \frac{d\boldsymbol{\pi}_m}{dt} \cdot \frac{(\nabla\mu'_\pi)^i}{T}, \quad (2-17)$$

and the relation

$$\mathbf{E}_*^r - \mathbf{E}_L^r = d_E \frac{d^2 \mathbf{p}}{dt^2}, \quad (2-18)$$

which is sometimes referred to as “the equation of intramolecular force balance” [Maugin 1988].

3. The constitutive relations

Since parameters T , ρ_m , \mathbf{E}_L^r , $(\nabla\mu'_\pi)^r$, and $\hat{\boldsymbol{e}}$ are independent, the Gibbs equation (2-18) yields the state equations

$$\begin{aligned} s &= -\left. \frac{\partial f}{\partial T} \right|_{\rho_m, (\nabla\mu'_\pi)^r, \mathbf{E}_L^r, \hat{\boldsymbol{e}}}, & \hat{\boldsymbol{\sigma}}_* &= \rho \left. \frac{\partial f}{\partial \hat{\boldsymbol{e}}} \right|_{T, \rho_m, (\nabla\mu'_\pi)^r, \mathbf{E}_L^r}, & \mu'_\pi &= \left. \frac{\partial f}{\partial \rho_m} \right|_{T, (\nabla\mu'_\pi)^r, \mathbf{E}_L^r, \hat{\boldsymbol{e}}}, \\ \mathbf{p} &= -\left. \frac{\partial f}{\partial \mathbf{E}_L^r} \right|_{T, \rho_m, (\nabla\mu'_\pi)^r, \hat{\boldsymbol{e}}}, & \boldsymbol{\pi}_m &= \left. \frac{\partial f}{\partial (\nabla\mu'_\pi)^r} \right|_{T, \rho_m, \mathbf{E}_L^r, \hat{\boldsymbol{e}}}. \end{aligned} \quad (3-1)$$

Let us decompose the free energy density f into a Taylor series in perturbations of the state parameters with respect to the original state of unlimited homogeneous medium with $\hat{\boldsymbol{e}} = 0$, $\hat{\boldsymbol{\sigma}}_* = 0$, $\mathbf{E}_L^r = 0$, $(\nabla\mu'_\pi)^r = 0$, $\mathbf{p} = 0$, $\boldsymbol{\pi}_m = 0$, $T = T_0$, $s = s_0$, $\rho = \rho_0$, $\rho_m = 0$, and $\mu'_\pi = \mu'_{\pi 0}$. For small perturbations, we retain quadratic terms in this decomposition which enables us to get the linear state equations. Therefore, the free energy density for isotropic material has the form

$$\begin{aligned} f &= f_0 - s_0(T - T_0) + \mu'_{\pi 0} \rho_m - \frac{C_V}{2T_0}(T - T_0)^2 + \frac{1}{2\rho_0}(K - \frac{2}{3}G)I_1^2 + \frac{1}{\rho_0}GI_2 + \frac{1}{2}d_\rho \rho_m^2 - \frac{1}{\rho_0}K\alpha_t I_1(T - T_0) \\ &\quad - \frac{1}{\rho_0}K\alpha_\rho I_1 \rho_m - \beta_{T\rho} \rho_m(T - T_0) - \frac{1}{2}\chi_m (\nabla\mu'_\pi)^r \cdot (\nabla\mu'_\pi)^r - \frac{1}{2}\chi_E \mathbf{E}_L^r \cdot \mathbf{E}_L^r + \chi_{Em} \mathbf{E}_L^r \cdot (\nabla\mu'_\pi)^r. \end{aligned}$$

Here $I_1 = \hat{\boldsymbol{e}} : \hat{\boldsymbol{I}} \equiv e$ and $I_2 = \hat{\boldsymbol{e}} : \hat{\boldsymbol{e}}$ are the first and second invariants of strain tensor, respectively, K is the modulus of volume elasticity at constant temperature and specific density of the induced mass, G is the shear modulus, α_t is the temperature coefficient of volume dilatation at uniform specific density of the induced mass, α_ρ is the coefficient of volume dilatation caused by the local displacement of mass at uniform temperature, C_V is the specific heat at constant deformation and specific density of the induced mass, χ_E is the dielectric susceptibility, $\beta_{T\rho}$ and d_ρ are the isothermal-isochoric coefficients of dependency of entropy and potential μ'_π on a specific density of the induced mass, and χ_m and χ_{Em} are

the coefficients that characterize the local displacement of mass and body polarization due to the gradient of potential μ'_π , respectively.

If the potential f is known, the constitutive equations (3-1) take on the form

$$s = s_0 + \frac{C_V}{T_0}(T - T_0) + \frac{1}{\rho_0}K\alpha_t e + \beta_{T\rho}\rho_m, \quad \hat{\sigma}_* = 2G\hat{e} + \left\{ \left(K - \frac{2}{3}G \right) e - K[\alpha_t(T - T_0) + \alpha_\rho\rho_m] \right\} \hat{\mathbf{I}},$$

$$\mu'_\pi = \mu'_{\pi 0} + d_\rho\rho_m - \beta_{T\rho}(T - T_0) - \frac{1}{\rho_0}K\alpha_\rho e, \quad (3-2)$$

$$\mathbf{p} = \chi_E \mathbf{E}_L^r - \chi_{Em}(\nabla\mu'_\pi)^r, \quad \boldsymbol{\pi}_m = -\chi_m(\nabla\mu'_\pi)^r + \chi_{Em} \mathbf{E}_L^r. \quad (3-3)$$

Taking into account (2-18) we rewrite the state equations (3-3) as follows:

$$\mathbf{p} = \chi_E \left(\mathbf{E}^r - d_E \frac{d^2 \mathbf{p}}{dt^2} \right) - \chi_{Em}(\nabla\mu'_\pi)^r, \quad \boldsymbol{\pi}_m = -\chi_m(\nabla\mu'_\pi)^r + \chi_{Em} \left(\mathbf{E}^r - d_E \frac{d^2 \mathbf{p}}{dt^2} \right). \quad (3-4)$$

We obtain kinetic relations based on (2-17) for entropy production. Let us assume that thermodynamic fluxes $\mathbf{j}_1 = \mathbf{J}_q$, $\mathbf{j}_2 = \mathbf{J}_{e^*}$, $\mathbf{j}_3 = \rho(d\mathbf{p}/dt)$, and $\mathbf{j}_4 = \rho(d\boldsymbol{\pi}_m/dt)$ are linear functions of the thermodynamic forces $\mathbf{X}_1 = -\nabla T/T^2$, $\mathbf{X}_2 = \mathbf{E}_*/T$, $\mathbf{X}_3 = \mathbf{E}_*^i/T$, and $\mathbf{X}_4 = -(\nabla\mu'_\pi)^i/T$:

$$\mathbf{j}_i = \sum_{j=1}^4 \mathcal{L}_{ij} \mathbf{X}_j, \quad (i = \overline{1, 4}). \quad (3-5)$$

Here \mathcal{L}_{ij} ($i, j = \overline{1, 4}$) are constant kinetic coefficients. In general, the relations (3-5) are nonlinear. If we take into account formulas (2-9) and (3-4) and exclude irreversible terms \mathbf{E}^i and $(\nabla\mu'_\pi)^i$ and reversible terms \mathbf{E}^r and $(\nabla\mu'_\pi)^r$ of vectors \mathbf{E} and $\nabla\mu'_\pi$, in the linearized approximation we obtain from (3-5) the following relations for the vectors of heat flux and electric current density:

$$\begin{aligned} \mathbf{J}_q &= -L_1^T \nabla T + L_1^E \mathbf{E} - L_1^\mu \nabla\mu'_\pi - L_1^d \frac{d^2 \mathbf{p}}{dt^2} + L_1^p \mathbf{p} + L_1^\pi \boldsymbol{\pi}_m, \\ \mathbf{J}_e &= -L_2^T \nabla T + L_2^E \mathbf{E} - L_2^\mu \nabla\mu'_\pi - L_2^d \frac{d^2 \mathbf{p}}{dt^2} + L_2^p \mathbf{p} + L_2^\pi \boldsymbol{\pi}_m, \end{aligned} \quad (3-6)$$

and the rheological constitutive relations for vectors of polarization and local mass displacement:

$$\begin{aligned} L_3^d \frac{d^2 \mathbf{p}}{dt^2} + \rho_0 \frac{d\mathbf{p}}{dt} - L_3^p \mathbf{p} - L_3^\pi \boldsymbol{\pi}_m &= -L_3^T \nabla T + L_3^E \mathbf{E} - L_3^\mu \nabla\mu'_\pi, \\ L_4^d \frac{d^2 \boldsymbol{\pi}_m}{dt^2} + \rho_0 \frac{d\boldsymbol{\pi}_m}{dt} - L_4^p \mathbf{p} - L_4^\pi \boldsymbol{\pi}_m &= -L_4^T \nabla T + L_4^E \mathbf{E} - L_4^\mu \nabla\mu'_\pi. \end{aligned} \quad (3-7)$$

Here

$$L_i^d = d_E \frac{\mathcal{L}_{i3}}{T_0}, \quad L_i^T = \frac{\mathcal{L}_{i1}}{T_0^2}, \quad L_i^E = \frac{\mathcal{L}_{i2} + \mathcal{L}_{i3}}{T_0}, \quad L_i^\mu = \frac{\mathcal{L}_{i4}}{T_0}, \quad L_i^\pi = \frac{\chi_{Em} \mathcal{L}_{i3} - \chi_E \mathcal{L}_{i4}}{T_0(\chi_E \chi_m - \chi_{Em}^2)}, \quad L_i^p = \frac{\chi_{Em} \mathcal{L}_{i4} - \chi_m \mathcal{L}_{i3}}{T_0(\chi_E \chi_m - \chi_{Em}^2)},$$

where $i = \overline{1, 4}$. Note that summands $L_3^d(d^2 \mathbf{p}/dt^2)$ and $L_4^d(d^2 \boldsymbol{\pi}_m/dt^2)$ in the left hand parts of (3-7) appear due to polarization inertia being taken into account while the summands $\rho_0(d\mathbf{p}/dt)$, $\rho_0(d\boldsymbol{\pi}_m/dt)$, $L_3^\pi \boldsymbol{\pi}_m$, $L_4^p \mathbf{p}$, $L_3^T \nabla T$, and $L_4^T \nabla T$ appear due to considering the irreversibility of the processes of local

mass displacement and polarization. According to (3-7), a body can be theoretically polarized not only in the electric field but also in a gradient of temperature as well as in a gradient of potential μ'_π . Therefore, the rheological relations (3-7) should describe both the surface polarization (the gradient of potential μ'_π may be significant in near-surface regions [Burak et al. 2008]) and the thermopolarization effect which consists in the linear response of the dielectric polarization to the temperature gradient.

Due to simple transformations, we can rewrite relations (3-7) as follows:

$$\mathbf{L}(\mathbf{p}) = \mathbf{L}_{pT}(\nabla T) - \mathbf{L}_{pE}(\mathbf{E}) + \mathbf{L}_{p\mu}(\nabla \mu'_\pi), \quad \mathbf{L}(\boldsymbol{\pi}_m) = \mathbf{L}_{\pi T}(\nabla T) - \mathbf{L}_{\pi E}(\mathbf{E}) + \mathbf{L}_{\pi\mu}(\nabla \mu'_\pi). \quad (3-8)$$

Here we introduce the operators

$$\begin{aligned} \mathbf{L} &= \frac{L_3^\pi}{\rho_0} \left(L_4^p - L_4^d \frac{d^2}{dt^2} \right) - \left(L_3^d \frac{d^2}{dt^2} + \rho_0 \mathbf{L}_p \right) \mathbf{L}_\pi, \quad \mathbf{L}_\pi = \frac{d}{dt} - \frac{1}{\tau_\pi}, \quad \mathbf{L}_p = \frac{d}{dt} - \frac{1}{\tau_p}, \\ \mathbf{L}_{p\alpha} &= L_3^\alpha \mathbf{L}_\pi + L_3^\pi \frac{L_4^\alpha}{\rho_0}, \quad \mathbf{L}_{\pi\alpha} = \frac{1}{\rho_0} (L_3^\alpha \mathbf{L}_{p2} + L_4^\alpha \mathbf{L}_{p1}), \quad \mathbf{L}_{p1} = L_3^d \frac{d^2}{dt^2} + \rho_0 \mathbf{L}_p, \quad \mathbf{L}_{p2} = L_4^p - L_4^d \frac{d^2}{dt^2}, \end{aligned}$$

where $\alpha = \{T, E, \mu\}$, $\tau_p = \rho_0/L_3^p$, and $\tau_\pi = \rho_0/L_4^\pi$.

The constitutive equations (3-2), (3-6), and (3-8), the linearized balance equations (2-1), (2-4), and (2-12), Maxwell's equations (2-5), the strain-displacement relation (2-14), and the balance equation of induced mass, which in linearized approximation looks like

$$\rho_m = -\nabla \cdot \boldsymbol{\pi}_m, \quad (3-9)$$

comprise a fundamental system of equations of linear augmented local gradient theory of deformable nonferromagnetic polarized isotropic solids in which account is taken of the polarization inertia and the irreversibility of both local mass displacement and polarization.

4. The key system of equations and a potential description

We shall study the ideal dielectrics for which $\rho_e = 0$ and $\mathbf{J}_e = 0$ and assume the isothermal approximation. We write the key equations in the linearized approximation for perturbations of the following functions: \mathbf{u} , \mathbf{E} , \mathbf{B} , and $\tilde{\mu}'_\pi = \mu'_\pi - \mu'_{\pi 0}$. Thus, we get

$$\rho_0 \frac{\partial^2 \mathbf{u}}{\partial t^2} = \left(K + \frac{1}{3} G - \frac{K^2 \alpha_\rho^2}{\rho_0 d_\rho} \right) \nabla (\nabla \cdot \mathbf{u}) + G \Delta \mathbf{u} - K \frac{\alpha_\rho}{d_\rho} \nabla \tilde{\mu}'_\pi + \rho_0 \mathbf{F}, \quad (4-1)$$

$$\mathbf{L}_{\pi\mu} (\Delta \tilde{\mu}'_\pi) + \frac{1}{d_\rho} \mathbf{L} (\tilde{\mu}'_\pi) = -\frac{K \alpha_\rho}{\rho_0 d_\rho} \mathbf{L} (\nabla \cdot \mathbf{u}) + \mathbf{L}_{\pi E} (\nabla \cdot \mathbf{E}), \quad (4-2)$$

$$\nabla \times \mathbf{E} = -\frac{\partial \mathbf{B}}{\partial t}, \quad \nabla \cdot \mathbf{B} = 0, \quad \mathbf{L}_\varepsilon (\nabla \cdot \mathbf{E}) + \rho_0 \mathbf{L}_{p\mu} (\Delta \tilde{\mu}'_\pi) = 0,$$

$$\mathbf{L} (\nabla \times \mathbf{B}) = \mu_0 \left[\mathbf{L}_\varepsilon \left(\frac{\partial \mathbf{E}}{\partial t} \right) + \rho_0 \mathbf{L}_{p\mu} \left(\frac{\partial (\nabla \tilde{\mu}'_\pi)}{\partial t} \right) \right]. \quad (4-3)$$

Here, $\mathbf{L}_\varepsilon = \varepsilon_0 \mathbf{L} - \rho_0 \mathbf{L}_{pE}$ and Δ is the Laplace operator. As may be seen in (4-3) the electrodynamics equations contain time derivatives of higher orders. The increase in the orders of these equations is due to accounting for the irreversibility of processes as well as the polarization inertia. Moreover, for the

potential $\tilde{\mu}'_\pi$ we obtain an equation which includes dynamic terms (for comparison, see [Burak et al. 2008]).

We see that (4-1)–(4-3) are interrelated. Therefore, this theory accommodates an electromechanical interaction even for isotropic materials.

Let us represent the displacement \mathbf{u} and mass force \mathbf{F} as sums of their potential and vortex components:

$$\mathbf{u} = \nabla\phi_u + \nabla \times \boldsymbol{\psi}_u, \quad \mathbf{F} = \nabla\Phi + \nabla \times \boldsymbol{\Psi}, \quad \nabla \cdot \boldsymbol{\psi}_u = 0, \quad \nabla \cdot \boldsymbol{\Psi} = 0, \quad (4-4)$$

Similarly, we represent the electric field \mathbf{E} and the magnetic field \mathbf{B} in terms of the scalar (electrical) potential ϕ_e and the vector potential \mathbf{A} :

$$\mathbf{E} = -\nabla\phi_e - \frac{\partial\mathbf{A}}{\partial t}, \quad \mathbf{B} = \nabla \times \mathbf{A}. \quad (4-5)$$

With the relationship

$$\phi_{em} = \varepsilon^{-1}[\mathbf{L}_\varepsilon\phi_e - \rho_0\mathbf{L}_{p\mu}\tilde{\mu}'_\pi], \quad (4-6)$$

we introduce the generalized potential ϕ_{em} , where ε is the dielectric permittivity of the medium. By neglecting the inertia of polarization and its irreversibility we have: $\varepsilon = \varepsilon_0 + \rho_0\chi_E$.

If the Lorentz gauge condition is modified in such a way:

$$\mathbf{L}(\nabla \cdot \mathbf{A}) + \varepsilon\mu_0\frac{\partial\phi_{em}}{\partial t} = 0, \quad (4-7)$$

then the electrodynamics equations (4-3) are reduced to two unrelated similar differential relations for vector \mathbf{A} and scalar ϕ_{em} potentials:

$$\mathbf{L}(\Delta\mathbf{A}) - \mu_0\mathbf{L}_\varepsilon\left(\frac{\partial^2\mathbf{A}}{\partial t^2}\right) = 0, \quad \mathbf{L}(\Delta\phi_{em}) - \mu_0\mathbf{L}_\varepsilon\left(\frac{\partial^2\phi_{em}}{\partial t^2}\right) = 0. \quad (4-8)$$

Note that the presence of operators \mathbf{L} and \mathbf{L}_{pE} in (4-8) leads to the dispersion of electromagnetic waves in an infinite medium. This dispersion was discussed in [Kondrat and Hrytsyna 2010] for the case of reversible processes of local mass displacement and polarization.

Substitution of (4-4) into (4-1) and (4-2) gives the equations:

$$G\Delta\boldsymbol{\psi}_u + \rho_0\boldsymbol{\Psi} - \rho_0\frac{\partial^2\boldsymbol{\psi}_u}{\partial t^2} = 0, \quad (4-9)$$

$$\left(K + \frac{4}{3}G - \frac{K^2\alpha_\rho^2}{\rho_0d_\rho}\right)\Delta\phi_u + \rho_0\Phi - \rho_0\frac{\partial^2\phi_u}{\partial t^2} = K\frac{\alpha_\rho}{d_\rho}\tilde{\mu}'_\pi, \quad (4-10)$$

$$\mathbf{L}\left([\mathbf{L}_\varepsilon\mathbf{L}_{\pi\mu} + \rho_0\mathbf{L}_{\pi E}\mathbf{L}_{\rho\mu}](\Delta\tilde{\mu}'_\pi) + \frac{1}{d_\rho}\mathbf{L}_\varepsilon\mathbf{L}(\tilde{\mu}'_\pi) + \frac{K\alpha_\rho}{\rho_0d_\rho}\mathbf{L}_\varepsilon\mathbf{L}(\Delta\phi_u) - \varepsilon(1 - \mathbf{L}_{\pi E})(\Delta\phi_{em})\right) = 0. \quad (4-11)$$

The system (4-8)–(4-11) can be solved consistently. First we find the potentials \mathbf{A} and ϕ_{em} from the homogeneous equations (4-8). Then, in the next step, the functions $\tilde{\mu}'_\pi$ and ϕ_u can be found based on (4-10) and (4-11). If the potentials ϕ_{em} and $\tilde{\mu}'_\pi$ are found, then in order to find ϕ_e we use differential equation (4-6). To determine the vector potentials $\boldsymbol{\psi}_u$ and \mathbf{A} homogeneous unrelated equations are obtained, which are also unrelated to the remaining equations of this system. However, to determine the potential $\boldsymbol{\psi}_u$ we use a relation identical to the ones obtained earlier in [Kondrat and Hrytsyna 2009b], whereas

for the potential A we get the modified equation due to accounting for the polarization inertia. Formula (4-11), unlike its analog obtained in [Kondrat and Hrytsyna 2009b], contains the generalized potential ϕ_{em} and dynamical terms, caused by accounting for the polarization inertia and the irreversibility of both the local mass displacement and polarization. From (4-8)–(4-11) it follows that in linear approximation the local mass displacement is not associated with the change of body shape. This process is related to the change of the body volume (the processes of compression-tension) and the electric scalar potential. The local displacement of mass is the cause of perturbation of the electromagnetic field.

5. Conclusions

We obtained a complete system of equations of the local gradient theory of deformable nonferromagnetic polarized isotropic solids in which the polarization inertia and the irreversibility of local mass displacement and polarization are taken into account. With the assumption that the body state is defined by the vector of the local electric field, we obtain the so-called equation of intramolecular force balance as well as the corresponding constitutive equations. It is shown that by accounting for the inertia of polarization and the above-mentioned irreversibility for the specific vector of polarization and the specific vector local mass displacement we got the rheological constitutive relations which include time derivatives of first and higher orders. The key system of equations is obtained for an isothermal approximation. This system is also written down relative to the scalar ϕ_u and vector ψ_u potentials of the vector displacement, the potential $\tilde{\mu}'_\pi$, the vector potential A , and the scalar generalized potential ϕ_{em} . Function ϕ_{em} is related to the scalar electric potential ϕ_e and the potential $\tilde{\mu}'_\pi$ by differential relation (4-6). The Lorentz gauge is generalized in such a way that equations for the vector potential of the electromagnetic field and for the generalized scalar potential are not interrelated and have similar structures. The effects of the mentioned irreversibility and polarization inertia on the interaction of the investigated fields is discussed.

References

- [Burak 1987] Y. Burak, “Constitutive equations of locally gradient thermomechanics”, *Dopov. Akad. Nauk URSS* **12** (1987), 19–23. In Ukrainian; translated in *Proc. Acad. Sci. Ukrain. SSR*.
- [Burak et al. 2008] Y. Burak, V. Kondrat, and O. Hrytsyna, “An introduction of the local displacements of mass and electric charge phenomena into the model of the mechanics of polarized electromagnetic solids”, *J. Mech. Mater. Struct.* **3**:6 (2008), 1037–1046.
- [Buryachenko and Pagano 2003] V. A. Buryachenko and N. J. Pagano, “Non-local models of stress field concentrations and effective thermoelastic properties of random structure composites”, *Math. Mech. Solids* **8**:4 (2003), 403–433.
- [Chapla et al. 2009] Y. Chapla, S. Kondrat, O. Hrytsyna, and V. Kondrat, “On electromechanical phenomena in thin dielectric films”, *Task Quart.* **13**:1 (2009), 145–154.
- [Ciancio 1989] V. Ciancio, “On the generalized Debye equation for media with dielectric relaxation phenomena described by vectorial internal thermodynamic variables”, *J. Non Equilib. Thermodyn.* **14**:3 (1989), 239–250.
- [Cimmelli and Ván 2005] V. A. Cimmelli and P. Ván, “The effects of nonlocality on the evolution of higher order fluxes in nonequilibrium thermodynamics”, *J. Math. Phys.* **46**:11 (2005), 112901.
- [Dolfin et al. 2004] M. Dolfin, M. Francaviglia, and L. Restuccia, “Thermodynamics of deformable dielectrics with a non-Euclidean structure as internal variable”, *Tech. Mech.* **24**:2 (2004), 137–145.
- [Eringen 1984] A. C. Eringen, “Theory of nonlocal piezoelectricity”, *J. Math. Phys.* **25**:3 (1984), 717–727.
- [Erofeyev 2003] V. I. Erofeyev, *Wave processes in solids with microstructure*, World Scientific, Singapore, 2003.

- [Forest and Amestoy 2008] S. Forest and M. Amestoy, “Hypertemperature in thermoelastic solids”, *C. R. Mécanique* **336**:4 (2008), 347–353.
- [de Groot and Mazur 1962] S. R. de Groot and P. Mazur, *Non-equilibrium thermodynamics*, North-Holland, Amsterdam, 1962.
- [Hrytsyna and Kondrat 2007] O. Hrytsyna and V. Kondrat, “Modelling of electro-magneto-thermo-mechanical processes in a viscous electrically conducting polarized fluid taking into account irreversibility of a local displacements of mass and electric charge”, *Physico-Mathematical Modelling and Informational Technologies* **5** (2007), 42–54. In Ukrainian.
- [Kafadar 1971] C. B. Kafadar, “Theory of multipoles in classical electromagnetism”, *Int. J. Eng. Sci.* **9**:9 (1971), 831–853.
- [Kondrat and Hrytsyna 2008a] V. Kondrat and O. Hrytsyna, “The equations of electro-magneto-thermo-mechanics of polarized nonferromagnetic solids taking into account a local displacement of mass”, *Physico-Mathematical Modelling and Informational Technologies* **8** (2008), 69–83. In Ukrainian.
- [Kondrat and Hrytsyna 2008b] V. F. Kondrat and O. R. Hrytsyna, “Equations of thermomechanics of deformable bodies with regard for irreversibility of local displacement of mass”, *Mat. Metody i Fiz.-Mekh. Polya* **51**:1 (2008), 169–177. In Ukrainian; translated in *J. Math. Sci.* **160**:4 (2009), 492–502.
- [Kondrat and Hrytsyna 2009a] V. Kondrat and O. Hrytsyna, “Linear theories of electromagnetomechanics of dielectrics”, *Physico-Mathematical Modelling and Informational Technologies* **9** (2009), 7–46. In Ukrainian.
- [Kondrat and Hrytsyna 2009b] V. F. Kondrat and O. R. Hrytsyna, “Mechanoelectromagnetic interaction in isotropic dielectrics with regard to the local displacement of mass”, *Mat. Metody i Fiz.-Mekh. Polya* **52**:1 (2009), 150–158. In Ukrainian; translated in *J. Math. Sci.* **168**:5 (2010), 688–698.
- [Kondrat and Hrytsyna 2010] V. Kondrat and O. Hrytsyna, “Electromagnetomechanical waves dispersion in local gradient dielectrics with polarization inertia”, *Physico-Mathematical Modelling and Informational Technologies* **11** (2010), 81–90. In Ukrainian.
- [Kuno 2004] M. Kuno, “Introduction to nanoscience and nanotechnology: a workbook”, 2004, Available at http://www.nd.edu/~djena/Kens_Notes.pdf.
- [Landau and Lifshitz 1982] L. D. Landau and E. M. Lifshitz, *Электродинамика сплошных сред*, 2nd ed., Nauka, Moscow, 1982. In Russian; translated as *Electrodynamics of continuous media*, Course of Theoretical Physics **8**, Pergamon, Oxford, 1984.
- [Ma and Cross 2003] W. H. Ma and L. E. Cross, “Strain-gradient-induced electric polarization in lead zirconate titanate ceramics”, *Appl. Phys. Lett.* **82**:19 (2003), 3293–3295.
- [Majdoub 2010] M. S. Majdoub, *Flexoelectricity and piezoelectricity in nanostructures and consequences for energy harvesting and storage*, Ph.D. thesis, University of Houston, 2010, Available at <http://gradworks.umi.com/34/16/3416806.html>.
- [Majdoub et al. 2008] M. S. Majdoub, P. Sharma, and T. Çağın, “Enhanced size-dependent piezoelectricity and elasticity in nanostructures due to the flexoelectric effect”, *Phys. Rev. B* **77**:12 (2008), 125424.
- [Majdoub et al. 2009] M. S. Majdoub, R. Maranganti, and P. Sharma, “Understanding the origins of the intrinsic dead layer effect in nanocapacitors”, *Phys. Rev. B* **79**:11 (2009), 115412.
- [Maugin 1988] G. A. Maugin, *Continuum mechanics of electromagnetic solids*, North-Holland Series in Applied Mathematics and Mechanics **33**, North-Holland, Amsterdam, 1988.
- [Mead 1961] C. A. Mead, “Anomalous capacitance of thin dielectric structures”, *Phys. Rev. Lett.* **6**:10 (1961), 545–546.
- [Mead 1962] C. A. Mead, “Electron transport mechanisms in thin insulating films”, *Phys. Rev.* **128**:5 (1962), 2088–2093.
- [Mindlin 1972] R. D. Mindlin, “Elasticity, piezoelectricity and crystal lattice dynamics”, *J. Elasticity* **2**:4 (1972), 217–282.
- [Papargyri-Beskou et al. 2009] S. Papargyri-Beskou, D. Polyzos, and D. E. Beskos, “Wave dispersion in gradient elastic solids and structures: a unified treatment”, *Int. J. Solids Struct.* **46**:21 (2009), 3751–3759.
- [Papenfuss and Forest 2006] C. Papenfuss and S. Forest, “Thermodynamical frameworks for higher grade material theories with internal variables or additional degrees of freedom”, *J. Non Equilib. Thermodyn.* **31**:4 (2006), 319–353.
- [Sharma et al. 2007] N. D. Sharma, R. Maranganti, and P. Sharma, “On the possibility of piezoelectric nanocomposites without using piezoelectric materials”, *J. Mech. Phys. Solids* **55**:11 (2007), 2328–2350.
- [Tagantsev 1986] A. K. Tagantsev, “Piezoelectricity and flexoelectricity in crystalline dielectrics”, *Phys. Rev. B* **34**:8 (1986), 5883–5889.

- [Tauchert and Guzelsu 1972] T. R. Tauchert and A. N. Guzelsu, “An experimental study of dispersion of stress waves in a fiber-reinforced composite”, *J. Appl. Mech. (ASME)* **39**:1 (1972), 98–102.
- [Ván 2003] P. Ván, “Weakly nonlocal irreversible thermodynamics”, *Ann. Phys. (8)* **12**:3 (2003), 146–173.
- [Yang 2006] J. S. Yang, “A review of a few topics in piezoelectricity”, *Appl. Mech. Rev. (ASME)* **59**:6 (2006), 335–345.
- [Yang and Yang 2004] J. S. Yang and X. M. Yang, “Electric field gradient effect and thin film capacitance”, *World J. Eng.* **1**:2 (2004), 41–45.
- [Yerofeyev and Sheshenina 2005] V. I. Yerofeyev and O. A. Sheshenina, “Waves in a gradient-elastic medium with surface energy”, *J. Appl. Math. Mech.* **69**:1 (2005), 57–69.

Received 24 Jan 2011. Revised 4 Jul 2011. Accepted 15 Dec 2011.

VASYL KONDRAT: kon@cmm.lviv.ua

Center of Mathematical Modeling of the Institute of Applied Mathematics and Mechanics, National Academy of Sciences of Ukraine, 15 D. Dudajeva St. 15, 79005 Lviv, Ukraine

OLHA HRYTSYNA: gryt@cmm.lviv.ua

Center of Mathematical Modeling of the Institute of Applied Mathematics and Mechanics, National Academy of Sciences of Ukraine, 15 D. Dudajeva St. 15, 79005 Lviv, Ukraine

<http://cmm.lviv.ua/hrytcyna.html>

ELECTROMAGNETOELASTIC WAVES IN A VORTEX LAYER OF A SUPERCONDUCTOR

BOGDAN T. MARUSZEWSKI, ANDRZEJ DRZEWIECKI AND ROMAN STAROSTA

Magnetic field enters the type-II superconducting body along a discrete arrangement of magnetic vortex lines. The paper aims at investigating the dispersion and amplitude distributions of magnetoelastic waves propagating solely in the vortex field of the superconducting layer. Our attention has been focused on the dispersion features and amplitudes for various wave velocities. The vortex field consists only of soft vortices (the superconducting crystal is free of lattice defects).

1. Introduction

Magnetic flux can penetrate the type-II superconductor in the form of Abrikosov vortices (also called flux lines, flux tubes or fluxons), each carrying a quantum of magnetic flux. Since the vortices are formed by the applied magnetic field, the supercurrent flows around of each of them. There exist also Lorentz force interactions among them, which give rise to an additional thermomechanical (stress) field in type-II superconductors. Near the lower critical magnetic intensity limit H_{c1} , this field has elastic character. However, if the density of the supercurrent is above its critical value and/or the temperature is sufficiently high, there occurs a flow (creep or diffusion) of vortex lines in the superconducting body. The *fluidity* of the vortex array has been also observed when the applied magnetic field approaches its upper critical limit H_{c2} [Blatter et al. 1994; Brandt 1995; Cyrot and Pavuna 1992]. Following a magnetothermomechanical model of interactions in such II-type superconductors both for the *lattice-like* and *fluid-like* states of the vortex field, where the specific definition of the vortex field stress tensor has been introduced [Maruszewski 1998; 2007], this paper aims at determining the dispersion and amplitude distributions of magnetoelastic waves propagating along soft vortices in the superconducting layer.

If the crystal lattice of the layer is free of lattice defects, there is a parallel arrangement of soft vortex cores (Figure 1, left). However, in real crystals, imperfections such as vacancies, dislocations, disclinations, grain boundaries, and interstitial atoms cause that the vortex lines can be curved or even tangled because of pinning (Figure 1, right). We have confined in the paper only to the *lattice-like* state. The choice of the geometry of the vortex field (layer) was motivated by a need to check if those magnetoelastic waves and electromagnetoelastic waves in such peculiar environment are possible to be guided.

The natural conditions where devices may use such a technological solution exist in space where temperature is about 4K and majority of elements and materials behave as superconductors. In the paper the particular analysis of the SH magnetoelastic and compressional and flexural electromagnetoelastic modes has been presented.

Partially supported by Poland's Ministry of Science and Higher Education (MNiSzW) grant 1101/T02/2006/30 and DS grant 21-320/2009.

Keywords: magnetoelastic waves, dispersion, superconductor.

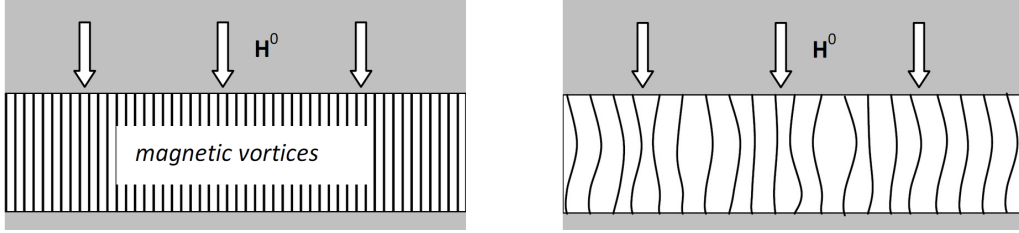


Figure 1. Vortices in a perfect crystal (left) and in a real one (right), where pinning can occur.

2. General wave equations

Let us now consider a problem which deals with the dynamics of the previously defined vortex field. Following the thermodynamical model of the electromagnetomechanical interactions in continuous media, i.e., the momentum balance with Hooke's law and the Maxwell equations in the moving frames with the first London equation we are able to formulate proper equations describing dynamics of the vortex field in the elastic superconductor. For the sake of simplicity thermal influences have been omitted. The governing equations of the electromagnetoelastic vortex waves read as follows [Maruszewski et al. 2007]:

$$\begin{aligned} \mu u_{i,jj} + \eta \dot{u}_{i,jj} + (\lambda + \mu) u_{j,ij} + \frac{1}{3} \eta \dot{u}_{j,ij} - \mu_0 (h_{r,i} - h_{i,r}) H_r^0 - \rho \ddot{u}_i &= 0, \\ \lambda_0^2 h_{i,kk} - h_i + u_{i,k} H_k^0 - u_{k,k} H_i^0 &= 0, \\ \lambda_0^2 e_{i,jj} - e_i + \mu_0 e_{ijk} \dot{u}_j H_k^0 &= 0, \end{aligned} \quad (1)$$

where u_k is the displacement vector of the vortex field point, H_r^0 is the applied magnetic field normal to the limiting surfaces of the layer (Figure 1), h_r is the small contribution to the total magnetic field in the layer comparing to H_r^0 and describes its perturbations, because the linear form of equations (1) results from

$$H_k = H_k^0 + h_k, \quad |h_k| \ll |H_k^0|. \quad (2)$$

Here e_k is the electric field intensity understood in the sense of (2), λ and μ are Lamé's constants, μ_0 is the permeability of vacuum, η is the viscosity coefficient (inside each vortex core flows a normal current, so the Ohmic resistivity occurs there [Cyrot and Pavuna 1992]), ρ is the vortex density [Maruszewski 2007; Maruszewski et al. 2007], and λ_0 is the London penetration depth. Any thermal influences on the considered waves have been omitted. The solutions of equations (1) are looked for in the form

$$f(x_1, x_3, t) = \tilde{f}(x_1) \exp[i(\omega t - kx_3)], \quad (3)$$

where $\tilde{f}(x_1)$ are the amplitudes of signals $u_1, u_2, u_3, h_1, h_2, h_3, e_1, e_2, e_3$ propagating in x_1 direction with the velocity v :

$$\tilde{f}(x_1) = \{u_1, u_2, u_3, h_1, h_2, h_3, e_1, e_2, e_3\} \quad (4)$$

if the geometry of the problem is as shown in Figure 2.

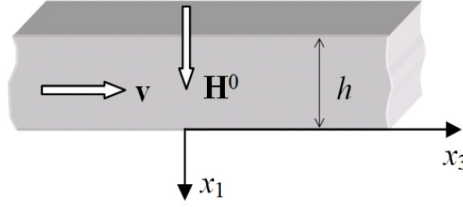


Figure 2. Geometry of the problem.

To facilitate the analysis of the waves, all the relations will be presented in the dimensionless form, with the help of the following substitutions, where \tilde{c} is the speed of light:

$$\begin{aligned}
 x_1 &= hx, & x_2 &= hy, & x_3 &= hz, & t &= T\tau, & T &= \frac{h}{v_T}, & v_T &= \sqrt{\frac{\mu}{\rho}}, & \Omega &= \omega T, \\
 c &= \frac{kv_T}{\omega} = \frac{v_T}{v}, & \tilde{\lambda}_0 &= \frac{\lambda_0}{h}, & \tilde{\mu} &= \frac{K}{\mu}, \\
 K &= \lambda + \frac{2}{3}\mu, & \tilde{\lambda} &= \frac{\lambda}{\mu}, & \tilde{\rho} &= \frac{\rho v_T^2}{\mu} = 1, & H^0 &= H_{c1}H_0, & E &= \tilde{c}\mu_0H_{c1}, \\
 c_1 &= \frac{v_T}{\tilde{c}}, & u_1 &= hu_x, & u_2 &= hu_y, & u_3 &= hu_z, \\
 \tilde{\eta} &= \eta \frac{h}{v_T}, & e_1 &= Ee_x, & e_2 &= Ee_y, & e_3 &= Ee_z, & \tilde{\mu} &= \frac{\mu_0 H_{c1}^2}{\mu}, \\
 h_1 &= H_{c1}h_x, & h_2 &= H_{c1}h_y, & h_3 &= H_{c1}h_z.
 \end{aligned} \tag{5}$$

3. SH magnetoelastic waves

Let us consider at the beginning the SH magnetoelastic wave propagating along the vortex layer shown in Figure 2. The general equations (1) in this case reduce to

$$\mu u_{i,jj} + \eta \dot{u}_{i,jj} + (\lambda + \mu)u_{j,ij} + \frac{1}{3}\eta \dot{u}_{j,ij} - \mu_0(h_{r,i} - h_{i,r})H_r^0 - \rho \ddot{u}_i = 0, \tag{6}$$

$$\lambda_0^2 h_{i,kk} - h_i + u_{i,k}H_k^0 - u_{k,k}H_i^0 = 0, \tag{7}$$

since the SH wave amplitudes in the layer are now looked for in the form (3) with

$$\tilde{f}(x_1) = \{u_2, h_2\}, \tag{8}$$

because

$$\mathbf{u} = [0, u_2, 0], \quad \mathbf{h} = [0, h_2, 0]. \tag{9}$$

Taking (5) into account, the SH wave equations (6) and (7) become in dimensionless form

$$\begin{aligned}
 (\tilde{\mu} + i\Omega\tilde{\eta})\frac{d^2u_y}{dx^2} + \frac{\Omega^2}{c^2}(v^2\tilde{\rho} - \tilde{\mu} - i\Omega\tilde{\eta})u_y + \tilde{\mu}H_0\frac{dh_y}{dx} &= 0, \\
 \tilde{\lambda}_0^2\frac{d^2h_y}{dx^2} - (\tilde{\lambda}_0^2\frac{\Omega^2}{c^2} + 1)h_y + H_0\frac{du_y}{dx} &= 0.
 \end{aligned} \tag{10}$$

On using relations (5) in (8), the solutions of (10) determine the following amplitudes of the SH magnetoelastic waves:

$$\begin{aligned} u_y &= S_1 e^{p_1 x} + S_2 e^{-p_1 x} + S_3 e^{p_2 x} + S_4 e^{-p_2 x}, \\ h_y &= -M(p_1, \Omega, c) S_1 e^{p_1 x} + M(p_1, \Omega, c) S_2 e^{-p_1 x} - M(p_2, \Omega, c) S_3 e^{p_2 x} + M(p_2, \Omega, c) S_4 e^{-p_2 x}, \end{aligned} \quad (11)$$

where

$$M(p_k, \Omega, c) = \frac{p_k}{\bar{\mu} H_0} + \frac{\Omega^2 (1 - 1/c^2)}{\bar{\mu} H_0 p_k}, \quad k = 1, 2.$$

The parameters p_1 and p_2 were determined from the characteristic equation

$$\tilde{\lambda}_0^2 A(\Omega) p^4 + [\tilde{\lambda}_0^2 B(\Omega, c) - F(\Omega, c) A(\Omega) - \mu_0 H_0^2] p^2 - F(\Omega, c) B(\Omega, c) = 0 \quad (12)$$

where

$$A(\Omega) = 1 + i\Omega\tilde{\eta}, \quad B(\Omega, c) = \frac{\Omega^2}{c^2} (c^2 - 1 - i\Omega\tilde{\eta}), \quad F(\Omega, c) = \tilde{\lambda}_0^2 \frac{\Omega^2}{c^2} + 1.$$

A detailed analysis of the characteristic equation shows that wave propagation is possible only if

$$B(\Omega, c) > 0. \quad (13)$$

From (13) we get that if SH magnetoelastic wave amplitude is a function of x , then

$$c = \frac{v}{v_r} < 1 \quad (14)$$

We neglect, from now on, viscous features of the vortex field, in view of their very weak influence on the propagation process; see [Cyrot and Pavuna 1992; Maruszewski et al. 2008].

Since the waves propagate along the layer, we should now take into account the proper boundary conditions for solving the set of equations (10). They follow from Figure 2, and read

$$h_y = 0 \quad \text{and} \quad \frac{du_y}{dx} = 0 \quad \text{for } x = -1 \text{ and } x = 0. \quad (15)$$

The first of these conditions expresses the continuity of the tangent component of the magnetic field intensity, while the second follows from the equality $\sigma_{yz} = 0$ (the surfaces are free of loadings).

Substituting (11) into (15) we obtain the set of algebraic equations

$$\begin{aligned} -M(p_1, \Omega, c) S_1 e^{-p_1} + M(p_1, \Omega, c) S_2 e^{p_1} - M(p_2, \Omega, c) S_3 e^{-p_2} + M(p_2, \Omega, c) S_4 e^{p_2} &= 0, \\ S_1 p_1 e^{-p_1} - S_2 p_1 e^{p_1} + S_3 p_2 e^{-p_2} + S_4 p_2 e^{p_2} &= 0, \\ -M(p_1, \Omega, c) S_1 + M(p_1, \Omega, c) S_2 - M(p_2, \Omega, c) S_3 + M(p_2, \Omega, c) S_4 &= 0, \\ S_1 p_1 - S_2 p_1 + S_3 p_2 + S_4 p_2 &= 0, \end{aligned} \quad (16)$$

or

$$\mathbf{W} \cdot \mathbf{S} = \mathbf{0}, \quad (17)$$

where

$$\mathbf{S} = \{S_1, S_2, S_3, S_4\}^T. \quad (18)$$

Hence we arrive at the dispersion relation for SH magnetoelastic wave in the form

$$\det \mathbf{W} = 0. \quad (19)$$

A unique solution for (19) exists if

$$c = 1. \tag{20}$$

Thus the SH wave is nondispersive and its amplitude is independent of x . (See [Oliner 1978, Chapter 5].) So, the supposition (14) is no longer valid. But the final conclusion is such that we are dealing only with the plane SH wave mode in the vortex layer, which propagates with constant velocity — (20).

4. Compressional (C) and flexural (F) electromagnetoelastic waves

Let us now focus on electromagnetoelastic waves propagating along the magnetic vortex field layer. Our aim is to answer the question of whether they can be guided by such a layer. It is well known that, besides the SH magnetoelastic waves considered in the previous section, compressional (symmetric) and flexural (antisymmetric) waves may also propagate along waveguides in the form of a rod, plate or ribbon [Achenbach 1976, Chapter 8; Oliner 1978, Chapter 5; Eringen and Şuhubi 1975, Chapter 7] (Figure 3).

The solutions of the C and F wave equations (1) are looked this time for in the form (3) where $\tilde{f}(x_1)$ now stands for

$$\tilde{f}(x_1) = \{u_1, u_3, h_1, h_3, e_2\} \tag{21}$$

since (see Figure 4)

$$\mathbf{u} = [u_1, 0, u_3], \quad \mathbf{h} = [h_1, 0, h_3], \quad \mathbf{e} = [0, e_2, 0]. \tag{22}$$

On using now (21) and (5) in (1) the dimensionless F and C wave equations read

$$\begin{aligned} & \left(\frac{4}{3} + \frac{1}{3}\tilde{G}\right)u_{x,xx} + \Omega^2(1 - c^2)u_x - \frac{1}{3}i\Omega c(\tilde{G} + 1)u_{z,x} = 0, \\ & u_{z,xx} + \Omega^2\left[1 - c^2\left(\frac{4}{3} + \frac{1}{3}\tilde{G}\right)\right]u_z - \frac{1}{3}i\Omega c(\tilde{G} + 1)u_{x,x} + i\tilde{\mu}H_0\Omega ch_x + \tilde{\mu}H_0h_{z,x} = 0, \\ & \tilde{\lambda}_0^2 h_{x,xx} - (1 + \tilde{\lambda}_0^2\Omega^2 c^2)h_x + i\Omega c H_0 u_z = 0, \\ & \tilde{\lambda}_0^2 h_{z,zz} - (1 + \tilde{\lambda}_0^2\Omega^2 c^2)h_z + H_0 u_{z,x} = 0, \\ & \tilde{\lambda}_0^2 e_{y,xx} - (1 + \tilde{\lambda}_0^2\Omega^2 c^2)e_y - i\Omega c_1 H_0 u_z = 0. \end{aligned} \tag{23}$$

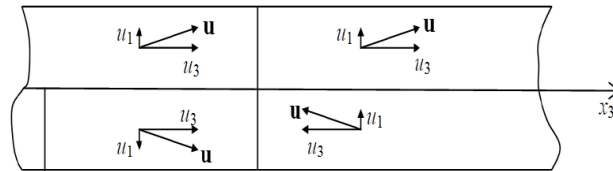


Figure 3. Symmetry of the vortex field displacements [Eringen and Şuhubi 1975]: symmetric-compressional wave (left pair) and antisymmetric-flexural wave (right pair).

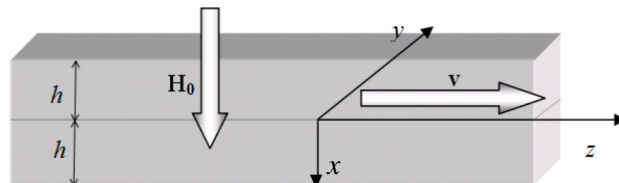


Figure 4. Geometry of the problem for the C and F waves in the vortex layer, following (5).

These equations should be completed by the electromagnetic field equations in vacuum:

$$h_{x,xx}^p - \Omega^2(c^2 - c_1^2)h_x^p = 0, \quad h_{z,xx}^p - \Omega^2(c^2 - c_1^2)h_z^p = 0, \quad e_{y,xx}^p - \Omega^2(c^2 - c_1^2)e_y^p = 0, \quad (24)$$

where superscript p denotes fields in a vacuum.

The jump and boundary conditions for (23) and (24) at the upper and lower planes of the layer read (see Figure 4)

$$\begin{aligned} \sigma_{xx}|_{x=-1} = 0 &\Rightarrow \frac{du_x}{dx}|_{x=-1} = 0; & \sigma_{zx}|_{x=-1} = 0 &\Rightarrow \frac{du_z}{dx}|_{x=-1} = 0; \\ (h_x = h_x^p)|_{x=0} &\text{ or } (e_y = e_y^p)|_{x=0}; & (h_z = h_z^p)|_{x=0}; & \\ \sigma_{xx}|_{x=1} = 0 &\Rightarrow \frac{du_x}{dx}|_{x=1} = 0; & \sigma_{zx}|_{x=1} = 0 &\Rightarrow \frac{du_z}{dx}|_{x=1} = 0; \\ (h_x = h_x^p)|_{x=1} &\text{ or } (e_y = e_y^p)|_{x=1}; & (h_z = h_z^p)|_{x=1}. & \end{aligned} \quad (25)$$

The desired C and F wave amplitudes are (using sh and ch to denote the hyperbolic sine and cosine)

$$\begin{aligned} u_x &= P(\xi_2)S_4 \text{ch}(\xi_2x) + P(\xi_2)S_3 \text{sh}(\xi_2x) + P(\xi_3)S_6 \text{ch}(\xi_3x) + P(\xi_3)S_5 \text{sh}(\xi_3x) + P(\xi_4)S_8 \text{ch}(\xi_4x) \\ &\quad + P(\xi_4)S_7 \exp(\xi_4x), \\ u_z &= Q(\xi_2)S_3 \text{ch}(\xi_2x) + Q(\xi_2)S_4 \text{sh}(\xi_2x) + Q(\xi_3)S_5 \text{ch}(\xi_3x) + Q(\xi_3)S_6 \text{sh}(\xi_3x) + Q(\xi_4)S_7 \text{ch}(\xi_4x) \\ &\quad + Q(\xi_4)S_8 \text{sh}(\xi_4x), \\ h_x &= S_3 \text{ch}(\xi_2x) + S_4 \text{sh}(\xi_2x) + S_5 \text{ch}(\xi_3x) + S_6 \text{sh}(\xi_3x) + S_7 \text{ch}(\xi_4x) + S_8 \text{sh}(\xi_4x), \\ h_z &= -\frac{i}{\Omega c} [\xi_2 S_4 \text{ch}(\xi_2x) + \xi_2 S_3 \text{sh}(\xi_2x) + \xi_3 S_6 \text{ch}(\xi_3x) + \xi_3 S_5 \text{sh}(\xi_3x) + \xi_4 S_8 \text{ch}(\xi_4x) + \xi_4 S_7 \text{sh}(\xi_4x)], \\ e_y &= -\frac{c_1}{c} [S_3 \text{ch}(\xi_2x) + S_4 \text{sh}(\xi_2x) + S_5 \text{ch}(\xi_3x) + S_6 \text{sh}(\xi_3x) + S_7 \text{ch}(\xi_4x) + S_8 \text{sh}(\xi_4x)], \end{aligned} \quad (26)$$

where

$$P(\xi) = -\frac{\xi(\tilde{G} + 1)(\tilde{\lambda}_0^2 \xi^2 - 1 - \tilde{\lambda}_0^2 \Omega^2 c^2)}{H_0[(4 + \tilde{G})\xi^2 + 3\Omega^2(1 - c^2)]}, \quad Q(\xi) = i \frac{\tilde{\lambda}_0^2 \xi^2 - 1 - \tilde{\lambda}_0^2 \Omega^2 c^2}{\Omega c H_0}.$$

The parameters ξ_m are the solutions of the characteristic equation

$$(A\xi^6 + B\xi^4 + C\xi^2 + D)(\Omega^2 c^2 \tilde{\lambda}_0^2 - \tilde{\lambda}_0^2 \xi^2 + 1) = 0, \quad (27)$$

whose coefficients A , B , C and D are given in the Appendix.

The amplitudes of the electromagnetic waves outside the layer read as follows:

– above the upper plane:

$$h_x^p = S_1[\text{ch}(\tilde{\xi}_1x) + \text{sh}(\tilde{\xi}_1x)], \quad h_z^p = -\frac{i\tilde{\xi}_1}{\Omega c} S_1[\text{ch}(\tilde{\xi}_1x) + \text{sh}(\tilde{\xi}_1x)], \quad e_y^p = -\frac{c_1}{c} S_1[\text{ch}(\tilde{\xi}_1x) + \text{sh}(\tilde{\xi}_1x)], \quad (28)$$

– below the lower plane:

$$h_x^p = S_2[\text{ch}(\tilde{\xi}_1x) - \text{sh}(\tilde{\xi}_1x)], \quad h_z^p = \frac{i\tilde{\xi}_1}{\Omega c} S_2[\text{ch}(\tilde{\xi}_1x) - \text{sh}(\tilde{\xi}_1x)], \quad e_y^p = -\frac{c_1}{c} S_2[\text{ch}(\tilde{\xi}_1x) + \text{sh}(\tilde{\xi}_1x)]. \quad (29)$$

Now using solutions (26), (28) and (29) in the boundary and jump conditions (25) we get a set of eight algebraic equations for S_1 through S_8 . They are given in the Appendix. After laborious calculations this set of eight equation splits into two uncoupled sets:

$$\mathbf{W}_C \cdot \mathbf{S}_C = \mathbf{0}, \quad (30)$$

$$\mathbf{W}_F \cdot \mathbf{S}_F = \mathbf{0}, \quad (31)$$

where

$$\mathbf{S}_C = \left\{ \frac{1}{2}(S_1 - S_2), S_4, S_6, S_8 \right\}^T, \quad \mathbf{S}_F = \left\{ \frac{1}{2}(S_1 + S_2), S_3, S_5, S_7 \right\}^T.$$

Hence the dispersion relations for the considered waves are

$$\text{– for compressional modes:} \quad \det \mathbf{W}_C = 0, \quad (32)$$

$$\text{– for flexural modes:} \quad \det \mathbf{W}_F = 0. \quad (33)$$

5. Numerical results

In this section we limit ourselves to the numerical analysis of the compressional and flexural electromagnetic wave propagation conditions since the SH magnetic wave is nondispersive propagating with the constant velocity and is amplitude independent of the thickness of the layer. All the calculations have been made for $\text{YBa}_2\text{Cu}_3\text{O}_{6+x}$, or YBCO, ceramics. We have restricted ourselves to the *lattice-like* state of the vortex field, so the external magnetic H_0 is taken slightly higher than the limiting lower magnetic field value H_{c1} .

Firstly, let us take care of the existence of the C and F waves in the layer. The conditions dealing with their existence result from characteristic equation (27). That situation is illustrated in Figure 5.

Before we start analysis of the amplitude distribution of the C and F waves in the layer we should consider their dispersion. Figure 6 shows the dispersion of the C waves calculated from (32), and the F waves, from (33).

Remark that both in the C and F wave cases only one single modes propagate. That feature is anomalous and differs from that for the classical elastic body where infinite number of modes propagate [Eringen and Şuhubi 1975, Chapter 7]. From Figure 6 it is also visible that waves C and F characterize anomalous dispersion: they propagate with acoustic velocity having optical frequencies (C wave has

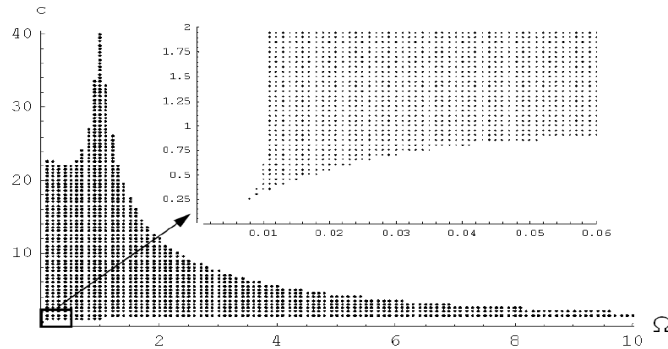


Figure 5. Area of existence of C and F waves.

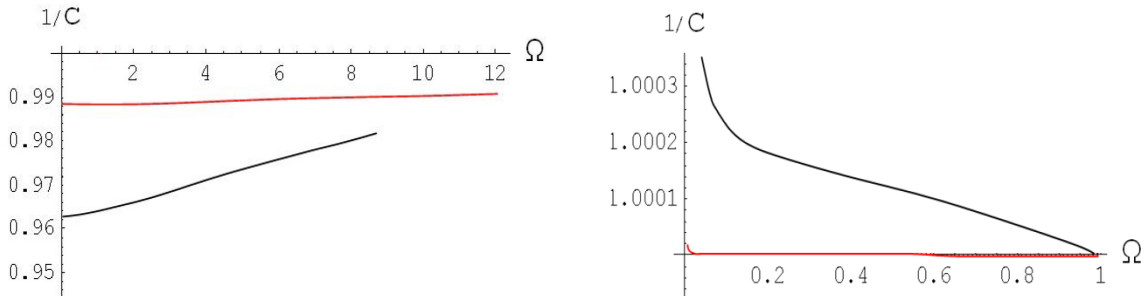


Figure 6. Dispersion of C waves (left) and of F waves (right) for $h = 10^{-7}$ m. Black: $H_0 = 1$; red: $H_0 = 10$.

higher frequency comparable to the frequency spectrum of the visible light than F wave has lower frequency comparable to the frequency spectrum of the infrared rays). Moreover, for both cases the dispersion decreases if the external magnetic field H_0 increases. Now let us take care of the amplitudes.

Compressional waves. The compressional (C) wave amplitudes for $h_x, h_z, e_y, u_x, u_z, \sigma_{xx}$ and σ_{xz} are presented in Figure 7. Shaded areas indicate the layer region.

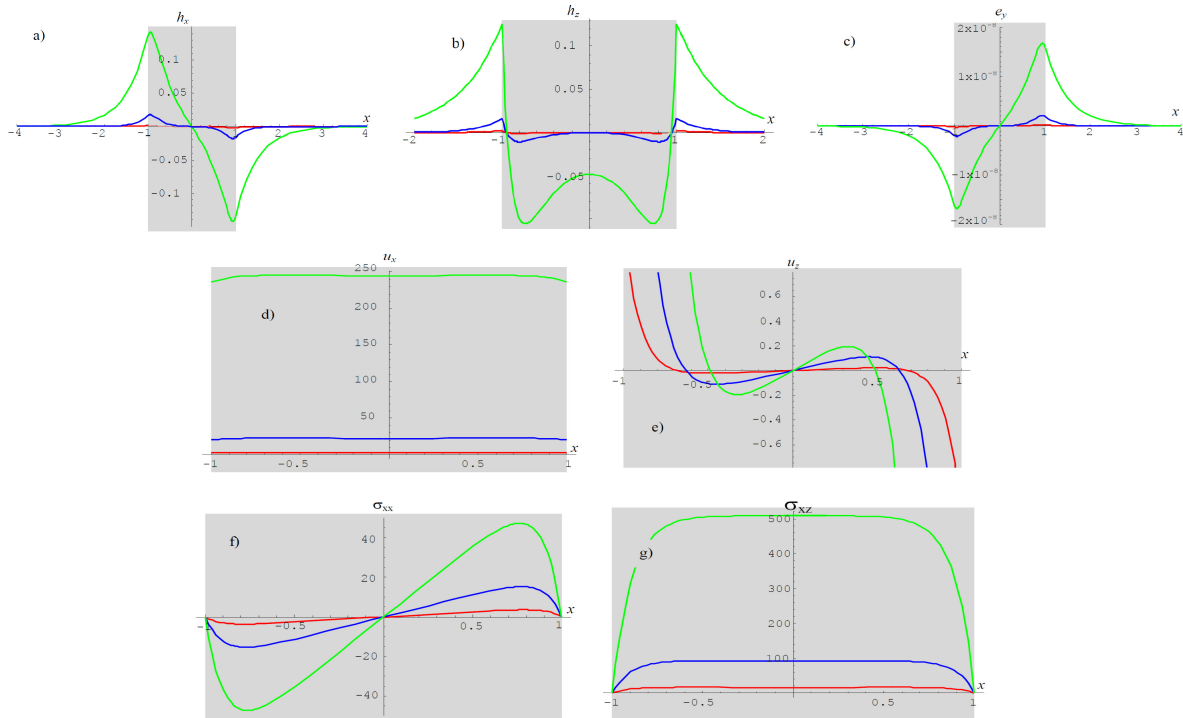


Figure 7. Compressional wave amplitudes for $H_0 = 1$ and $h = 10^{-7}$ m. Top row: h_x, h_z, e_y . Middle row: u_x, u_z . Bottom row: σ_{xx}, σ_{xz} . Green: $\Omega = 0.2$. Blue: $\Omega = 0.6$. Red: $\Omega = 0.9$.

The simple look at the drawings in Figure 7 shows that in the case of the electromagnetic part of the C waves (top row) their amplitudes reach extremal values at the lateral planes of the layer and are continuous across them. But the mechanical part of the C waves behave differently (middle and bottom rows). They naturally exist only between the lateral planes of the layer. Then the longitudinal u_x and shear σ_{xz} modes are symmetric with respect to the middle surface of the layer. But the general conclusion for all modes is such that all their amplitudes decreases if the frequency Ω increases.

Flexural waves. The flexural (F) wave amplitudes for $h_x, h_z, e_y, u_x, u_z, \sigma_{xx}$ and σ_{xz} are presented in Figure 8.

The properties of the F wave amplitudes differ from their C counterpart. For example, h_x and e_z amplitudes are extremal at the middle surface of the layer and do not “feel” its lateral planes disappearing smoothly in infinity. Then antisymmetric h_z is extremal at the above planes. The mechanical mode amplitudes behave as follows:

- u_x mode is linear and antisymmetric vanishing at the middle surface; it exist solely inside the layer.
- u_z is symmetric with respect to the middle surface reaching there extremum.

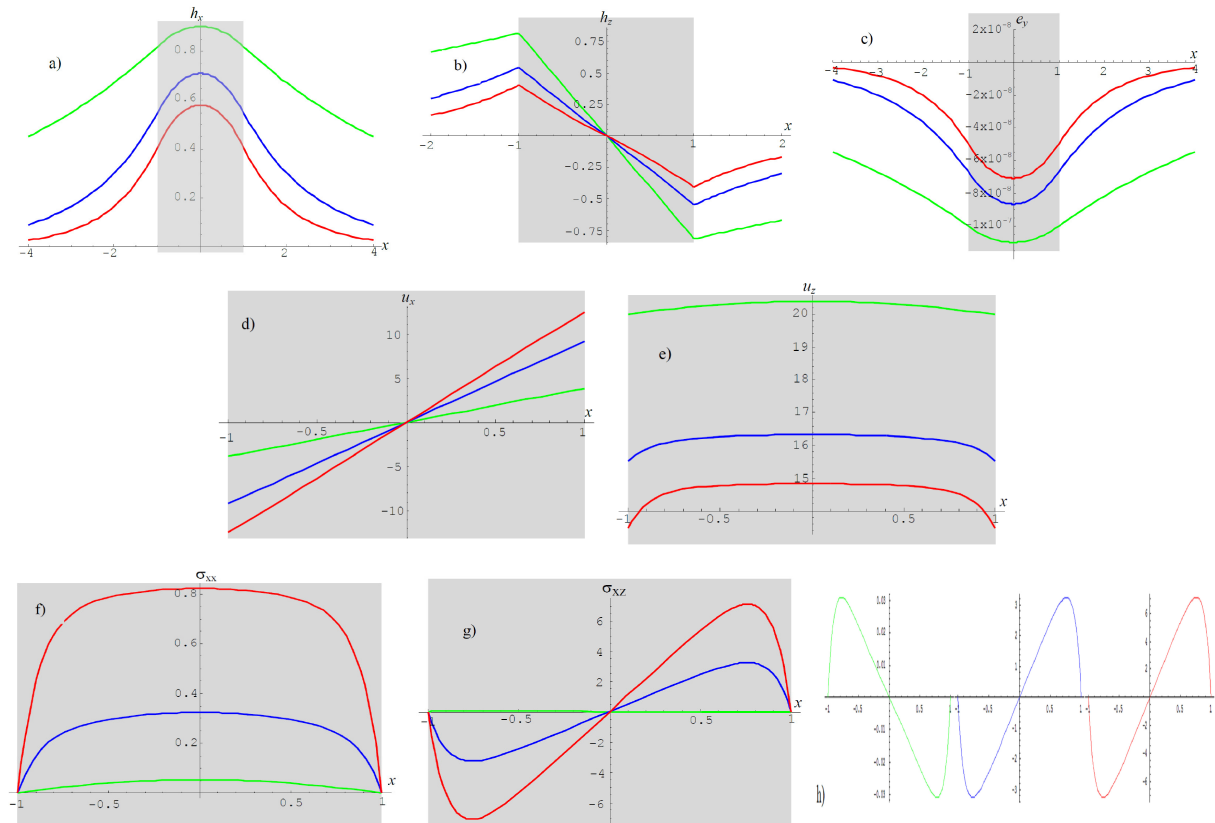


Figure 8. Flexural wave amplitudes for $H_0 = 1$ and $h = 10^{-7}$ m. Green: $\Omega = 0.2$. Blue: $\Omega = 0.6$. Red: $\Omega = 0.9$. Top row: h_x, h_z, e_y . Middle row: u_x, u_z . Bottom row: σ_{xx}, σ_{xz} . The last panel, (h), shows the same graphs as (g) but at different scales.

- σ_{xx} (the trace part of the stress associated with the wave propagation direction) behaves like u_z ; however, it vanishes at the lateral planes.
- σ_{xz} is antisymmetric with respect to the middle plane vanishing at the lateral surfaces. However it behaves anomalously; from the last two panels in the bottom row of Figure 8 we see that there exists a frequency Ω_{cr} for which σ_{xz} values are equal to zero across the layer, so the σ_{xz} stress values change sign if they are observed for $\Omega < \Omega_{cr}$ or for $\Omega > \Omega_{cr}$.

According to the dependence of Ω the electromagnetic mode amplitudes decrease if the frequency Ω increases contrary to the mechanical modes behavior (Figure 8).

6. Conclusions

The considerations made in the paper show that two general types of waves can propagate in the vortex array existing solely in the superconducting layer. The first one deals with the SH magnetoelastic modes and the second type concerns electromagnetoelastic compressional and flexural modes. It is known that layers can be used in some situations as waveguides. Investigations made in the paper confirmed that guided signal transmission along the magnetic vortex field is possible. Natural conditions for such an application exist in free space, so such a technology, which is not energy consuming, might be used in space ships or other similar equipment.

Except for classical properties, electromagnetoelastic C and F waves involve the same anomalous features, as seen in Figure 8(c), (g), (h). The u_x mode is linearly distributed across the layer, which differs from the classical (mechanical non-vortex) situation. But a much more interesting result is presented in Figure 8 (g), (h). We see that there exists a definite critical frequency Ω_{cr} for which the amplitude of the F σ_{xz} mode vanishes across the entire layer. That means that for such critical frequency Ω_{cr} σ_{xz} mode does not propagate.

Appendix: The coefficients of (27) and the algebraic equations encoded in (30)–(31)

The coefficients of (27) are given by

$$\begin{aligned}
 A &= \tilde{\lambda}_0^2(4 + \tilde{G}), \\
 B &= -4(3\Omega^2 c^2 \tilde{\lambda}_0^2 + 1) - \tilde{G}(3\Omega^2 c^2 \tilde{\lambda}_0^2 + 1) - 4H_0^2 \tilde{\mu} + 7\Omega^2 \tilde{\lambda}_0^2 + \tilde{G}(\Omega^2 \tilde{\lambda}_0^2 - H_0^2 \tilde{\mu}), \\
 C &= 4\Omega^2 c^2 (3\Omega^2 c^2 \tilde{\lambda}_0^2 + 2) + \Omega^2 [\tilde{G} c^2 (3\Omega^2 c^2 \tilde{\lambda}_0^2 + 2) + 7(H_0^2 c^2 \tilde{\mu} - 2\Omega^2 c^2 \tilde{\lambda}_0^2 - 1)] \\
 &\quad + \Omega^2 [\tilde{G}(H_0^2 c^2 \tilde{\mu} - 2\Omega^2 c^2 \tilde{\lambda}_0^2 - 1) - 3(H_0^2 \tilde{\mu} - \Omega^2 \tilde{\lambda}_0^2)], \\
 D &= -4\Omega^2 c^4 (\Omega^2 c^2 \tilde{\lambda}_0^2 + 1) - \Omega^4 c^2 [\tilde{G} c^2 (\Omega^2 c^2 \tilde{\lambda}_0^2 + 1) + 3H_0^2 c^2 \tilde{\mu} - 7(\Omega^2 c^2 \tilde{\lambda}_0^2 + 1)] \\
 &\quad + \Omega^4 [\tilde{G} c^2 (\Omega^2 c^2 \tilde{\lambda}_0^2 + 1) + 3(H_0^2 c^2 \tilde{\mu} - \Omega^2 c^2 \tilde{\lambda}_0^2 - 1)].
 \end{aligned}$$

We next give the algebraic equations satisfied for S_1, S_2, \dots, S_8 . Let

$$Y(\xi) = \frac{1}{3}(4 + \tilde{G})P(\xi)\xi - \frac{1}{3}i\Omega c(\tilde{G} - 2)Q(\xi) \quad \text{and} \quad Z(\xi) = [-Q(\xi)\xi + i\Omega cP(\xi)],$$

where sh and ch denote the hyperbolic sine and cosine. Then

$$\begin{aligned}
 Y(\xi_2) \operatorname{ch} \xi_2 S_3 - Y(\xi_2) \operatorname{sh} \xi_2 S_4 + Y(\xi_3) \operatorname{ch} \xi_3 S_5 - Y(\xi_3) \operatorname{sh} \xi_3 S_6 + Y(\xi_4) \operatorname{ch} \xi_4 S_7 - Y(\xi_4) \operatorname{sh} \xi_4 S_8 &= 0, \\
 Z(\xi_2) \operatorname{ch} \xi_2 S_3 - Z(\xi_2) \operatorname{sh} \xi_2 S_4 + Z(\xi_3) \operatorname{ch} \xi_3 S_5 - Z(\xi_3) \operatorname{sh} \xi_3 S_6 + Z(\xi_4) \operatorname{ch} \xi_4 S_7 - Z(\xi_4) \operatorname{sh} \xi_4 S_8 &= 0, \\
 \tilde{\xi}_1 (\operatorname{ch} \tilde{\xi}_1 - \operatorname{sh} \tilde{\xi}_1) S_1 + \xi_2 \operatorname{sh} \xi_2 S_3 - \xi_2 \operatorname{ch} \xi_2 S_4 - \xi_3 \operatorname{sh} \xi_3 S_5 - \xi_3 \operatorname{ch} \xi_3 S_6 + \xi_4 \operatorname{sh} \xi_4 S_7 - \xi_4 \operatorname{ch} \xi_4 S_8 &= 0, \\
 (\operatorname{ch} \tilde{\xi}_1 - \operatorname{sh} \tilde{\xi}_1) S_1 - \operatorname{ch} \xi_2 S_3 + \operatorname{sh} \xi_2 S_4 - \operatorname{ch} \xi_3 S_5 + \operatorname{sh} \xi_3 S_6 - \operatorname{ch} \xi_4 S_7 + \operatorname{sh} \xi_4 S_8 &= 0, \\
 Y(\xi_2) \operatorname{ch} \xi_2 S_3 + Y(\xi_2) \operatorname{sh} \xi_2 S_4 + Y(\xi_3) \operatorname{ch} \xi_3 S_5 + Y(\xi_3) \operatorname{sh} \xi_3 S_6 + Y(\xi_4) \operatorname{ch} \xi_4 S_7 + Y(\xi_4) \operatorname{sh} \xi_4 S_8 &= 0, \\
 Z(\xi_2) \operatorname{ch} \xi_2 S_3 + Z(\xi_2) \operatorname{sh} \xi_2 S_4 + Z(\xi_3) \operatorname{ch} \xi_3 S_5 + Z(\xi_3) \operatorname{sh} \xi_3 S_6 + Z(\xi_4) \operatorname{ch} \xi_4 S_7 + Z(\xi_4) \operatorname{sh} \xi_4 S_8 &= 0, \\
 \tilde{\xi}_1 (\operatorname{ch} \tilde{\xi}_1 - \operatorname{sh} \tilde{\xi}_1) S_2 + \xi_2 \operatorname{sh} \xi_2 S_3 + \xi_2 \operatorname{ch} \xi_2 S_4 + \xi_3 \operatorname{sh} \xi_3 S_5 + \xi_3 \operatorname{ch} \xi_3 S_6 + \xi_4 \operatorname{sh} \xi_4 S_7 + \xi_4 \operatorname{ch} \xi_4 S_8 &= 0, \\
 (\operatorname{ch} \tilde{\xi}_1 - \operatorname{sh} \tilde{\xi}_1) S_2 - \operatorname{ch} \xi_2 S_3 - \operatorname{sh} \xi_2 S_4 - \operatorname{ch} \xi_3 S_5 - \operatorname{sh} \xi_3 S_6 - \operatorname{ch} \xi_4 S_7 - \operatorname{sh} \xi_4 S_8 &= 0.
 \end{aligned}$$

References

- [Achenbach 1976] J. Achenbach, *Wave propagation in elastic solids*, North-Holland, Amsterdam, 1976.
- [Blatter et al. 1994] G. Blatter, M. V. Feigelman, V. B. Geshkenbein, A. L. Larkin, and V. M. Vinokur, “Vortices in high-temperature superconductors”, *Rev. Mod. Phys.* **66** (1994), 1125–1388.
- [Brandt 1995] E. H. Brandt, “The flux-line lattice in superconductors”, *Rep. Prog. Phys.* **58** (1995), 1465–1594.
- [Cyrot and Pavuna 1992] M. Cyrot and D. Pavuna, *Introduction to superconductivity and high- T_c materials*, World Scientific, Singapore, 1992.
- [Eringen and Şuhubi 1975] A. C. Eringen and E. S. Şuhubi, *Elastodynamics*, vol. 2, Academic Press, New York, 1975.
- [Maruszewski 1998] B. T. Maruszewski, “Superconducting fullerenes in a nonconventional thermodynamical model”, *Arch. Mech.* **50** (1998), 497–508.
- [Maruszewski 2007] B. T. Maruszewski, “On a nonclassical thermoviscoelastic stress in the vortex field in the type-II superconductor”, *Phys. Stat. Sol. B* **24** (2007), 919–927.
- [Maruszewski et al. 2007] B. T. Maruszewski, A. Drzewiecki, and R. Starosta, “Anomalous features of the thermomagnetoelastic field in a vortex array in a superconductor: propagation of Love’s waves”, *J. Thermal Stresses* **30** (2007), 1049–1065.
- [Maruszewski et al. 2008] B. T. Maruszewski, A. Drzewiecki, and R. Starosta, “Propagation of a surface wave in a vortex array along a superconducting heterostructure”, *J. Mech. Mat. Struct.* **3** (2008), 1097–1104.
- [Oliner 1978] A. A. Oliner, *Waveguides for acoustic surface waves*, edited by A. A. Oliner, Springer, New York, 1978.

Received 24 Jan 2011. Revised 25 Oct 2011. Accepted 13 Jan 2012.

BOGDAN T. MARUSZEWSKI: bogdan.maruszewski@put.poznan.pl
Institute of Applied Mechanics, Poznan University of Technology, ul. Jana Pawla II 24, 60-965 Poznan, Poland

ANDRZEJ DRZEWIECKI: andrzej.drzewiecki@put.poznan.pl
Institute of Applied Mechanics, Poznan University of Technology, ul. Jana Pawla II 24, 60-965 Poznan, Poland

ROMAN STAROSTA: roman.starosta@put.poznan.pl
Institute of Applied Mechanics, Poznan University of Technology, ul. Jana Pawla II 24, 60-965 Poznan, Poland

SUBMISSION GUIDELINES

ORIGINALITY

Authors may submit manuscripts in PDF format online at the Submissions page. Submission of a manuscript acknowledges that the manuscript is original and has neither previously, nor simultaneously, in whole or in part, been submitted elsewhere. Information regarding the preparation of manuscripts is provided below. Correspondence by email is requested for convenience and speed. For further information, write to one of the Chief Editors:

Davide Bigoni	bigoni@ing.unitn.it
Iwona Jasiuk	ijasiuk@me.concordia.ca
Yasuhide Shindo	shindo@material.tohoku.ac.jp

LANGUAGE

Manuscripts must be in English. A brief abstract of about 150 words or less must be included. The abstract should be self-contained and not make any reference to the bibliography. Also required are keywords and subject classification for the article, and, for each author, postal address, affiliation (if appropriate), and email address if available. A home-page URL is optional.

FORMAT

Authors can use their preferred manuscript-preparation software, including for example Microsoft Word or any variant of $\text{T}_{\text{E}}\text{X}$. The journal itself is produced in $\text{L}^{\text{A}}\text{T}_{\text{E}}\text{X}$, so accepted articles prepared using other software will be converted to $\text{L}^{\text{A}}\text{T}_{\text{E}}\text{X}$ at production time. Authors wishing to prepare their document in $\text{L}^{\text{A}}\text{T}_{\text{E}}\text{X}$ can follow the example file at www.jomms.net (but the use of other class files is acceptable). At submission time only a PDF file is required. After acceptance, authors must submit all source material (see especially Figures below).

REFERENCES

Bibliographical references should be complete, including article titles and page ranges. All references in the bibliography should be cited in the text. The use of Bib $\text{T}_{\text{E}}\text{X}$ is preferred but not required. Tags will be converted to the house format (see a current issue for examples); however, for submission you may use the format of your choice. Links will be provided to all literature with known web locations; authors can supply their own links in addition to those provided by the editorial process.

FIGURES

Figures must be of publication quality. After acceptance, you will need to submit the original source files in vector format for all diagrams and graphs in your manuscript: vector EPS or vector PDF files are the most useful. (EPS stands for Encapsulated PostScript.)

Most drawing and graphing packages—Mathematica, Adobe Illustrator, Corel Draw, MATLAB, etc.—allow the user to save files in one of these formats. Make sure that what you're saving is vector graphics and not a bitmap. If you need help, please write to graphics@msp.org with as many details as you can about how your graphics were generated.

Please also include the original data for any plots. This is particularly important if you are unable to save Excel-generated plots in vector format. Saving them as bitmaps is not useful; please send the Excel (.xls) spreadsheets instead. Bundle your figure files into a single archive (using zip, tar, rar or other format of your choice) and upload on the link you been given at acceptance time.

Each figure should be captioned and numbered so that it can float. Small figures occupying no more than three lines of vertical space can be kept in the text (“the curve looks like this:”). It is acceptable to submit a manuscript with all figures at the end, if their placement is specified in the text by means of comments such as “Place Figure 1 here”. The same considerations apply to tables.

WHITE SPACE

Forced line breaks or page breaks should not be inserted in the document. There is no point in your trying to optimize line and page breaks in the original manuscript. The manuscript will be reformatted to use the journal's preferred fonts and layout.

PROOFS

Page proofs will be made available to authors (or to the designated corresponding author) at a Web site in PDF format. Failure to acknowledge the receipt of proofs or to return corrections within the requested deadline may cause publication to be postponed.

Special issue

Trends in Continuum Physics (TRECOP 2010)

Preface	BOGDAN T. MARUSZEWSKI, WOLFGANG MUSCHIK, JOSEPH N. GRIMA and KRZYSZTOF W. WOJCIECHOWSKI	225
The inverse determination of the volume fraction of fibers in a unidirectionally reinforced composite for a given effective thermal conductivity	MAGDALENA MIERZWICZAK and JAN ADAM KOŁODZIEJ	229
Analytical-numerical solution of the inverse problem for the heat conduction equation	MICHAŁ CIAŁKOWSKI, ANDRZEJ MAĆKIEWICZ, JAN ADAM KOŁODZIEJ, UWE GAMPE and ANDRZEJ FRĄCKOWIAK	239
Analysis of stress-strain distribution within a spinal segment	ZDENKA SANT, MARIJA CAUCHI and MICHELLE SPITERI	255
A mesh-free numerical method for the estimation of the torsional stiffness of long bones	ANITA USCIOLOWSKA and AGNIESZKA FRASKA	265
Rayleigh-type wave propagation in an auxetic dielectric	ANDRZEJ DRZEWIECKI	277
Local gradient theory of dielectrics with polarization inertia and irreversibility of local mass displacement	VASYL KONDRAT and OLHA HRYTSYNA	285
Electromagnetoelastic waves in a vortex layer of a superconductor	BOGDAN T. MARUSZEWSKI, ANDRZEJ DRZEWIECKI and ROMAN STAROSTA	297

